



**OFF-DESIGN ANALYSIS OF A HIGH BYPASS TURBOFAN USING A PULSED  
DETONATION COMBUSTOR**

THESIS

Caitlin R. Thorn, Captain, USAF

AFIT/GAE/ENY/10-M26

**DEPARTMENT OF THE AIR FORCE  
AIR UNIVERSITY**

**AIR FORCE INSTITUTE OF TECHNOLOGY**

---

---

**Wright-Patterson Air Force Base, Ohio**

APPROVED FOR PUBLIC RELEASE; DISTRIBUTION UNLIMITED

The views expressed in this thesis are those of the author and do not reflect the official policy or position of the United States Air Force, Department of Defense, or the United States Government. This material is declared a work of the U.S. Government and is not subject to copyright protection in the United States.

AFIT/GAE/ENY/10-M26

**OFF-DESIGN ANALYSIS OF A HIGH BYPASS TURBOFAN USING A PULSED  
DETONATION COMBUSTOR**

THESIS

Presented to the Faculty

Department of Aeronautics and Astronautics

Graduate School of Engineering and Management

Air Force Institute of Technology

Air University

Air Education and Training Command

In Partial Fulfillment of the Requirements for the  
Degree of Master of Science in Aeronautical Engineering

Caitlin R. Thorn, BS

Captain, USAF

March 2010

APPROVED FOR PUBLIC RELEASE; DISTRIBUTION UNLIMITED


AFIT/GAE/ENY/10-M26

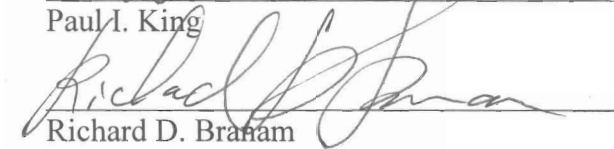
**OFF-DESIGN ANALYSIS OF A HIGH BYPASS TURBOFAN USING A PULSED  
DETONATION COMBUSTOR**

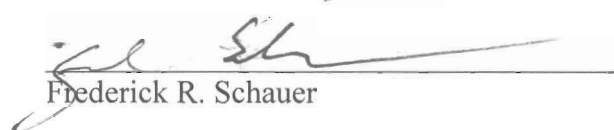
Caitlin R. Thorn, BS

Captain, USAF

Approved:

  
\_\_\_\_\_  
Paul I. King

  
\_\_\_\_\_  
Richard D. Bramam

  
\_\_\_\_\_  
Frederick R. Schauer

18 Mar 10  
Date

18 Mar 2010  
Date

18 Mar 2010  
Date

## **Abstract**

Past research has indicated that implementation of a pulsed detonation combustor (PDC) into a high-bypass turbofan engine yields a more efficient engine at design conditions. It is proposed that performance gains can be made utilizing this hybrid engine off-design. A hybrid high-bypass turbofan engine with a PDC model was evaluated for a range of Mach numbers, altitudes, and fill fractions in the Numerical Propulsion System Simulation (NPSS). Results were compared to a conventional baseline high-bypass turbofan engine that shares the same architecture with the hybrid. The NPSS baseline engine was validated using the Aircraft Engine Design System (AEDsys) program and the net thrust and specific fuel consumption agreed to within one percent. The effect of detonation on the core air flow is calculated using a closed form solution for the Chapman-Jouguet Mach number with a total energy correction applied. Results indicate that fill fraction can be adjusted to reduce the TSFC to that of the baseline engine and lower at some thrust levels. With careful selection of design parameters, results suggest a pulsed detonation combustor may be an appropriate candidate for inclusion in a hybrid turbofan engine.

## **Acknowledgments**

This thesis could not have been written without the help of many different people. I want to first thank Capt Ionio Andrus for answering many of my questions during the early months of my study as I sought to understand and build on his work. I wish to thank Tom Lavelle for his guidance in helping me learn a programming language I first thought I would never understand. Thanks go to Dr. Fred Schauer and Major Kurt Rouser for their time and input. I would especially like to thank my advisor, Dr. King, for his patience, time, input, and faith that I could accomplish this work. And finally to my newborn son and husband, thank you for your love and support as I completed this research.

Caitlin R. Thorn

## Table of Contents

	Page
Abstract .....	iv
Acknowledgements .....	vi
Table of Contents .....	vi
List of Figures .....	ix
List of Tables .....	xi
List of Symbols .....	xii
List of Abbreviations .....	xviii
I. Introduction .....	1
Purpose .....	2
Procedure .....	3
Significance of Research .....	4
Organization .....	4
II. Literature Review .....	6
Introduction.....	6
Combustion Waves.....	7
Chapman-Jouguet Theory .....	8
Zeldovich-von Nuemann-Doring Theory .....	11
Thermodynamic Cycle Analysis .....	13
Pulsed Detonation Engine Cycle .....	16

	Page
Prior Work on Hybrid-Pulse Detonation Engines .....	18
III. Baseline and Hybrid Models.....	22
Introduction .....	22
Baseline High Bypass Turbofan Engine in AEDsys and NPSS.....	22
Hybrid Turbofan Engine and Pulsed Detonation Combustor in NPSS.....	27
Hybrid Turbofan Engine Off-Design .....	32
IV. Analysis and Results.....	36
Introduction .....	36
Baseline Turbofan Off-Design Performance.....	36
Hybrid Turbofan Engine Off-Design Results.....	39
Code Verification and Operating Limit.....	39
Component Data.....	43
Hybrid Turbofan Performance Comparison.....	48
Component Performance .....	61
Component Adiabatic Efficiencies.....	64
Parameter Design Choices.....	68
V. Conclusions and Recommendations .....	72
Introduction .....	72
Hybrid Turbofan Engine Off-Design Performance .....	72
Recommendations .....	73



	Page
Appendix A.....	75
Appendix B.....	82
Appendix C.....	90
Appendix D.....	98
Bibliography .....	130
Vita.....	133

## List of Figures

Figure	Page
2.1. Stationary One-Dimensional Combustion Wave.....	7
2.2. Hugoniot Curve with Rayleigh Lines .....	10
2.3. Thermodynamic Property Variations Across a ZND Detonation Wave .....	12
2.4. Detonation Structure .....	13
2.5. Ideal PDE, Humphrey, and Brayton Cycle Temperature-Entropy Diagrams.....	14
2.6. PDE Cycle Stages .....	17
2.7. Relationship Between Equivalence Ratio and Detonation Wave Speed .....	20
2.8. Relationship Between Fill Fraction and Detonation Wave Speed.....	21
3.1. Baseline NPSS High Bypass Turbofan Engine Configuration .....	23
3.2. Pulsed Detonation Combustor Configuration.....	28
4.1. Throttle Hook Baseline Engine Comparison Using NPSS and AEDsys.....	37
4.2. Low Pressure Spool Adiabatic Efficiencies for NPSS Off-Design .....	38
4.3. High Pressure Spool Adiabatic Efficiencies for NPSS Off-Design.....	38
4.4. Maximum Operating Limit Baseline and Hybrid Engine.....	41
4.5. Throttle Hooks Baseline and Hybrid Engine Comparison .....	48
4.6. Throttle Hooks Hybrid Engine (various fill fractions) .....	51
4.7. Throttle Hooks Hybrid Engine (various frequencies).....	53
4.8. Thrust Variation with Flight Mach Number and Fill Fraction .....	55
4.9. TSFC Variation with Fill Fraction.....	59

Figure	Page
4.10. Mass Flow Rate Variation with Thrust.....	60
4.11. Fan Pressure Ratio Variation with $T_{t2}/T_0$ .....	62
4.12. HPC Ratio Variation with $T_{t2}/T_0$ .....	62
4.13. LPT Ratio Variation with $T_{t2}/T_0$ .....	63
4.14. Bypass Ratio Variation with $T_{t2}/T_0$ .....	63
4.15. Throttle Hooks Inlet Efficiency .....	64
4.16. Throttle Hooks Fan Efficiency.....	65
4.17. Throttle Hooks HPT Efficiency .....	65
4.18. Throttle Hooks LPT Efficiency .....	66
4.19. Throttle Hooks LPC Efficiency .....	66
4.20. Throttle Hooks HPC Efficiency .....	67
4.21. Throttle Hooks Burner Efficiency .....	67
4.22. Throttle Hooks Frequency Design Choice.....	69
4.23. Throttle Hooks Equivalence Ratio Design Choice .....	70
4.24. Throttle Hooks Purge Fraction Design Choice .....	71

## **List of Tables**

Table	Page
2.1. Qualitative Differences Between Detonation and Deflagration in Gases.....	8
3.1. Baseline Engine Parameters.....	23
3.2. AEDsys Baseline Turbofan Engine Input Parameters .....	24
3.3. Baseline Model NPSS Adiabatic Efficiency Inputs.....	25
3.4. NPSS Thermodynamics Packages .....	26
3.5. Hybrid Engine On-Design Configuration.....	27
4.1. Hybrid Engine Test Data .....	40
4.2. NPSS Component Interface Data at SLS.....	43
4.3. NPSS Component Interface Data at Cruise .....	44
4.4. Combustor Properties SLS and Cruise .....	47

## List of Symbols

### Symbol

$a$	Speed of sound in a fluid (ft/s)
$\alpha$	Bypass ratio
$A$	Area (ft <sup>2</sup> )
$Alt$	Altitude (ft)
$A_{phy}$	Cross sectional area (ft <sup>2</sup> )
$AR_{valve}$	Area ratio of detonation tube inlet valves to detonation tubes
$A_{tube}$	Detonation tube cross-sectional area (ft <sup>2</sup> )
$c_p$	Constant pressure specific heat (Btu/lbm R)
$c_v$	Nozzle gross thrust coefficient
$dP_qP$	Pressure loss
$e$	Polytropic efficiency
$e_{cH}$	High pressure compressor polytropic efficiency
$e_{cL}$	Low pressure compressor polytropic efficiency
$e_f$	Fan polytropic efficiency
$e_{tH}$	High pressure turbine polytropic efficiency
$e_{tL}$	Low pressure turbine polytropic efficiency
$\eta$	Adiabatic efficiency
$\eta_b$	Burner adiabatic efficiency
$\eta_{cH}$	High pressure compressor adiabatic efficiency

## Symbol

$\eta_{cL}$	Low pressure compressor adiabatic efficiency
$\eta_f$	Fan adiabatic efficiency
$\eta_{tH}$	High pressure turbine adiabatic efficiency
$\eta_{tL}$	Low pressure turbine adiabatic efficiency
$e_{tb}$	Work rate or power
$f$	Cycle frequency (1/s)
$f_m$	Mass fuel-air ratio
$ff$	Fill fraction
$F_g$	Gross thrust (lbf)
$F_n$	Net thrust (lbf)
$\gamma$	Ratio of specific heats
$h$	Static enthalpy (Btu/lbm)
$h^\circ$	Heat of reaction (Btu/lbm)
$h_0$	Enthalpy at beginning of cycle (Btu/lbm)
$h_{tbexit}$	Turbine exit enthalpy (Btu/lbm)
$\Delta h$	Difference in enthalpy between two models (Btu/lbm)
$h_{pr}$	Fuel lower heating value (Btu/lbm)
$imp$	Impulse function (lbf)
$l_{tube}$	Tube length (in)
$M_{CJ}$	Chapman-Jouguet Mach number

## Symbol

$M_{\text{valve}}$	Valve Mach number
$m_{\text{fill air}}$	Mass of pure air mixed with fuel during cycle (lbm)
$m_{\text{fuel}}$	Mass of fuel used for one fill cycle (lbm)
$m_{\text{fuel-air mix}}$	Fuel-air mass for fill (lbm)
$m_{\text{purge air}}$	Purge air mass (lbm)
$\dot{m}$	Mass flow rate (lbm/s)
$\dot{m}_{\text{core air}}$	Mass flow rate of air through detonation tubes and internal bypass (lbm/s)
<u><math>\dot{m}_{\text{tube air}}</math></u>	Mass flow rate through detonation tubes (lbm/s)
$\dot{m}_{\text{IEP}}$	Mass flow rate through internal bypass (lbm/s)
<u><math>\dot{m}_{\text{flux}}</math></u>	Mass flux (lbm/(A*s))
$\dot{m}_{\text{vo}}$	Maximum mass flow rate when detonation valve is open (lbm/s)
$n_{\text{tubes}}$	Number of detonation tubes
$N_c$	Corrected speed (rpm)
$P_0$	Freestream static pressure (lbf/ft <sup>2</sup> )
$P_r$	Reduced pressure (lbm/s)
$P_s$	Static pressure (lbf/ft <sup>2</sup> )
$P_t$	Total pressure (lbf/ft <sup>2</sup> )
$\frac{\Delta P}{P}$	Unscaled normalized pressure drop
$pf$	Purge fraction

## Symbol

$\pi_b$	Burner pressure ratio
$\pi_{cL}$	Low pressure compressor pressure ratio
$\pi_{cH}$	High pressure compressor pressure ratio
$\pi_d$	Diffuser pressure ratio
$\pi_f$	Fan pressure ratio
$\pi_n$	Nozzle pressure ratio
$\pi_{nf}$	Fan nozzle pressure ratio
$\pi_r$	Isentropic freestream recovery pressure ratio
$\pi_{tH}$	High pressure turbine pressure ratio
$\pi_{tL}$	Low pressure turbine pressure ratio
$q$	Heat flux (Btu/lbm)
$q_{add}$	Heat flux into system (Btu/lbm)
$\bar{q}$	Non-dimensional heat addition
$R_s$	Gas constant based on static conditions (Btu/(lbm*R))
$S$	Entropy (Btu/lbm R)
$\tau_{cL}$	Low pressure compressor temperature ratio
$\tau_{cH}$	High pressure compressor temperature ratio
$\tau_f$	Fan temperature ratio
$\tau_r$	Adiabatic freestream recovery enthalpy ratio
$\tau_{tH}$	High pressure turbine temperature ratio



## Symbol

$\tau_{tL}$	Low pressure turbine temperature ratio
$\tau_{tb}$	Total temperature ratio across turbine
$\tau_{vo}$	Valve open time fraction
$t_{blowdown}$	Blowdown time (s)
$t_{cycle}$	Cycle time (s)
$t_{fill}$	Fill time (s)
$t_{purge}$	Purge time (s)
$T_0$	Freestream static temperature (R)
$T_s$	Static temperature (R)
$T_t$	Total temperature (R)
$T_{t4}$	Total temperature at turbine inlet (R)
$u$	Fluid velocity (ft/s)
$u_{CJ}$	Chapman-Jouguet detonation wave velocity (ft/s)
$V$	Velocity (ft/s)
$V_{\text{purge air}}$	Purge air volume per cycle (ft <sup>3</sup> )
$V_{\text{fuel-air mix}}$	Fuel-air mixture volume per cycle (ft <sup>3</sup> )
$W$	Total mass flow (lbm/s)
$\Psi$	Non-dimensional temperature ratio
$\eta_b$	Burner adiabatic efficiency
$\eta_c$	Compressor adiabatic efficiency

## Symbol

$\eta_n$	Nozzle efficiency
$\eta_t$	Turbine adiabatic efficiency
$\pi_b$	Burner pressure ratio $\left( \frac{P_{t2}}{P_{t1}} \right)$
$\pi_c$	Compressor total pressure ratio
$\pi_{dmax}$	Maximum inlet pressure ratio
$\pi_n$	Main nozzle inlet pressure ratio $\left( \frac{P_{t4}}{P_{t3}} \right)$
$\pi_{nf}$	Fan nozzle pressure ratio $\left( \frac{P_{t19}}{P_{t17}} \right)$
$\pi_t$	Total pressure ratio across turbine
$\phi$	Entropy function
$\rho$	Density (lbm/ft <sup>3</sup> )
$\rho_t$	Static density (lbm/ft <sup>3</sup> )
$\gamma$	Ratio of specific heats

## **List of Abbreviations**

### Abbreviation

AED <sub>sys</sub>	Aircraft Engine Design System
BLD	Bleed
BPR	Bypass ratio
CJ	Chapman-Jouguet
CTOH	High pressure spool power take-off coefficient
CTOL	Low pressure spool powertake-off coefficient
CVCCE	Constant volume combustion cycle engine
DDT	Deflagration to detonation time
FAR	Mass fuel-to-air ratio
FPR	Fan pressure ratio
HBTF	High bypass turbofan
HP	High pressure
HPC	High pressure compressor
HPT	High pressure turbine
iBPR	Internal bypass ratio
LP	Low pressure
LPC	Low pressure compressor
LPT	Low pressure turbine
MFP	Mass flow parameter

## Abbreviation

MN	Mach number
NASA	National Aeronautics and Space Administration
NIST	National Institute of Standards and Technology
NPSS	Numerical Propulsion System Simulation
OPR	Overall pressure ratio
PDC	Pulsed detonation combustor
PDE	Pulsed detonation engine
PR	Pressure ratio
PTO	Power take off
RPM	Revolutions per minute
SFC	Specific fuel consumption
TIT	Turbine inlet temperature
TSFC	Thrust specific fuel consumption
VSH	Variable specific heats
WAR	Water-to-air ratio
ZND	Zeldovich, Von Neumann, and Doring

# **OFF-DESIGN ANALYSIS OF A HIGH BYPASS TURBOFAN USING A PULSED DETONATION COMBUSTOR**

## **I. Introduction**

Since the early 1940's, pulsed detonation engines (PDE) have been studied as a means of increasing burn efficiency in an engine as a result of its supersonic detonative mode of combustion over conventional subsonic deflagration. Detonations provide a much more efficient means of combusting a fuel-oxidizer mixture due to increased thermodynamic efficiency as a result of the pressure-rise associated with detonation. Additionally, with its potential for a cycle time of more than ten times that of a traditional pulsejet engine and fewer moving parts to maintain, PDEs hold the promise for applications across the flight envelope spanning subsonic, supersonic and hypersonic flight.

More advanced concepts such as a hybrid-PDE have been studied in which a pulsed detonation combustor (PDC) is incorporated into a gas turbine engine as the primary combustion system with the intention of increasing efficiency by utilizing the strengths of both engines. In this type of system the exhaust from the detonation chamber drives the downstream turbine which provides power to the compressor, which, in turn, provides the air flow to fill and purge the detonation chamber. Although a novel idea, the hybrid system is not without its challenges. Low-vapor pressure hydrocarbon fuels must be used efficiently as key PDE cycle parameters such as ignition time and deflagration to

detonation time depend on the properties of the fuel. Noise is also a substantial issue as detonations are significantly louder than deflagration combustion. The periodic, high-pressure pulses must be assessed on turbine performance and the life of the engine. The first flight of an aircraft powered by a PDE took place on January 31, 2008 operating under its own power for 10 seconds at an altitude of approximately 100 feet. With this demonstration proving that a PDE can be integrated into an aircraft frame without experiencing structural problems, PDEs are increasingly recognized as a realizable technology for future aerospace propulsion.

## **Purpose**

A substantial amount of work on PDEs and hybrid PDEs has been accomplished, with significant developments being made in the last fifteen years. The theoretical analysis of Petters and Felding (Petters and Felding, 2002:6) indicated that a PDE-hybrid with the same inlet airflow as a baseline turbofan engine produced a 2% higher thrust and an 11% reduction in thrust specific fuel consumption (TSFC). Similar studies by Andrus (Andrus, 2007:81) showed that an optimal hybrid engine operating at design conditions could yield an 8% decrease in TSFC while maintaining thrust.

The experimental work of Schauer et al. (Schauer et al., 2003), Deng et al. (Deng et al., 2008), and Rasheed et al. (Rasheed et al., 2005) all investigated a detonation driven turbine at design conditions; however, the only experimental work done on PDEs at off-design conditions to date is that of Glaser et al. (Glaser et al., 2004). Glaser's work

suggests performance gains can be made by varying key parameters such as equivalence ratio and fill fraction. The objective of this thesis is to build on Andrus's (Andrus, 2007) work by performing a simulated off-design analysis of a hybrid-PDE design to evaluate the effects on thrust and TSFC.

## **Procedure**

The procedure for performing the off-design analysis closely mirrors the steps used by Andrus in performing his comparative analysis of a high bypass turbofan using a pulsed detonation combustor with a conventional baseline turbofan. A baseline high-bypass turbofan is modeled in both the Numerical Propulsion System Simulation (NPSS) and in the Aircraft Engine Design system (AEDsys) programs. The comparison is made to ensure identical engine configuration between the two programs. The NPSS program is the primary software program used in this thesis to evaluate the off-design performance of a hybrid-PDE. It was developed via a cooperative effort between industry and NASA to predict and analyze the aerothermodynamic behavior of commercial jet aircraft, military applications, and space transportation with the goal of reducing development time and cost of a new engine by half. AEDsys was developed by Mattingly (Mattingly et al., 2006) for educational use in the field of gas turbine engine design and allows the user to perform design point and parametric cycle analysis for various engines.

After validating the accuracy of the baseline engine in both AEDsys and NPSS, a hybrid-PDE model with the identical configuration as the baseline engine, with the

exception of a pulsed detonation combustor replacing the conventional combustor, is developed in NPSS and run at off-design conditions. An analysis of the hybrid engine performance is evaluated for a range of Mach numbers, altitudes, and fill fractions. The effects on thrust and TFSC are compared to that of the NPSS baseline engine running at the same off-design conditions.

### **Significance of Research**

Much research has been done on turbofan engines with a pulsed detonation combustor at design conditions, but there is a very limited amount of literature on the performance of these engines off-design. Because the majority of an engine's operation are at off-design conditions, significant cost savings could be realized if hybrid turbofan engines are more efficient than conventional engines. In addition, a hybrid engine may be cheaper to build and less expensive to maintain than a conventional engine, offering additional long term savings.

### **Organization**

This thesis compares the performance of a hybrid-PDE to that of a conventional turbofan using the NPSS program. Chapter two contains a thorough discussion of pulsed detonation thermodynamics as well as prior work on PDEs. Chapter three describes the baseline turbofan model used in AEDsys and NPSS, as well as the hybrid-PDE engine and its combustor section. Chapter four is a comprehensive analysis of the hybrid-PDE



performance as compared to that of the conventional baseline engine. Chapter five contains the conclusions of this research as well as recommendations for future work.

## II. Literature Review

### Introduction

This section presents a thorough discussion of the underlying thermodynamics of the hybrid-PDE engine as the results of this thesis are essentially governed by the basic models of detonation to include the Chapman-Jouguet and Zeldovich-von Nuemann-Doring (ZND) theories.

The Chapman-Jouguet theory allows for the calculation of the detonation velocity of a detonation wave with known pressures and densities of the unburned gases for a given  $q$ . The steady state solution of the detonation wave requires knowledge of the equilibrium thermodynamic calculations. Experimental results have shown to agree well with the detonation velocities resulting from this theory.

Zeldovich, von Nuemann, and Doring (Kuo, 1986) present a model for detonation wave structure in which parameters such as detonation limits, initiation energy, tube diameter, etc. are known. Unlike the Chapman-Jouguet theory, experimental measurements do not agree with the model calculations, mainly because the ZND structure is unstable and only observed experimentally under transient conditions. Experimental observations show that the self-sustained detonations have a three-dimensional cell structure; however, there are currently no acceptable theories that define this cell structure.

## Combustion Waves

In order to understand how a pulsed detonation combustor can be more efficient than a conventional combustor, it is first necessary to understand the differences between the detonations and deflagrations of the two burners that produce engine thrust. A detonation is a supersonic shock wave that propagates through a fluid due to an energy release in a reaction zone. A deflagration is a wave that propagates at a subsonic rate by heat transfer. Detonations generate higher pressures and have increased wave speeds, thus producing greater thrust than deflagrations. Figure 2.1 shows a schematic of a stationary one-dimensional combustion wave in which subscript one and two denote conditions of the unburned gases ahead of the wave and burned gases behind the wave, respectively. Deflagration and detonation wave properties are compared in Table 2.1.

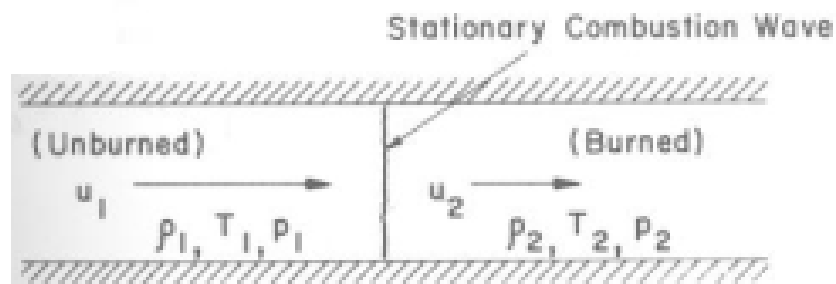


**Figure 2.1 Stationary one-dimensional combustion wave (Kuo, 1986:233)**

**Table 2.1. Qualitative differences between detonation and deflagration in gases (Kuo, 1986:234)**

	Detonation	Deflagration
$u_1/a_1$	5-10	0.0001-0.03
$u_2/u_1$	0.4-0.7	4-6
$p_2/p_1$	13-55	~0.98
$T_2/T_1$	8-21	4-16
$\rho_2/\rho_1$	1.7-2.6	0.06-0.25

A combustion wave is formed in a tube when a combustible gas mixture is ignited at the closed end of a tube. The properties in Table 2.1 show that the burned gases are higher in temperature and density than the unburned gases. This increase in density initiates a compression wave that travels towards the deflagration wave front, causing the wave to accelerate. Density increases as the deflagration wave continues, causing more and more compression waves to form. The waves accelerate as pressure and density increase, thus causing them to amalgamate at the deflagration wave front. If the tube is sufficiently long, a shock wave will form that is strong enough to ignite the mixture ahead of the wave front. A detonation is obtained as the continuous compression waves in the reaction zone keep the shock from decaying. The detonation is inherently self-sustaining in that the detonation front initiates a chemical reaction by compression by diffusing heat.

### **Chapman-Jouguet Theory**

To solve for the Hugoniot curve on which the Chapman-Jouguet points are found, we must first start with the conservation equations (Glassman, 1996:226):

$$\rho_1 u_1 = \rho_2 u_2 \quad (2.1)$$

$$p_1 + \rho_1 u_1^2 = p_2 + \rho_2 u_2^2 \quad (2.2)$$

$$c_p T_1 + \frac{1}{2} u_1^2 + q = c_p T_2 + \frac{1}{2} u_2^2 \quad (2.3)$$

$$\begin{aligned} p_1 &= \rho_1 R T_1 \\ p_2 &= \rho_2 R T_2 \end{aligned} \quad (2.4)$$

where Eqs. 2.1, 2.2, and 2.3 are the mass, momentum, and energy respectively. Equation 2.4 is simply the equation of state. The four equations can be reduced to one equation with two unknowns,  $p_2$  and  $\rho_2$ , by combining Eqs. 2.1 and 2.2 to yield (Kuo, 1986:236):

$$\rho_1^2 u_1^2 = \frac{p_2 - p_1}{\frac{1}{\rho_1} - \frac{1}{\rho_2}} = \dot{m}_{f_{ax}}^2 \quad (2.5)$$

or in terms of Mach number:

$$\gamma M_1^2 = \frac{\frac{p_2}{p_1} - 1}{1 - \frac{\rho_1}{\rho_2}} \quad (2.6)$$

where Eqs. 2.5 and 2.6 are known as the Raleigh-line relation.

The Hugoniot relation can be found by combining Eqs. 2.1 - 2.4 to yield (Glassman, 1996:228):

$$\frac{\gamma}{\gamma - 1} \left( \frac{p_2}{\rho_2} - \frac{p_1}{\rho_1} \right) - \frac{1}{2} (p_2 - p_1) \left( \frac{1}{\rho_1} - \frac{1}{\rho_2} \right) = q \quad (2.7)$$

where  $q$  is the heat flux. The Hugoniot curve as shown in Fig. 2.2 is a plot of the specific volume ( $1/\rho$ ) and pressure of the burned gases for given values of heat flux, specific volume and pressure of the unburned gases.

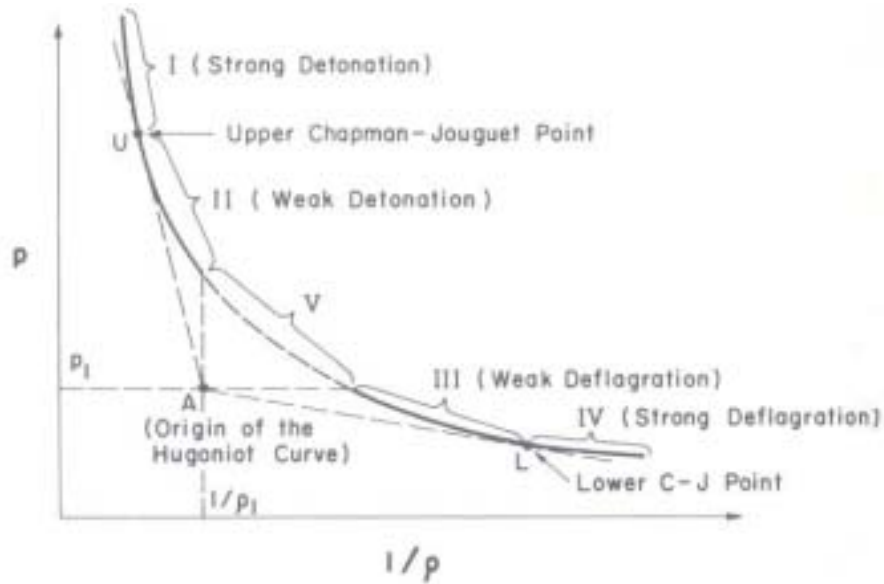


**Figure 2.2 Hugoniot curve with Rayleigh lines (Kuo, 1986:238)**

The plot is broken up into five regions constructed by drawing tangents and vertical and horizontal lines from the origin ( $1/\rho_1, p_1$ ) to the curve. The two Chapman-Jouguet points are at the tangents to the curve and are referred to as the upper and lower C-J points at the upper and lower Rayleigh lines, respectively. Of the five regions, only regions I, II, and III are physically possible. Region V does not bound a valid solution as  $p_2$  and  $1/\rho_2$  are greater than  $p_1$  and  $1/\rho_1$  and thus would require a compression wave to move in the negative direction. Region IV is also ruled out as the heat addition stipulates supersonic flow; however, it is not possible to have heat addition and advance past the sonic condition in a constant area duct. Regions I and II are the detonation regions of the

curve and represent strong and weak detonations, respectively. These regions are eliminated due to the structure of the detonation wave discussed in the next section. Region III is the weak deflagration region and is often observed in most experimental conditions; however, since deflagration is not of interest in this thesis, region III is irrelevant to this work as well. The upper C-J point is of importance to this research in that the wave speed at this point corresponds to a minimum detonation wave speed and implies that the Mach number of the burned gases must be equal to one. The method used in this work to calculate the velocity of the wave at this point will be discussed later in this chapter.

### **Zeldovich-von Nuemann-Doring Theory**

The Zeldovich-von Nuemann-Doring (ZND) model is a one-dimensional model of the structure of a detonation wave. The model assumes a one-dimensional, steady flow with limited reactions in the shock wave region. As shown in Fig. 2.3 the detonation wave consists of a thin shock wave region followed by a thick deflagration region consisting of an induction and reaction zone. The reactants are initially heated by the shock wave to a temperature which ensures a high enough reaction rate in which the deflagration can propagate at the same speed as the shock wave. The thin shock layer results in a sharp spike in temperature, pressure, and density. The peak pressure reached in this region is referred to as the von Neumann spike. This is followed by relatively steady profiles through the induction zone due to a slowly increasing rate of reaction immediately behind the shock front.

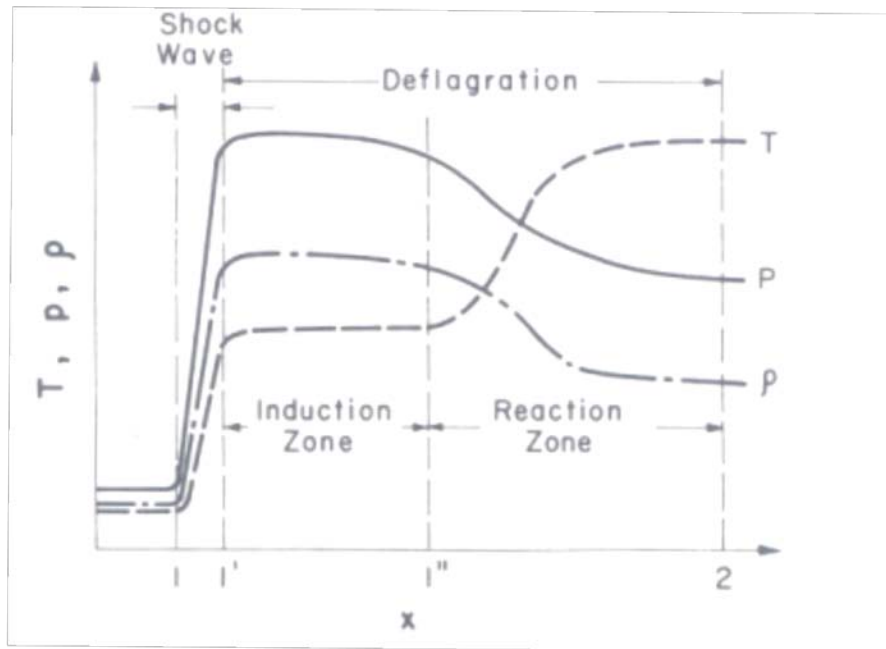


**Figure 2.3 Thermodynamic property variations across a ZND detonation wave (Kuo, 1986:261)**

The properties change drastically again as reaction rate increases and then reach their equilibrium values once the reaction has completed. The ZND detonation structure may also be shown on Fig. 2.4 beginning at the Hugoniot origin and moving up along the left of the curve until it reaches the von Neumann spike. At this point the pressure decreases and the path merges with the Hugoniot curve to the upper C-J point.

Although these models assume a detonation to be one-dimensional, it should be acknowledged that detonation waves moving in tubes are actually three-dimensional and nonsteady in nature in which the flow proceeds in a cyclic manner with shock velocity fluctuations about the equilibrium C-J value.



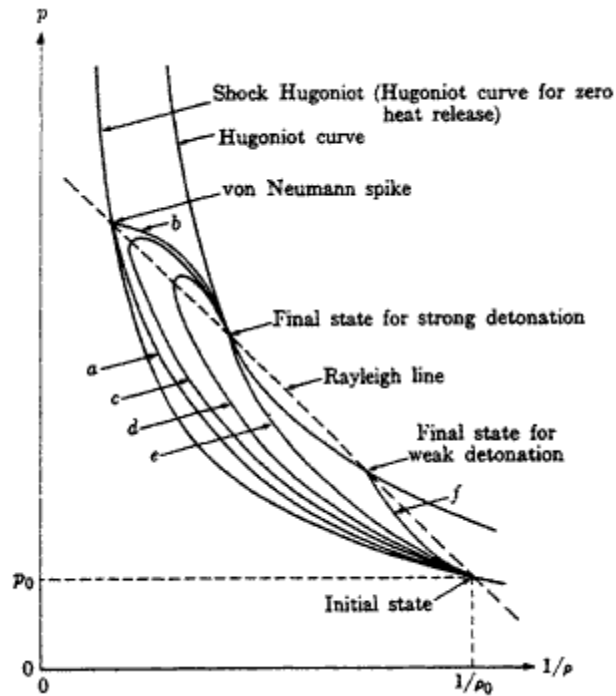
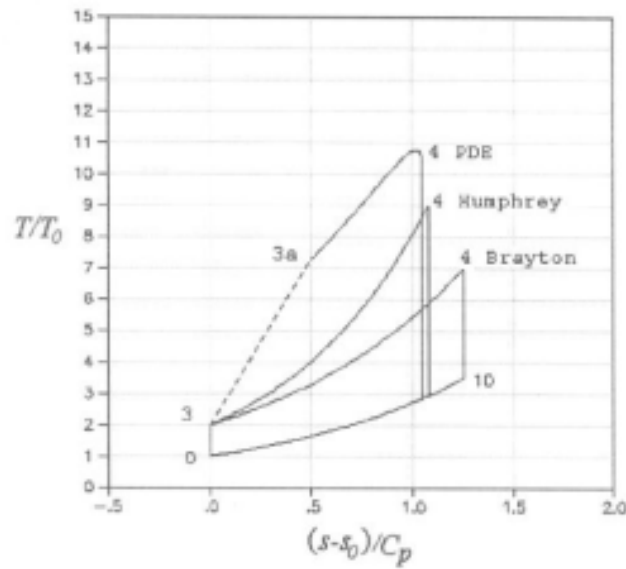


Figure 2.4 Detonation structure (Williams, 1985:193)

### Thermodynamic Cycle Analysis

The pulsed detonation engine thermodynamic cycle is described by Heiser and Pratt (Heiser and Pratt, 2002:2) as being identical to that of an ideal Humphrey cycle used in turbojets and ramjets with the exception of heat addition during the combustion process. The ideal Humphrey cycle is sometimes used to estimate the thermal efficiency of the PDE cycle as it replaces the Brayton cycle's constant-pressure heat addition process with a constant-volume heat addition process. The T-s diagram of these three processes is shown in Fig. 2.5.



**Figure 2.5 Ideal PDE, Humphrey, and Brayton cycle temperature-entropy diagrams (Heiser, 2002:4)**

The thermal efficiency of the PDE cycle is slightly greater than that of the Humphrey cycle and much greater than that of the Brayton cycle. The thermal efficiency of the PDE cycle as proposed by Heiser is identical to that of the Fickett-Jacobs cycle as described by Wintenberger (Wintenberger and Sheperd, 2004:12) in which an upper limit is computed to be the amount of mechanical work in a cycle produced by an unsteady detonation process.

In Fig. 2.5, from state 0 to 3, an isentropic, adiabatic compression takes place in all three cycles, raising the temperature to  $T_3$ . It is the process from state 3 to 4 in which the PDE, Humphrey, and Brayton cycles differ. In the Brayton cycle, a constant pressure heat addition takes place and increases the temperature  $T_3$  of the combustor inlet to  $T_4$  at the combustor outlet. From state 3 to 4 in the PDE cycle, the ZND detonation wave is

seen in which the process is constrained by the Chapman-Jouguet condition, requiring the Mach number at state 4 to be sonic. The path from state 3 to 4 differs slightly from that of the Brayton and Humphrey cycles in that from state 3 to 3a the heat addition process generates entropy via the adiabatic normal shock wave, and from state 3a to 4 entropy is generated via a constant area heat addition process. The process from state 4 to 10 and state 10 to 0 of the three cycles are identical in that an isentropic expansion process takes place followed by a heat rejection to close the cycle.

The derivation for the solutions for the Chapman-Jouguet Mach number, the entropy difference from states 3 to 4, and cycle thermal efficiency are shown in Appendix A. They are given here by Eqs. 2.8, 2.9, and 2.10 respectively:

$$M_{cj}^2 = (\gamma + 1) \left( \frac{\bar{q}}{\psi} \right) + 1 + \sqrt{\left[ (\gamma + 1) \left( \frac{\bar{q}}{\psi} \right) + 1 \right]^2 - 1} \quad (2.8)$$

$$\frac{s_4 - s_3}{c_p} = -\ln \left[ M_{cj}^2 \left( \frac{\gamma + 1}{1 + \gamma M_{cj}^2} \right)^{\frac{\gamma + 1}{\gamma}} \right] \quad (2.9)$$

$$\eta_{th} = 1 - \left[ \frac{1}{M_{cj}^2} \left( \frac{1 + \gamma M_{cj}^2}{\gamma + 1} \right)^{\frac{\gamma + 1}{\gamma}} - 1 \right] / \bar{q} \quad (2.10)$$

where

$$\bar{q} = \frac{q_{add}}{c_p T_0} = \frac{h_4 - h_3}{c_p T_0} = \frac{\eta_b (FAR) h_{py}}{c_p T_0} \quad (2.11)$$

and

$$\psi = T_3 / T_0 \quad (2.12)$$

The Chapman-Jouguet Mach number is calculated using the non-dimensional heat addition  $q$  and  $\psi$ , the ratio of static temperature at state 3 to the free-stream static temperature at state 0.  $M_{CJ}$  is then used to calculate the entropy rise from state 3 to 4 and the thermal efficiency of the cycle. According to Heiser and Pratt (Heiser and Pratt, 2002), all the fluid properties at the detonation tube exit can be solved for using Eqs. 2.9 and 2.13 to solve for the entropy and pressure at state 4.

$$\frac{p_4}{p_0} = \frac{1 + \gamma M_{CJ}^2}{\gamma + 1} \frac{p_3}{p_0} \geq 1 \quad (2.13)$$

The PDE thermodynamics as described by Heiser and Pratt is used in this thesis with the addition of a correction factor by Dyer and Kaemming (Dyer and Kaemming, 2002:5). They note that using the pressure and entropy at the detonation tube exit to solve for all the properties of the fluid at this point is inaccurate because it ignores the eventual pressure loss that the gas will go through due to expansion waves. They propose using entropy and the change in enthalpy liberated by the combustion process to solve for the properties at the detonation tube exit. Available energy is calculated using the known CJ entropy originally calculated by Heiser and Pratt (Heiser and Pratt, 2002:3), Eq. 2.9, with the known system enthalpy of  $(h_0 + q_{add})$ , with  $q_{add}$  being the heat flux into the system, to ensure that energy is conserved.

### **Pulsed Detonation Engine Cycle**

A basic understanding of the PDE cycle is necessary to understand how the combustor section of the hybrid PDE performs in this research. The cycle consists of four

distinct processes: fill phase, detonation initiation, detonation wave propagation, and purge phase. The combustor is then recharged with another fuel/air mixture and the cycle repeats.

Figure 2.6 illustrates the various stages in a pulsed detonation engine cycle. At

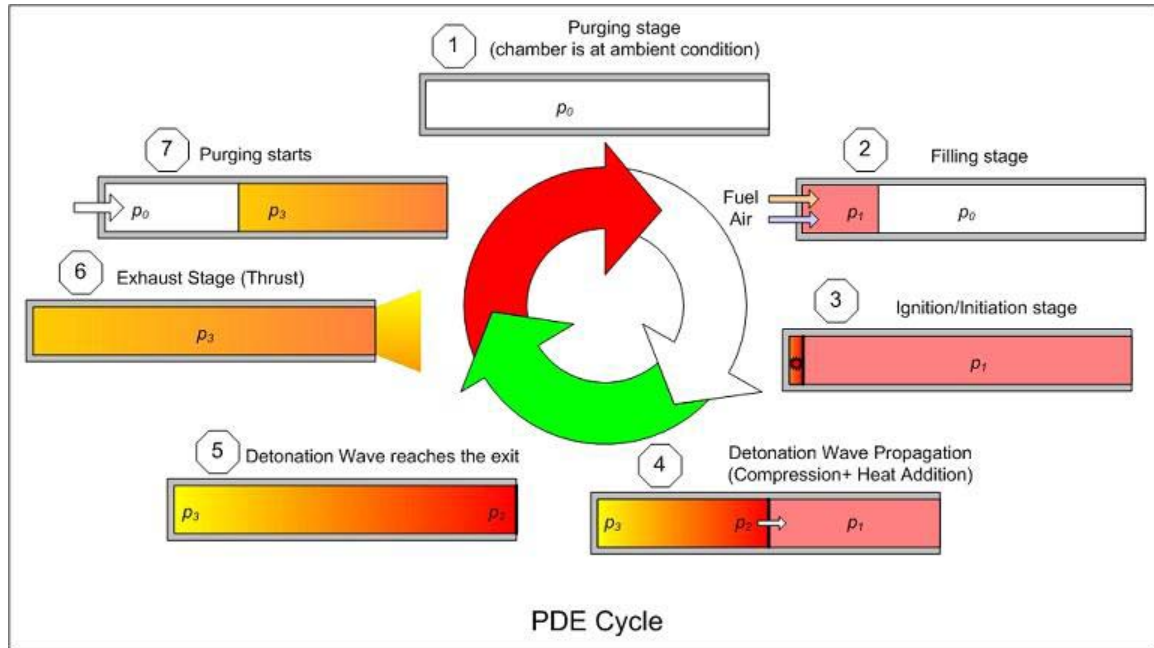


**Figure 2.6 PDE cycle stages**

station one in the diagram, the detonation chamber is at ambient conditions. The fill phase is shown at station 2 as a valve that seals one end of the detonation chamber opens, permitting the fuel/air mixture into the chamber. The volume of the fuel/air mixture at ambient conditions to the tube volume is the fill fraction ( $ff$ ). This is one of the variables analyzed in this research to determine engine performance over a range of values.

After the fuel/air mixture enters the chamber, the valve closes and a detonation wave is initiated near the closed end of the chamber as shown at station 3 of the figure. At the onset of this stage, a spark plug deposits a spark that causes a deflagration wave to

form at the end of the tube. The deflagration wave propagates through the tube and transitions to a detonation wave before reaching the open end of the tube. This transition is known as the deflagration to detonation transition (DDT), and the time elapsed between the formation of the deflagration wave and detonation wave is known as the DDT transition time. The detonation wave then propagates to the tube exit at the Chapman-Jouguet condition. As shown by station 4 in Fig. 2.6, the region ahead of the detonation wave contains the unburned gas at state one. The burned gas at state 2 just behind the wave is at a significantly higher pressure and temperature than state one; however, the burned gas at state 3 near the closed end of the chamber will have a lower temperature and pressure than the gas at state 2 with an intermediate condition existing between states 2 and 3.

Upon reaching the end of the tube, the detonation wave exits, producing the thrust of the engine. The purge phase begins as a pressure differential in the tube creates rarefaction waves which propagate into the tube and expel the burned gases. Pressure and temperature in the chamber eventually decay to ambient levels and the exhaust velocity goes to zero. The detonation tube can then be filled with a new fuel/air mixture to begin the cycle once again.

### **Prior Work on Hybrid-Pulse Detonation Engines**

A significant amount of research, both experimental and analytical, has been done on integrating a pulsed detonation combustor into a turbine system with the hopes of increasing thrust and decreasing fuel consumption of an aircraft engine. Petters and

Felder (Petters and Felder, 2002:4) and Andrus (Andrus, 2007:81) demonstrated that, in theory, a pulsed detonation hybrid engine can reduce TSFC by 8 to 10% at design conditions. GE Global Research (Rasheed et al., 2005) built and evaluated an eight tube PDC integrated with a single-stage axial turbine. Results indicated the ability to produce detonations at 10 and 20 Hz conditions showing promise for operability over a wide range of conditions. Noise signatures and internal structural damage due to the cyclic pulsations of the detonations are a cause for concern in implementing a PDC into a turbine system. Caldwell and Gutmark (Caldwell and Gutmark, 2008:1) performed experimental studies to ascertain the flow field and suggest that shock reflection and blowdown jet interaction length and time scales could minimize noise and structural damage. During Schauer et al. (Schauer et al., 2003:1) testing of a PDE into a radial turbine, the turbine withstood all detonations into the inlet, as well as significantly weakened the strength of the detonation shocks in the exhaust nozzle. This experimental work (Rasheed et al., 2005) (Caldwell and Gutmark, 2008) (Schauer et al., 2003) among others prove that after overcoming a few hurdles, these engines can become a reality.

Though much work has been performed on hybrid-PDEs at design conditions, hardly any off-design analysis, either experimentally or analytically, has been accomplished. Off-design analysis determines the performance of an engine at a given set of conditions for a fixed geometry determined from a design operating point. Glaser et al. (Glaser et al., 2004:1) experimentally investigated the off-design performance of a pulsed detonation engine by varying the equivalence ratio and fill fraction parameters. Their PDE system utilized a single stainless steel PDE tube 1" in diameter and 24" in length. A

fuel/oxidizer mixture of ethylene and oxygen was injected into the tube via a controlled solenoid valve. A relationship between the wave speed and the equivalence ratio was found and is shown in Fig. 2.7.

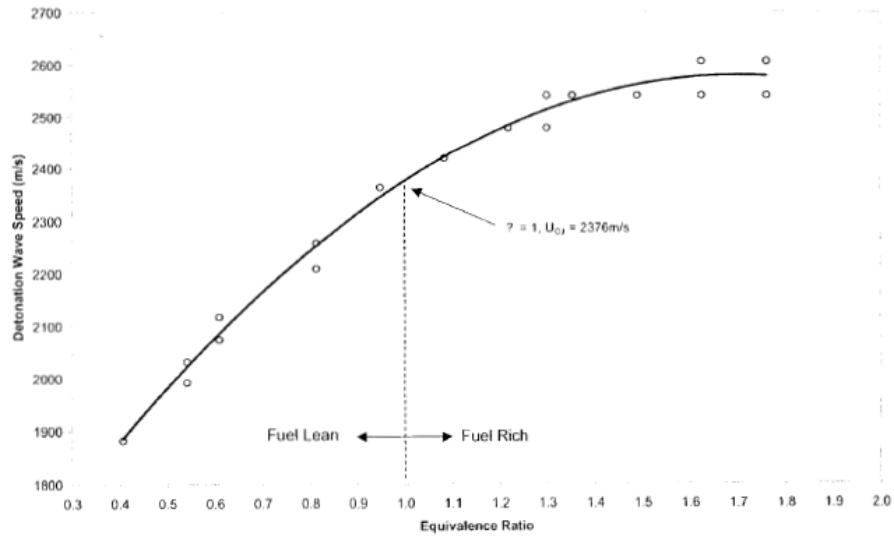


**Figure 2.7 Relationship between equivalence ratio and detonation wave speed (Glaser et al., 2004:6)**

As can be seen from the plot, the wave speed increases with equivalence ratio before leveling out at a maximum equivalence ratio of 1.7 and wave speed of 2583 m/s. The effect of fill fraction on wave speed was also determined. These results can be seen in Fig. 2.8.



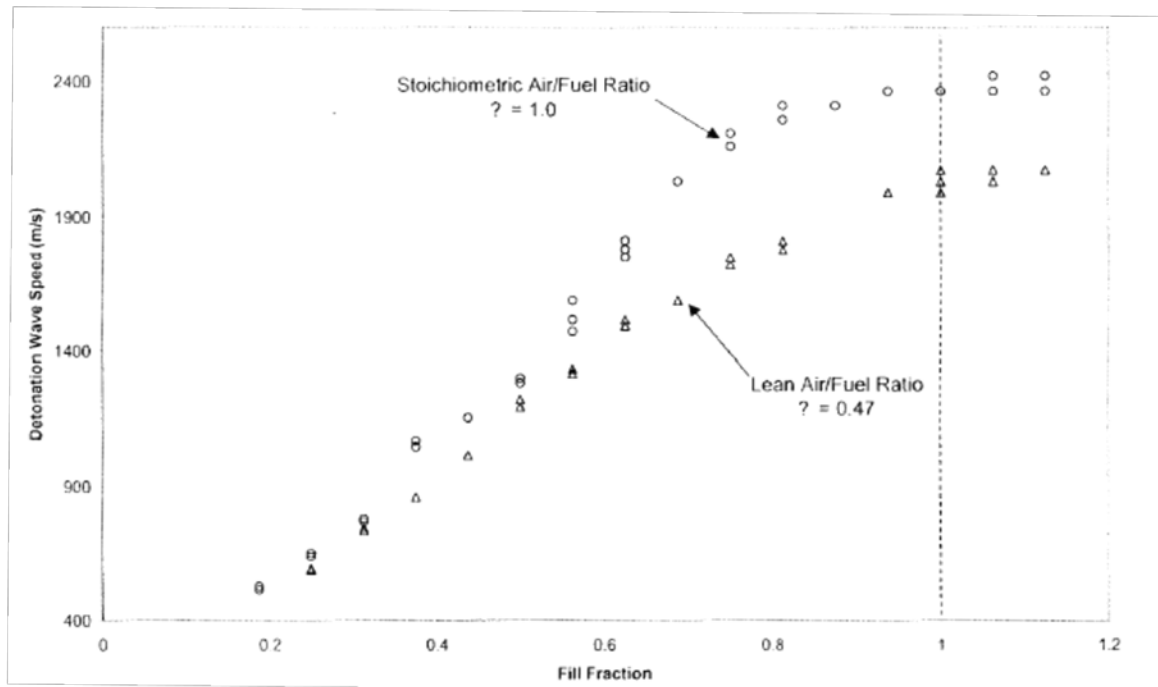


**Figure 2.8 Relationship between fill fraction and detonation wave speed (Glaser et al., 2004:7)**

Two different air/fuel ratios were investigated, with the two mixtures diverging at a fill fraction of approximately 0.6 before leveling off at a fill fraction of about 1.0. These results indicate that performance gains may be made at an equivalence ratio greater than one and a completely filled detonation tube. Although these tests were not performed on a hybrid-PDE, they indicate favorable results for pulsed detonation off-design studies, thus furthering the need for hybrid-PDE off-design research.

Chapter three will describe the baseline and hybrid-PDE models in AEDsys and NPSS and detail how the pulsed detonation thermodynamics are incorporated into the hybrid combustor section to solve for the hybrid engine performance.

### **III. Baseline and Hybrid Models**

#### **Introduction**

To ensure the accuracy of the baseline model in NPSS, it was compared to the same baseline model in AEDsys (Mattingly et al., 2002) at the design point. The baseline turbofan models were run in off-design mode in both the AEDsys and NPSS programs and the results compared. The hybrid turbofan model was developed and run off-design and its performance compared to that of the baseline model off-design. This chapter describes the baseline and hybrid models, including the changes made to the hybrid model to perform an off-design analysis.

#### **Baseline High Bypass Turbofan Engine in AEDsys and NPSS**

The modeled engine is based on the parameters of the TF-39-GE-1C engine used on the C-5 Galaxy, as this engine has known operating parameters and is relevant to the Air Force. The component efficiencies were unknown, however, and were selected to correspond to a technology level projected ten to twenty years in the future. The efficiencies can be found in Mattingly's Table 4.4 (Mattingly et al., 2002:107) under level 4 technology. Table 3.1 shows the parameters for the TF-39-GE-1C engine as compared with the notional baseline of the engine modeled.

**Table 3.1 Parameters for baseline engine**

Engine	TF39-GE-1C	Baseline Model
Aircraft	C-5	N/A
Mach number	0.0	0.0
Altitude (ft)	0.0	0.0
Fn (lbf)	40805	41500
Weight (lb)	7186	N/A
Length (in)	100	N/A
Max Diam (in)	203	N/A
BPR	8	8
FPR	1.56	1.56
OPR	26	26
TSFC (1/h)	0.315	0.325
Mass flow (lbm/s)	1549	1500
Max TIT (R)	2810	2900

Some of the baseline parameters are slightly different than those for the TF39-GE-1C engine and were chosen for simplicity.

The baseline engine coded in NPSS utilizes the architecture of a high bypass split stream turbofan as described by Mattingly (Mattingly et al., 2002:569-587). The model reference stations and NPSS configuration are shown in Fig. 3.1.

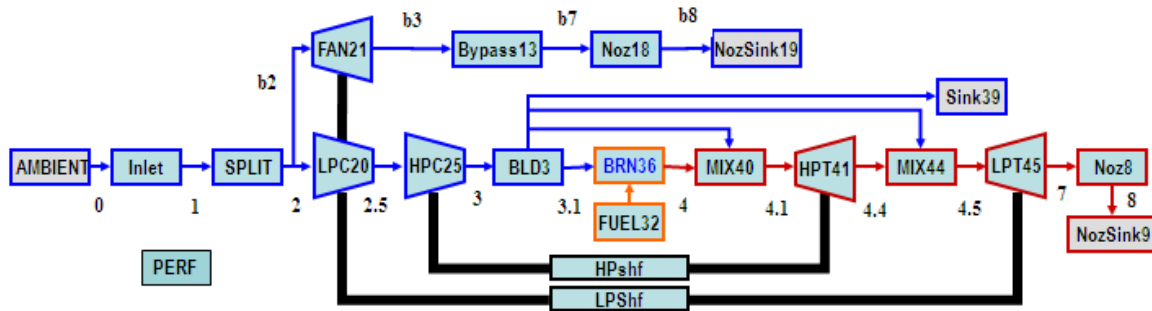


**Figure 3.1 Baseline NPSS high bypass turbofan engine configuration with reference stations**

In Fig. 3.1, the core and bypass flows split at the fan entry and two mixers are employed, one at the burner exit to combine the fluid exiting the burner with bleed flow (MIX40) and another at the high pressure turbine exit to combine the fluid exiting the turbine with bleed flow (MIX44). The bleeds are 5.0%, which is the default value in AEDsys. The model file that defines the baseline NPSS engine is found in Appendix B.

The engine was also modeled in AEDsys in order to compare results to the NPSS model and ensure its accuracy. Table 3.2 shows the input variables for the AEDsys baseline turbofan engine.

**Table 3.2 AEDsys baseline turbofan engine input parameters**

Input Variables	Value
Mach Number	0.0
Altitude	0.0 ft
Temperature	518.67 R
Pressure	14.696 psia
Mass Flow	1500 lbm/s
Tt4	2900 R
Compr Press Ratio	26
LPC PR	1.56
Fan PR	1.56
Bypass Ratio	8
Fuel Heating Value	18400 BTU/lbm
Cp Compressor	0.2415 BTU/lbm R
gamma c	1.3986
Cp Turbine	1.2957
Bleed Air	1%
Coolant Air	5%
Coolant Air 2	5%
Diffuser Max Press Ratio	0.995
Burner Press Ratio	0.96
Nozzle Press Ratio	0.985
Fan Press Ratio	0.98
Fan Polytropic Eff	0.89
LPC Polytropic Eff	0.89
HPC Polytropic Eff	0.90
HPT Polytropic Eff	0.89
LPT Polytropic Eff	0.89
Burner Eff	0.995
Mech Shaft LP Spool Eff	0.99
Mech Shaft HP Spool Eff	0.99
Max Tt4	3200 R
Max Comp Press Ratio	32
Max Press at station 3	650 psia
Max Temp at station 3	1860 R
Max % Ref RPM - LP Spool	110
Max % Ref RPM - HP Spool	110

All parameters in Table 3.2 are also input into NPSS with the exception of the polytropic efficiencies. NPSS requires adiabatic efficiency inputs for turbines and compressors as compared to the AEDsys requirement for polytropic efficiency inputs. The two efficiencies are related by Eqs. 3.1 and 3.2 (Oates, 1997: 214 & 222):

$$\eta_c = \frac{\pi_c^{(\gamma_c-1)/\gamma_c} - 1}{\pi_c^{(\gamma_c-1)/\gamma_c e_c} - 1} \quad (3.1)$$

$$\eta_t = \frac{1 - \pi_t^{e_t(\gamma_t-1)/\gamma_t}}{1 - \pi_t^{(\gamma_t-1)/\gamma_t}} \quad (3.2)$$

These relationships are used to calculate the adiabatic efficiencies used in the baseline NPSS model listed in Table 3.3.

**Table 3.3 Baseline model NPSS adiabatic efficiency inputs**

NPSS efficiency inputs	Value
Fan adiabatic eff	0.8827
LPC adiabatic eff	0.8827
HPC adiabatic eff	0.8573
HPT adiabatic eff	0.9057
LPT adiabatic eff	0.9084

The other difference between the AEDsys and NPSS programs is the thermodynamic model. The AEDsys thermodynamic package is a subroutine termed FAIR. FAIR is an 8<sup>th</sup> order polynomial fit to JANAF specific heat data for pure air, and CEA data for vitiated air (Mattingly et al., 2002: 89-91). NPSS however, gives the user control over the thermodynamic quantities by offering a choice of six different thermodynamic packages. Table 3.4 lists the available models and provides a description of each. The NPSS data in this thesis was generated using the GasTbl thermodynamics

package as it is the simplest to implement in NPSS and a close match to the AEDsys thermodynamic package. However, the GasTbl package is limited to results whose equivalence ratio is less than one; therefore, solutions with equivalence ratios greater than one could not be investigated.

**Table 3.4 NPSS Thermodynamics Packages**

Package	Description
CEA	Implementation of NASA chemical equilibrium code
Janaf	Implementation of NIST gas properties prepared by Honeywell
GasTbl	Package developed by Pratt & Whitney based on Therm, but adding humidity calculations and some chemical
AllFuel	Package developed by General Electric that contains gas properties and fuel properties
INGTherm	Package used to calculate the properties of ideal gases, contains only properties for Helium and Zenon at present
FPT	Package used to define NPSS table and/or functions that describe the thermodynamic properties of the fluid

The differences in the thermodynamics packages account for a 1.0% difference in net thrust and 0.8% difference in TSFC at SLS of the baseline engine in NPSS and AEDsys at the design point. Andrus (Andrus, 2007:23) provides a complete explanation on how the thermodynamics packages differ and how they contribute to these differences.

## Hybrid Turbofan Engine and Pulsed Detonation Combustor in NPSS

The hybrid-PDE model contains the identical architecture of the baseline turbofan model shown in Fig. 3.1, with the exception of the burner section which is replaced by a pulsed detonation combustor (PDC). The NPSS Model code for the hybrid turbofan engine can be found in Appendix C.

The hybrid engine and PDC inputs are listed in Table 3.5.

**Table 3.5 Hybrid engine on-design configuration**

Input Variables	Value
Mass Flow	1500 lbm/s
Tt4	2900 R
Compr Press Ratio	26
LPC PR	1.56
Fan PR	1.56
Bypass Ratio	8
Tube Inner Diameter	2.1 in
Tube Length	36 in
Number of Tubes	24 in
ARvalve	0.7
Mvalve	0.8
Equivalence Ratio	0.9012
Frequency	64.906 Hz
Purge Fraction	0.5
Fuel Heating Value	18400 BTU/lbm
Cp Compressor	0.2415 BTU/lbm R
gamma c	1.3986
Cp Turbine	1.2957
Bleed Air	1%
Coolant Air	5%
Coolant Air 2	5%
Diffuser Max Press Ratio	0.995
Burner Press Ratio	0.96
Nozzle Press Ratio	0.985
Fan Press Ratio	0.98
Fan Adiabatic Eff	0.8827
LPC Adiabatic Eff	0.8827
HPC Adiabatic Eff	0.8573
HPT Adiabatic Eff	0.9057
LPT Adiabatic Eff	0.9084
Burner Eff	0.995
Mech Shaft LP Spool Eff	0.99
Mech Shaft HP Spool Eff	0.99
Max Tt4	3200 R
Max Comp Press Ratio	32
Max Press at station 3	650 psia
Max Temp at station 3	1860 R
Max % Ref RPM - LP Spool	110
Max % Ref RPM - HP Spool	110

The inputs in Table 3.5 are identical to those of the baseline engine in NPSS, with the exception of the new parameters added for the PDC section: tube dimensions, number of tubes,  $AR_{\text{valve}}$ ,  $M_{\text{valve}}$ , equivalence ratio, frequency, and purge fraction.  $AR_{\text{valve}}$  is the ratio of the inlet valve cross-sectional area to the detonation tube cross-sectional area and  $M_{\text{valve}}$  is the Mach number into the valve. The values of these parameters are the results of a parametric study performed for optimal engine performance at SLS. Altitude, Mach number, and fill fraction are the parameters varied to analyze the hybrid engine performance off-design. The NPSS PDC burner element (BRN36) configuration is shown in Fig. 3.2.

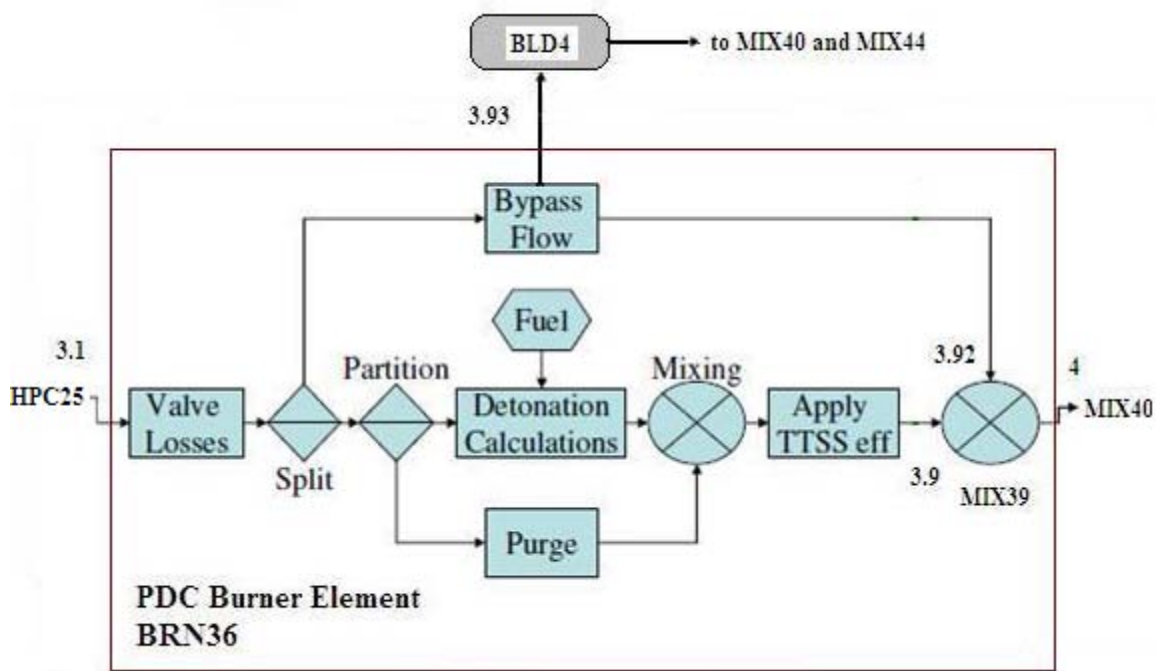


**Figure 3.2 Pulsed Detonation Combustor (BRN36) configuration with station numbers**



Flow leaves the high pressure compressor and enters the pulsed detonation combustor. The flow control at the detonation tube inlet is modeled as a pressure loss  $\Delta P/P$  term between the inlet and detonation tubes. This pressure loss matches the dry-duct pressure loss experienced by the conventional combustor. For the flow going into the tubes, this dry duct pressure loss is intended to represent pressure loss through a valve. Since the detonation engine operates at a higher equivalence ratio than conventional engines, it requires less air to mix with the fuel for a similar enthalpy generation. Balancing the mass flow through the tubes necessitates shunting some of the air around the detonation tubes through an internal bypass. The mass flow rate through the internal bypass ( $\dot{m}_{iBP}$ ) is defined as:

$$\dot{m}_{iBP} = \dot{m}_{core\_air} - \dot{m}_{tube\_air} \quad (3.2)$$

where  $\dot{m}_{core\_air}$  is the combined mass flow rate entering the PDC before it is split. The internal bypass ratio (iBPR) equals:

$$iBPR = \frac{\dot{m}_{iBP}}{\dot{m}_{tube\_air}} \quad (3.3)$$

In order to determine the mass flow rate into the detonation tubes ( $\dot{m}_{tube\_air}$ ), the fill fraction ( $ff$ ) and purge fraction ( $pf$ ) must first be defined. The fill air is the air mixed with the fuel, while the purge air is the unmixed portion. The purge air is used to expel the burned gases and also serves to cool the detonation tubes between cycles. The fill and purge fractions are defined in terms of volume of air for their respective portions of the tube filling process:

$$ff = \frac{V_{fuel-air\_mix}}{A_{tube} * l_{tube}} \quad (3.4)$$

$$pf = \frac{V_{purge\_air}}{A_{tube} * l_{tube}} \quad (3.5)$$

Since the air is stopped in the tube when the valve is closed, total density ( $\rho_t$ ) can be found. The purge and fuel-air masses are calculated by multiplying the total density by the tube volume and the purge fraction and fill fractions, respectively:

$$m_{purge\_air} = pf \cdot V_{tube} \cdot \rho_t \quad (3.6)$$

$$m_{fuel-air\_mix} = ff \cdot V_{tube} \cdot \rho_t \quad (3.7)$$

where  $V_{tube} = A_{tube} * l_{tube}$ .

Equations 3.6 and 3.7 represent the amount of purge air and fuel-air mixture that flow into one tube during each cycle. The amount of air to send through the valve at the opening of the detonation tube is calculated in Eqs. 3.8 - 3.12:

$$m_{fuel-air\_mix} = m_{fill\_air} + m_{fuel} \quad (3.8)$$

$$\frac{m_{fuel-air\_mix}}{m_{fill\_air}} = \frac{m_{fill\_air}}{m_{fill\_air}} + \frac{m_{fuel}}{m_{fill\_air}} \quad (3.9)$$

$$\frac{m_{fuel-air\_mix}}{m_{fill-air}} = 1 + FAR \quad (3.10)$$

$$m_{fill\_air} = \frac{m_{fuel-air\_mix}}{1 + FAR} \quad (3.11)$$

$$m_{fill\_air} = \frac{ff * V_{tube} * \rho_t}{1 + FAR} \quad (3.12)$$

where  $m_{\text{fill air}}$  is the mass of the air that is detonated and  $m_{\text{fuel}}$  is the fuel used during one cycle. Once the mass of air flowing into the tubes during one cycle is known, the time averaged steady state mass flow rate into the detonation tubes ( $\dot{m}_{\text{tubes\_air}}$ ) is calculated by multiplying the total mass of air into the tubes by the user inputs of frequency ( $f$ ) and the number of tubes ( $n_{\text{tubes}}$ ):

$$\dot{m}_{\text{tubes\_air}} = (m_{\text{fill\_air}} + m_{\text{pulse\_air}}) * f * n_{\text{tubes}} \quad (3.13)$$

The thermodynamics within the pulsed detonation combustor are modeled after the work of Heiser and Pratt (Heiser and Pratt, 2002:1) with a Dyer and Kaemming correction (Dyer and Kaemming, 2002:1) to more accurately conserve system energy. To calculate the detonation properties at the tube exit, implementation into NPSS required a few modifications to Equations 2.7 and 2.8. The quantity  $\left(\frac{\dot{q}}{\psi}\right)$  as defined by Eqs. 2.11 and 2.12 is rearranged as:

$$\left(\frac{\dot{q}}{\psi}\right) = \frac{h_4 - h_3}{C_p T_3} \quad (3.14)$$

This allows for burner inlet and exit enthalpies, specific heat, and inlet engine temperature parameters to be used to solve for the Chapman-Jouguet Mach number, Eq. 2.8, and entropy gain across the burner, Eq. 2.9. The pressure rise across the shock is then calculated as:

$$\frac{p_4}{p_0} = \frac{1 + \gamma M_{\text{CJ}}^2}{\gamma + 1} \frac{p_3}{p_0} \geq 1 \quad (3.15)$$

Having solved for the pressure and entropy at the detonation tube exit, all properties of the fluid at this point (station 4) are solved for through thermodynamic relationships. However, as mentioned in the previous chapter, instead of using the pressure and entropy at the detonation tube exit to solve for all the properties of the fluid at this point, which ignores the eventual pressure loss that the gas will go through due to expansion waves, entropy and the change in enthalpy liberated by the combustion process are used to solve for the properties at the detonation tube exit. Available energy is calculated using the known CJ entropy originally calculated by Heiser and Pratt (Heiser and Pratt, 2002:1), Eq. 2.9, with the known system enthalpy of ( $h_0 + q_{add}$ ) in order to ensure that energy is conserved within the system. The NPSS PDC burner element code is found in Appendix D.

Rasheed et al. (Rasheed et al., 2006) showed that exhausting a pulsed detonation combustor directly into a turbine lowers the turbine efficiency and has structural ramifications affecting the engine life. The hybrid model is based on the assumption that the flow into the turbine is steady flow. A subelement to the PDC was created that allows for the application of a pressure drop and enthalpy loss, however, no such loss is applied in this model.

### **Hybrid Turbofan Engine Off-Design**

Fill fraction is the primary method of thrust control as prior work on PDEs indicated that performance gains may be made at fill fractions other than one (Glaser et al., 2004:1). Frequency and equivalence ratio can also be used as variables to throttle the

engine as shown by the work of Schauer et al.(Schauer et al., 2001:6) and Hoke et al. (Hoke et al., 2005:2). Frequency is chosen to be a user input and constant throughout flight, whereas for the hybrid engine to operate at altitudes above 13,000 ft, the equivalence ratio has to be varied to gain the maximum thrust at a given Mach number and altitude. Therefore, the equivalence ratio is adjusted at each operating condition to yield maximum thrust. The engine constraints are shown at the bottom of Table 3.2 and controls were implemented into the solver to ensure the model stayed within these constraints.

When running the NPSS solver off-design, an error was given for the constant area mixer, MIX39, which combines the flow coming out of the detonation tubes with the internal bypass flow of the PDC. In design mode, the user provides a Mach number for the tube flow into the mixer, which determines the primary entrance area of the mixer. The area of the internal bypass flow entering the mixer is determined by varying the area until the static pressure of the two streams equal. This conserves energy, continuity, and momentum when mixing the flows exiting the tubes and the internal bypass flow into one.

Running the model in off-design mode at various fill fractions, Mach numbers, and altitudes, however, yielded a static pressure difference between the two flows when entering MIX39. As the fill fraction decreases from the design fill fraction, the mass of the fill air decreases, thus there is less mass flow entering the tubes and more flow entering the internal bypass as shown in Eqs. 3.13 and 3.2, respectively:

$$\dot{m}_{tube\_air} = (m_{fill\_air} + m_{purge\_air}) * f * n_{tubes} \quad (3.13)$$

$$\dot{m}_{iBP} = \dot{m}_{core\_air} - \dot{m}_{tube\_air} \quad (3.2)$$

As the mass flow of the internal bypass increases, the static pressure ( $p$ ) decreases for a fixed area. The internal bypass flow behaves as pipe flow, and as mass flow increases, velocity increases (assuming incompressible flow), Eq. 3.16, and thus the static pressure must decrease to maintain a constant total pressure ( $p_t$ ) shown in Eq. 3.17:

$$\dot{m} = \rho AV \quad (3.16)$$

$$\frac{1}{2} \rho V^2 + p = p_t = const \quad (3.17)$$

This yields a lower static pressure entering the mixer from the internal bypass than from the detonation tubes. The NPSS MIX39 requires that the incoming streams have equal static pressures in order to mix. To converge to a solution off-design, the static pressure of the internal bypass flow entering the mixer must be increased to match the static pressure of the flow coming out of the detonation tubes into the mixer. This is accomplished by decreasing the mass flow of the internal bypass, as mass flow and static pressure have an inverse relationship as seen from Eqs. 3.16 and 3.17. To decrease the mass flow of the internal bypass, a bleed was implemented, shown in Fig. 3.2 as BLD4, in which the mass flow is bled from the internal bypass until the static pressure of the two streams entering MIX39 match. The bleed flow then enters back into MIX40 and MIX44 on either side of the low pressure turbine. The flow is equally divided into MIX40 and MIX44 and does not present a static pressure error. MIX39 caused an NPSS convergence error because there is an unequal amount of independent (9) and dependent variables

(10). The internal bleed is added as an independent variable to be varied until the static pressure of the two flows entering the mixer equal.

MIX39 allows for the flow exiting the PDC to cool to below the temperature constraint before entering the turbine, however, it has the potential to be the source of a significant pressure loss. No pressure loss term is applied to the mixer in this model, but the possibility of such a loss is recognized.

The next chapter utilizes this PDC combustor configuration to analyze the hybrid turbofan performance at off-design conditions as compared to the conventional baseline model.

## **IV. Analysis and Results**

### **Introduction**

This chapter contains the performance of the baseline turbofan evaluated at off-design conditions in AEDsys and NPSS and an off-design analysis of the hybrid turbofan modeled in NPSS. The baseline turbofan is evaluated in two programs to establish a foundation for comparing the engine off-design.

### **Baseline Turbofan Off-Design Performance**

The on-design baseline model yields a thrust variation of approximately 1.0% and thrust specific fuel consumption (TSFC) variation of approximately 0.8% between AEDsys and NPSS. This deviation is due to differences in the thermodynamic models of the two programs in specific heat and enthalpy. The baseline turbofan model is run off-design in both AEDsys and NPSS. Throttle hooks are shown in Fig. 4.1 across six different Mach number and altitude levels. The throttle hooks are generated by varying the fuel-air ratio (FAR) to match a selected a thrust value, which is then plotted against the corresponding TSFC. As seen in the figure, the two programs display agreement at the design point; however, the solutions diverge at higher Mach numbers and altitudes. This divergence is due to differences in off-design component efficiencies. The AEDsys program component adiabatic efficiencies do not change from their on-design values, whereas the NPSS program utilizes component maps for off-design performance. Variation in efficiencies for NPSS at off-design conditions is shown in Figs. 4.2 and 4.3.



The baseline turbofan is run at maximum thrust at maximum  $T_{t4}$  at SLS, and at maximum  $\pi_c$  at all other altitudes. The AEDsys low pressure and high pressure spool efficiencies remain constant at 0.99 as expected. The NPSS low pressure compressor and turbine and high pressure compressor efficiencies change as  $N_c/(N_c \text{ design})$  increases. The high pressure turbine efficiency remains constant; however, the fan efficiency experiences a severe drop as it moves away from the design speed. The variations for the NPSS efficiencies are expected and may account for the differences in the throttle hook results between AEDsys and NPSS.

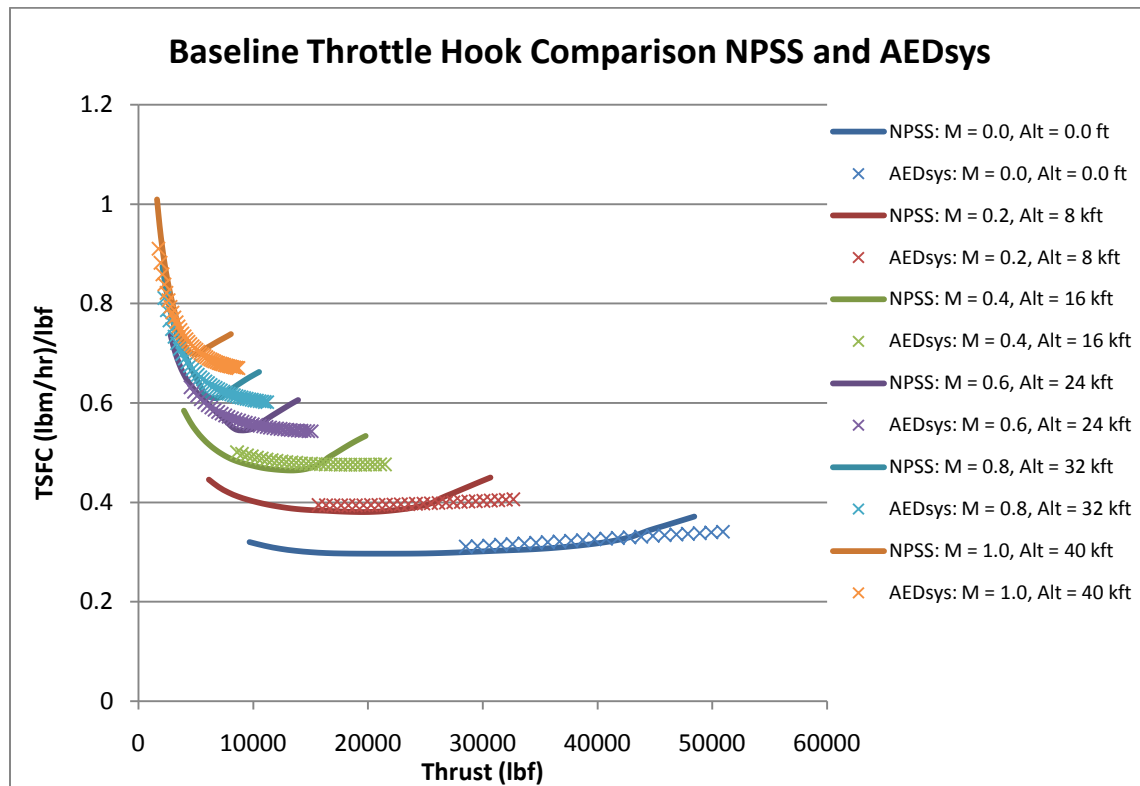


**Figure 4.1 Throttle hook baseline engine comparison using NPSS and AEDsys**

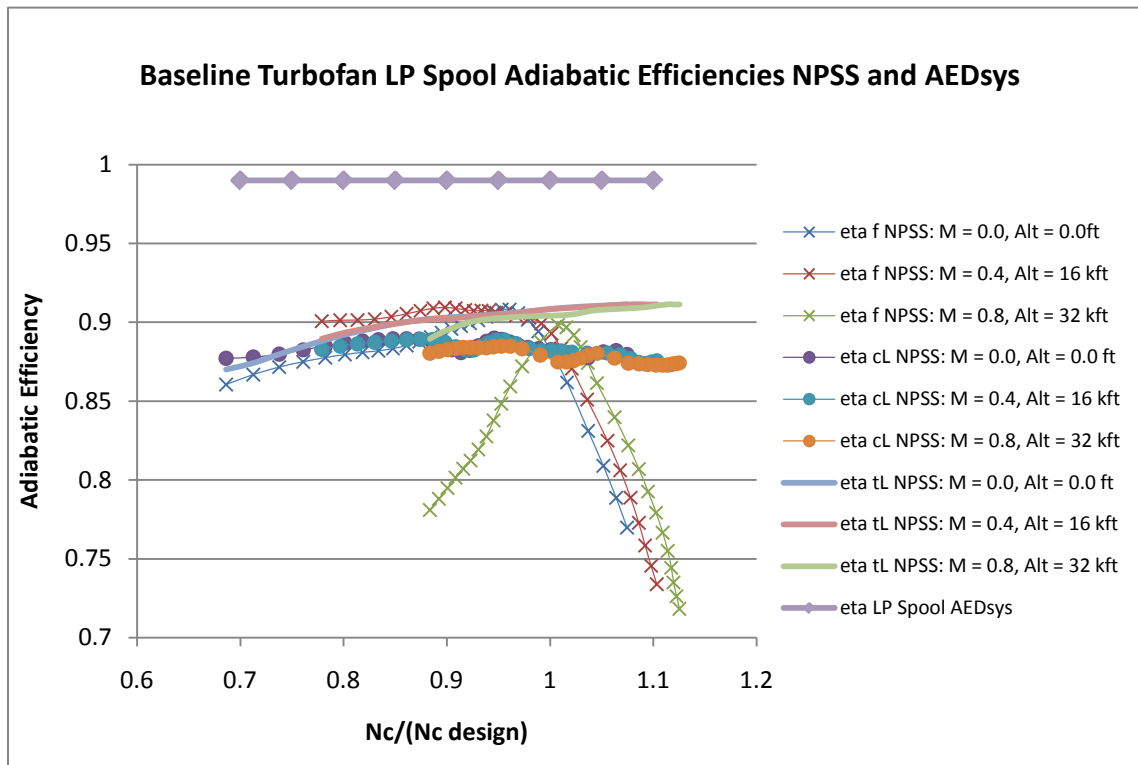


Figure 4.2 Low pressure spool adiabatic efficiencies for NPSS and AEDsys off-design

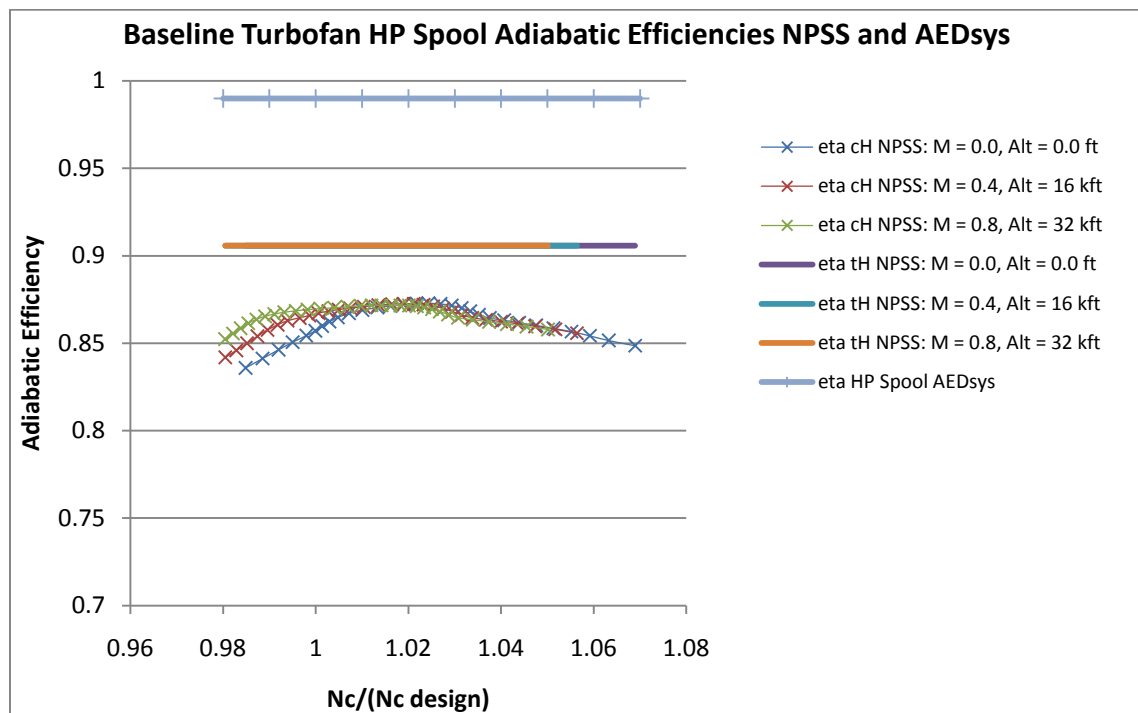


Figure 4.3 High pressure spool adiabatic efficiencies for NPSS and AEDsys off-design

## Hybrid Turbofan Off-Design Results

The hybrid turbofan model is evaluated off-design over a range of Mach numbers, altitudes, and fill fractions to determine the effects on engine performance. Engine constraints are placed in NPSS to ensure that the model does not violate the maximum engine control values of  $T_{t4}$ ,  $\pi_c$ ,  $P_{t3}$  and  $T_{t3}$ , and  $N_c/(N_c \text{ design})$  as listed as the bottom of Table 3.2.

## Code Verification and Operating Limit

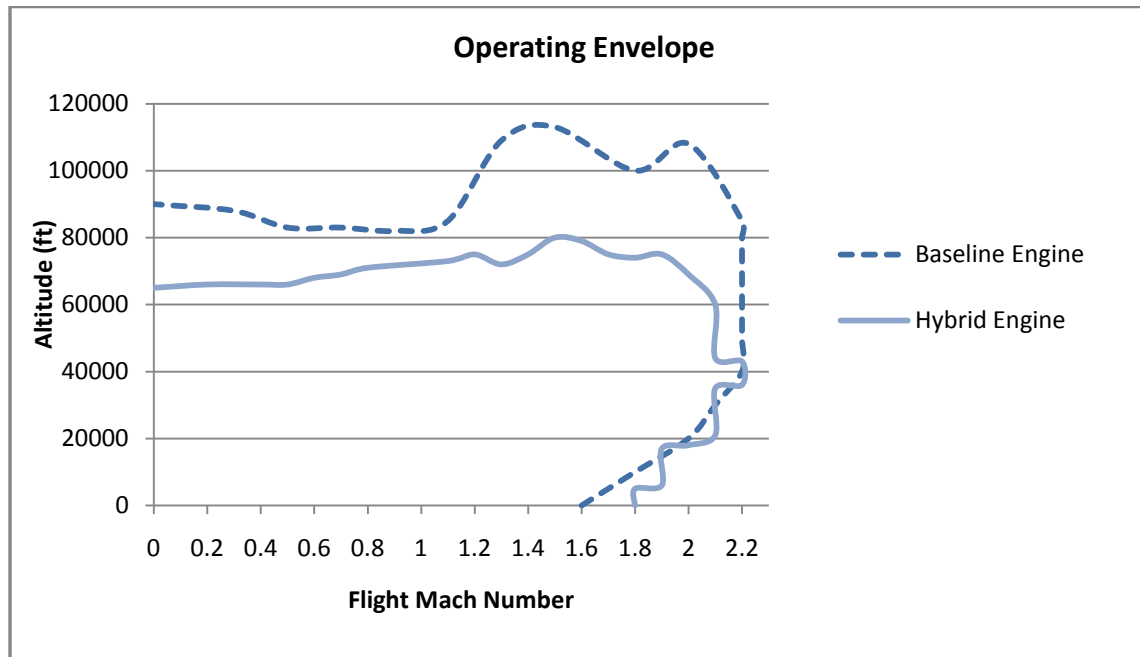
The hybrid engine is run in NPSS at the design point in off-design mode to validate the off-design code for the engine. Table 4.1 shows the engine data at the design point in both design and off-design mode. The data is very similar with a TSFC and thrust variation of 0.26% and 0.01%, respectively.

The engine operating envelope is found for both the baseline and hybrid engines in NPSS and shown in Fig. 4.4. The envelope is attained by running the model at sea level at increasing flight Mach numbers until NPSS no longer converges to a solution. The far right boundary is obtained by gradually increasing the flight altitude at the maximum Mach number. The top boundary is found via a similar method. The models are run off-design at maximum thrust and a fill fraction of 1.0 using the on-design parameters shown in Table 3.5 with the exception of the equivalence ratio. The design equivalence ratio only allows the hybrid engine to operate at a maximum of 13,000 ft. To obtain maximum performance, the equivalence ratio is varied to yield the maximum thrust at the flight Mach number and altitude. This is accomplished in NPSS by varying

the FAR, which is a user input, to yield the maximum thrust at a particular flight condition. Thus, the equivalence ratio varies along the operating limit line ranging from a minimum of 0.79 at  $M = 1.7$  and  $Alt = 75,000$  ft to a maximum of 0.93 at  $M = 1.8$  and  $Alt = 0.0$  ft. The baseline engine has a higher altitude limit of 113,000 ft as compared to that of the hybrid engine with a maximum of 80,000 ft. Both models have the same Mach number limit of 2.2.

**Table 4.1 Hybrid engine test data showing the design point and the design point run at off-design using NPSS**

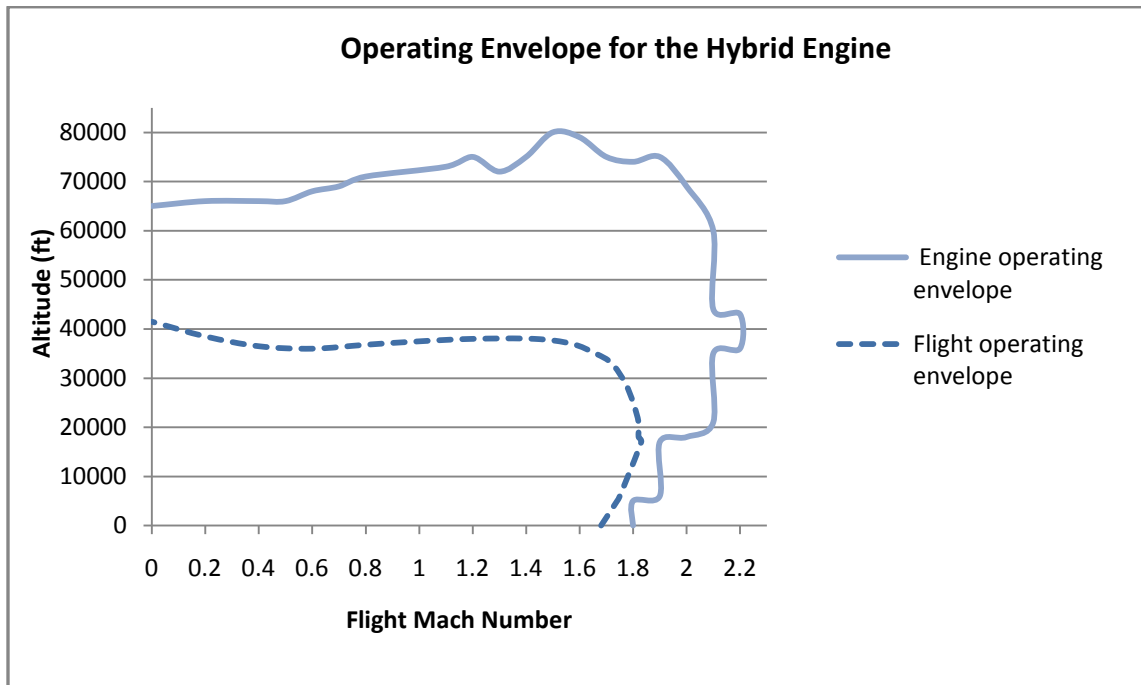
NCP NPSS_1.6.5 - Rev: -- model: PDC HBTF			
run by: Caitlin	solutionMode= STEADY_STATE	converge= 1	
case: 2	time: 0.000	timeStep=0.0500	therm_package=GasTb1
iter/pas/Jac/Broy= 4/ 4/ 0/ 2	run: 12/08/09 13:10:32		
Design Values			
Pidmax= 0.99500	Pi b = 1.46943	Eta b = 0.99500	Pi n = 0.98500
Eta f = 0.88270	Eta cL = 0.88270	Eta CH = 0.85730	Eta tH = 0.90570
e f = 0.89210	e cL = 0.89210	e CH = 0.89982	e tH = 0.89259
gam2 = 1.39978	gam25 = 1.39963	gam3 = 1.35506	gam4 = 1.27739
Eta mL = 0.99000	Eta MH = 0.9900	gam5 = 1.31906	
PTO L = 0.0kw	PTO H = 106.8kw	hPr = 18400	
Bleed = 1.00%	Cool 1 = 1.00%	Cool 2 = 1.00%	Pi nf = 0.98000
** Thrust scale DOES NOT APPLY...			
Converged? (0 - no, 1 - yes)			
	CASE 0: DESIGN	CASE 1: OFFDESIGN	
Mach Number at 0	0.0100	0.0100	
Temperature at 0	518.6700	518.6700	
Pressure at 0	14.6960	14.6960	
Altitude at 0	0.0000	0.0000	
Total Temp at 4	3648.0	3648.3	
Pi r	1.0001	1.0001	
/ Tau r	1.0000	1.0000	
Pi d	0.9950	0.9950	
/ Tau f	1.5600	1.5600	
Pi cL	1.534	1.534	
/ Tau cL	1.5600	1.5600	
Pi CH	16.6667	16.7164	
/ Tau CH	2.3730	2.3750	
Tau m1	0.9953	0.9968	
Pi tH	0.2842	0.2838	
/ Tau tH	0.7783	0.7780	
Tau m2	0.9964	0.9980	
Pi tL	0.2553	0.2553	
/ Tau tL	0.7503	0.7503	
LP Spool RPM (% reference pt)	100.000	99.987	
HP Spool RPM (% reference pt)	100.000	100.005	
Alpha	8.000	8.002	
Pt19/P19	1.5212	1.5212	
P0/P19	1.0000	1.0000	
Mach Number at 19	0.8003	0.8003	
Pt9/p9	1.8524	1.8524	
P0/p9	0.8664	0.8666	
Mach Number at 9	1.0000	1.0000	
Mass Flow Rate at 0	1500.0000	1499.9210	
Corr Mass Flow at 0	1499.9263	1499.8473	
Flow Area at 0 (ft2)	1757.3935	1757.3010	
Flow Area* at 0 (ft2)	30.3652	30.3636	
Flow Area at 8 and 18 (ft2)	22.7472	22.7472	
MB - Fuel/Air Ratio (f)	0.06161	0.06161	
Overall Fuel/Air Ratio (fo)	0.00301	0.00300	
Specific Thrust (F/m0)	32.1463	32.1439	
Thrust Spec Fuel Consumption (s)	0.3410	0.3401	
Thrust (Fn)	47699.0467	47692.9194	
Fuel Flow Rate (lbm/hr)	16264.8674	16220.1770	
Propulsive Efficiency (%)	2.0466	2.0465	
Thermal Efficiency (%)	40.2805	40.3875	
Overall Efficiency (%)	0.8244	0.8265	



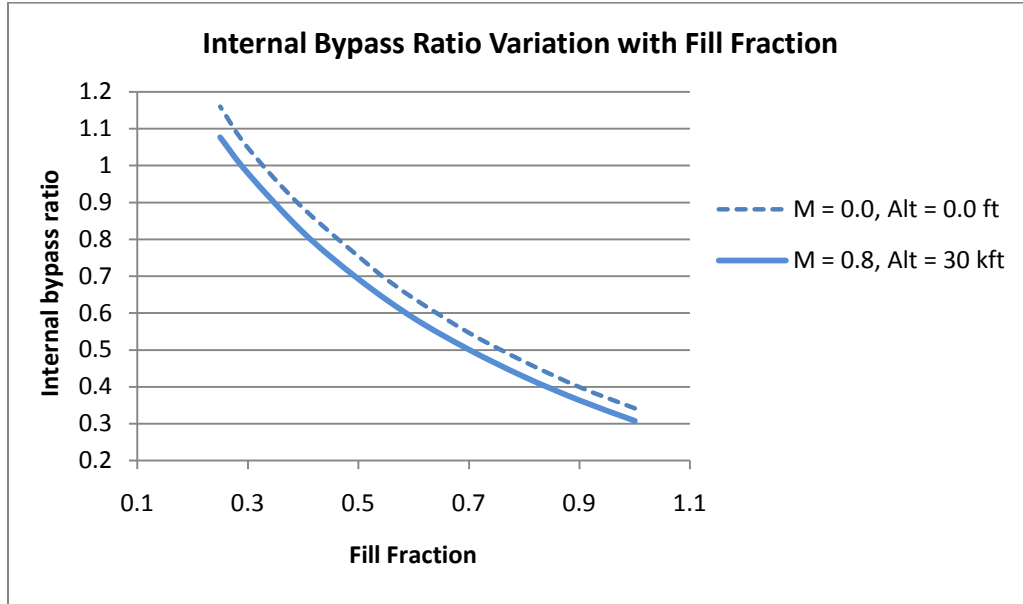
**Figure 4.4a Mach number and altitude operating envelope at maximum thrust, baseline and hybrid engine using NPSS**

Figure 4.4b shows the aircraft flight operating envelope as compared to the operating envelope of the engine. The flight operating envelope is estimated using a lift to drag ratio at cruise conditions on the order of 10 with each engine supporting 100,000 lbs of weight. This comes from an assumed thrust to weight ratio of 0.4 for a 40,000 lb engine. The flight envelope is much smaller than that of the engine, with a maximum altitude of 38,000 ft and a maximum Mach number of 1.83. The hybrid engine's flight altitude is constrained to lower than that of a conventional aircraft; however, it is still acceptable for flight. The lower altitude limit of the hybrid engine is due to the limitations of the internal bypass. The internal bypass ratio is on the order of 0.3 at a fill fraction on 1.0. This ratio increases as the fill fraction is throttled to lower values as seen in Fig. 4.4c. Figure 4.4c is generated by selecting the fill fraction and varying the FAR upward to

increase thrust. At the FAR for maximum thrust, any more increase in FAR results in non convergence in NPSS due to the internal bleed air equaling zero and the static pressure of the internal bypass flow entering MIX39 no longer equaling the static pressure of the flow exiting the detonation tubes.



**Figure 4.4b Mach number and altitude engine and flight operating envelope for the hybrid engine at maximum thrust using NPSS**



**Figure 4.4c Internal bypass ratio variation with fill fraction at SLS and cruise conditions at maximum thrust**

### Component Data

Component interface data for the baseline and hybrid engines at sea level static and cruise conditions are shown in Tables 4.2 and 4.3. The models are run at the configuration shown in Table 3.5 at maximum thrust and a fill fraction of 1.0. At SLS, the hybrid engine has a 12.7% greater thrust than the baseline engine, but at a cost of a 5.3% increase in TSFC. At cruise conditions of  $M = 0.8$  and  $Alt = 30,000$  ft, the hybrid engine has a thrust gain of 14.7% over the baseline and it also has a lower TSFC by 3.1%. These results are summarized in Table 4.3c and indicate that the hybrid engine could yield better performance than the baseline at cruise conditions.

**Table 4.2a NPSS component interface data for the baseline engine at SLS, maximum thrust**

*****														
NCP	NPSS_1.6.5 - Rev: --		model:Baseline HBTF >		run by: Caitlin		solutionMode= STEADY_STATE		converge= 1		case: 0			
time: 0.000	timeStep:0.0500		therm_package:GasTb1		Mode: DESIGN		iter/pas/Jac/Broy= 5/ 7/ 1/ 3		run: 01/07/10 11:28:56					
*****														
Summary Output Data														
MN	alt	dTs	W	Fg	Fn	TSFC	wfuel	WAR	OPR					
0.010	0.0	0.00	1500.0	42189.2	41668.8	0.3238	13491.12	0.0000	25.870					
INPUT FLOW														
FL0	INLET.F_I	W	gamt	Pt	Tt	Ps	Ts	MN	V	Aphy/144.	FAR	Rs	imp	
FL1	SPLIT.F_I	1500.00	1.39978	14.697	518.68	14.696	518.67	0.0100	11.16	1757.394	0.0000	0.06856	3719559.18	
FLb2	Fan21.F_I	1500.00	1.39978	14.623	518.68	12.329	493.97	0.5000	544.91	40.864	0.0000	0.06856	97950.38	
FLb3	Bypass13.F_I	1333.33	1.39978	14.623	518.68	12.329	493.97	0.5000	544.91	36.324	0.0000	0.06856	87067.00	
FLb7	Noz18.F_I	1333.33	1.39963	22.812	598.26	19.286	569.80	0.5000	585.02	24.947	0.0000	0.06856	93528.29	
FLb8	NozSink19.F_I	1333.33	1.39963	22.812	598.26	19.286	569.80	0.5000	585.02	24.947	0.0000	0.06856	93528.29	
FL2	LPC20.F_I	1333.33	1.39963	22.356	598.26	14.696	530.38	0.8003	903.41	19.734	0.0000	0.06856	79200.91	
FL25	HPC25.F_I	166.67	1.39978	14.623	518.68	12.329	493.97	0.5000	544.91	4.540	0.0000	0.06856	10883.38	
FL3	BLD3.F_I	166.67	1.39963	22.812	598.26	19.286	569.80	0.5000	585.02	3.118	0.0000	0.06856	11691.04	
FL31	BRN36.F_I	166.67	1.35513	380.206	1419.66	357.634	1397.08	0.3015	543.78	0.444	0.0000	0.06856	25662.10	
FL41	HPT41.F_I	148.33	1.35513	380.206	1419.66	357.634	1397.08	0.3015	543.78	0.395	0.0000	0.06856	22839.27	
FL4	MIX40.F_I	152.08	1.28210	364.998	2900.00	0.000	0.00	0.0000	0.00	0.000	0.0253	0.00000	0.00	
FL41	HPT41.F_I	160.41	1.28490	364.998	2830.35	0.000	0.00	0.0000	0.00	0.000	0.0239	0.00000	0.00	
FL44	MIX44.F_I	160.41	1.30753	86.673	2112.70	0.000	0.00	0.0000	0.00	0.000	0.0239	0.00000	0.00	
FL45	LPT45.F_I	168.75	1.30942	86.673	2080.75	0.000	0.00	0.0000	0.00	0.000	0.0227	0.00000	0.00	
FL7	Noz8.F_I	168.75	1.33650	17.608	1472.58	13.929	1387.80	0.6000	1072.95	5.810	0.0227	0.06861	17280.63	
BL 3	Sink39.F_I	1.67	1.35513	380.206	1419.66	0.000	0.00	0.0000	0.00	0.000	0.0000	0.00000	0.00	
FL8	NozSink9.F_I	168.75	1.33650	17.344	1472.58	14.696	1412.26	0.5024	905.79	6.638	0.0227	0.06861	18797.76	
BURNERS														
BRN36	TTout	eff	dPqP	LHV	wfuel	FAR								
BRN36	2900.00	0.9950	0.0400	18400	3.74753	0.02526								

**Table 4.2b NPSS component interface data for the hybrid engine at SLS, maximum thrust (ff = 1)**

NCP		NPSS_1.6.5 - Rev: --		model:		PDC HBTF		run by:		Caitlin		solutionMode= STEADY_STATE		converge= 1		case: 0											
time: 0.000		timeStep:0.0500		therm_package:GasTb1				Mode:		DESIGN		iter/pas/Jac/Broy= 5/ 7/ 1/ 3		run: 03/06/10 09:14:22													
Summary Output Data																											
MN		alt		dTs		W		Fg		Fn		TSFC		wfue1		WAR		OPR									
0.010		0.0		0.00		1500.0		48246.4		47725.9		0.3408		16264.87		0.0000		38.020									
INPUT FLOW																											
		W		gamt		Pt		Tt		Ps		Ts		MN		V		Aphy/144.		FAR		Rs		imp			
FL0		INLET.F_I		1500.00		1.39978		14.697		518.68		14.696		518.67		0.0100		11.16		1757.394		0.0000		0.06856		3719559.18	
FL1		SPLIT.F_I		1500.00		1.39978		14.623		518.68		13.078		502.60		0.4000		439.70		48.575		0.0000		0.06856		111974.73	
FLb2		Fan21.F_I		1333.33		1.39978		14.623		518.68		13.078		502.60		0.4000		439.70		43.177		0.0000		0.06856		99533.09	
FLb3		Bypass13.F_I		1333.33		1.39963		22.812		598.26		20.477		579.73		0.4000		472.07		29.626		0.0000		0.06856		106920.73	
FLb7		Noz18.F_I		1333.33		1.39963		22.812		598.26		20.477		579.73		0.4000		472.07		29.626		0.0000		0.06856		106920.73	
FLb8		NozSink19.F_I		1333.33		1.39963		22.356		598.26		14.696		530.38		0.8003		903.41		19.734		0.0000		0.06856		79200.91	
FL2		LPC20.F_I		166.67		1.39978		14.623		518.68		13.078		502.60		0.4000		439.70		5.397		0.0000		0.06856		12441.64	
FL25		HPC25.F_I		166.67		1.39963		22.812		598.26		20.477		579.73		0.4000		472.07		3.703		0.0000		0.06856		13365.09	
FL3		BLD3.F_I		166.67		1.35513		380.206		1419.66		341.620		1380.32		0.4000		717.35		0.348		0.0000		0.06856		20825.70	
FL31		BRN36.F_I		148.33		1.35513		380.206		1419.66		357.849		1397.30		0.3000		541.11		0.397		0.0000		0.06856		22930.36	
F1393		BLD4.F_I		0.00		1.39978		14.696		518.67		0.000		0.00		0.0000		0.00		0.000		0.0000		0.00000		0.00	
F139		MIX39.F_I1		115.15		1.25230		558.776		3648.04		362.681		3336.85		0.8500		2286.33		0.172		0.0408		0.06865		17160.29	
F1392		MIX39.F_I2		37.70		1.35513		364.998		1419.66		362.684		1417.30		0.0969		175.89		0.310		0.0000		0.06856		16413.70	
FL4		MIX40.F_I		152.85		1.27177		454.794		3161.21		424.475		3114.86		0.3305		862.59		0.482		0.0305		0.06863		33574.07	
FL41		HPT41.F_I		161.18		1.27494		454.794		3081.06		363.352		2934.54		0.6000		1523.69		0.317		0.0288		0.06862		24210.48	
FL44		MIX44.F_I		161.18		1.29532		125.458		2387.41		96.133		2246.04		0.6500		1455.77		0.959		0.0288		0.06862		20572.88	
FL45		LPT45.F_I		169.52		1.29759		125.458		2343.79		96.089		2204.00		0.6500		1443.34		0.999		0.0274		0.06862		21426.97	
FL7		Noz8.F_I		169.52		1.31902		32.033		1758.62		28.857		1714.71		0.4000		789.10		4.734		0.0274		0.06862		23827.24	
BL 3		Sink39.F_I		1.67		1.35513		380.206		1419.66		0.000		0.00		0.0000		0.00		0.000		0.0000		0.00000		0.00	
FL8		NozSink9.F_I		169.52		1.31902		31.552		1758.62		17.033		1511.92		1.0000		1859.66		3.000		0.0274		0.06862		17157.42	
F1394		NozSink1.F_I		0.00		1.50617		14.696		0.00		0.000		0.00		0.0000		0.00		0.000		0.0000		0.00000		0.00	
BURNERS																											
BRN36		TTout		eff		dPqP		LHV		wfue1		FAR															
BRN36		4443.75		0.9950		0.0400		18400		4.51802		0.06161															



**Table 4.3a NPSS component interface data for the baseline engine at cruise, maximum thrust**

NCP NPSS\_1.6.5 - Rev: -- model:Baseline HBTF > run by: Caitlin solutionMode= STEADY\_STATE converge= 1 case: 1  
time: 0.000 timestep:0.0500 therm\_package:GasTbI Mode: OFFDESIGN iter/pas/Jac/Broy= 19/ 29/ 1/17 run: 01/21/10 15:05:18

Summary Output Data														
MN	alt	dTs	W	Fg	Fn	TSFC	wfuel	WAR	OPR					
0.800	30000.0	0.00	779.5	30754.6	11483.9	0.6705	7700.22	0.0000	31.841					
INPUT FLOW														
			W	gamt	Pt	Tt	Ps	Ts	MN	V	Aphy/144.	FAR	Rs	imp
FL0	INLET.F_I		779.47	1.40010	6.679	464.31	4.364	411.69	0.8000	795.44	34.249	0.0000	0.06856	40793.83
FL1	SPLIT.F_I		779.47	1.40010	6.646	464.31	0.000	0.00	0.0000	0.00	0.000	0.0000	0.00000	0.00
FLb2	Fan21.F_I		685.97	1.40010	6.646	464.31	0.000	0.00	0.0000	0.00	0.000	0.0000	0.00000	0.00
FLb3	Bypass13.F_I		685.97	1.39969	10.978	564.78	0.000	0.00	0.0000	0.00	0.000	0.0000	0.00000	0.00
FLb7	Noz18.F_I		685.97	1.39969	10.978	564.78	0.000	0.00	0.0000	0.00	0.000	0.0000	0.00000	0.00
FLb8	NozSink19.F_I		685.97	1.39969	10.758	564.78	5.699	470.64	1.0000	1063.58	19.734	0.0000	0.06856	38871.01
FL2	LPC20.F_I		93.49	1.40010	6.646	464.31	0.000	0.00	0.0000	0.00	0.000	0.0000	0.00000	0.00
FL25	HPC25.F_I		93.49	1.39969	12.369	568.03	0.000	0.00	0.0000	0.00	0.000	0.0000	0.00000	0.00
FL3	BLD3.F_I		93.49	1.35799	212.674	1370.63	0.000	0.00	0.0000	0.00	0.000	0.0000	0.00000	0.00
FL31	BRN36.F_I		83.21	1.35799	212.674	1370.63	0.000	0.00	0.0000	0.00	0.000	0.0000	0.00000	0.00
FL4	MIX40.F_I		85.35	1.28227	204.167	2882.66	0.000	0.00	0.0000	0.00	0.000	0.0257	0.00000	0.00
FL41	HPT41.F_I		90.02	1.28514	204.167	2811.73	0.000	0.00	0.0000	0.00	0.000	0.0243	0.00000	0.00
FL44	MIX44.F_I		90.02	1.30729	50.031	2111.99	0.000	0.00	0.0000	0.00	0.000	0.0243	0.00000	0.00
FL45	LPT45.F_I		94.70	1.30927	50.031	2077.93	0.000	0.00	0.0000	0.00	0.000	0.0231	0.00000	0.00
FL7	Noz8.F_I		94.70	1.34283	7.178	1360.36	0.000	0.00	0.0000	0.00	0.000	0.0231	0.00000	0.00
BL 3	Sink39.F_I		0.93	1.35799	212.674	1370.63	0.000	0.00	0.0000	0.00	0.000	0.0000	0.00000	0.00
FL8	NozSink9.F_I		94.70	1.34283	7.070	1360.36	4.364	1201.26	0.8714	1456.01	6.638	0.0231	0.06861	8456.78
BURNERS														
		Ttout	eff	dPqP	LHV	wfuel	FAR							
BRN36		2882.66	0.9950	0.0400	18400	2.13895	0.02571							

**Table 4.3b NPSS component interface data for the hybrid engine at cruise, maximum thrust (ff = 1)**

NCP NPSS\_1.6.5 - Rev: -- model:PDC HBTF run by: Caitlin solutionMode= STEADY\_STATE converge= 1 case: 1  
time: 0.000 timestep:0.0500 therm\_package:GasTbI Mode: OFFDESIGN iter/pas/Jac/Broy= 14/ 25/ 1/12 run: 03/06/10 09:14:23

Summary output Data														
MN	alt	dTs	W	Fg	Fn	TSFC	wfuel	WAR	OPR					
0.800	30000.0	0.00	754.2	31818.0	13173.0	0.6495	8556.12	0.0000	44.695					
INPUT FLOW														
			W	gamt	Pt	Tt	Ps	Ts	MN	V	Aphy/144.	FAR	Rs	imp
FL0	INLET.F_I		754.16	1.40010	6.679	464.31	4.364	411.69	0.8000	795.44	33.137	0.0000	0.06856	39469.29
FL1	SPLIT.F_I		754.16	1.40010	6.646	464.31	5.877	448.29	0.4228	438.76	48.575	0.0000	0.06856	51394.06
FLb2	Fan21.F_I		665.31	1.40010	6.646	464.31	5.891	448.58	0.4188	434.74	43.177	0.0000	0.06856	45615.04
FLb3	Bypass13.F_I		665.31	1.39972	10.473	547.22	9.272	528.51	0.4209	474.28	29.626	0.0000	0.06856	49361.74
FLb7	Noz18.F_I		665.31	1.39972	10.473	547.22	9.272	528.51	0.4209	474.28	29.626	0.0000	0.06856	49361.74
FLb8	NozSink19.F_I		665.31	1.39972	10.263	547.22	5.441	456.01	1.0000	1046.81	19.734	0.0000	0.06856	37108.89
FL2	LPC20.F_I		88.85	1.40010	6.646	464.31	5.763	445.79	0.4558	471.77	5.397	0.0000	0.06856	5781.91
FL25	HPC25.F_I		88.85	1.39971	11.408	552.82	10.142	534.56	0.4134	468.50	3.703	0.0000	0.06856	6702.35
FL3	BLD3.F_I		88.85	1.35941	197.081	1346.97	177.010	1309.17	0.4002	699.99	0.348	0.0000	0.06856	10798.37
FL31	BRN36.F_I		79.07	1.35941	197.081	1346.97	185.469	1325.49	0.3001	527.96	0.397	0.0000	0.06856	11889.13
F1393	BLD4.F_I		0.00	1.39978	14.696	518.67	0.000	0.00	0.0000	0.00	0.000	0.0000	0.00000	0.00
F139	MIX39.F_I1		62.83	1.25587	298.535	3524.52	188.177	3203.63	0.8744	2308.19	0.172	0.0393	0.06864	9165.29
F1392	MIX39.F_I2		18.62	1.35941	189.197	1346.97	188.167	1345.03	0.0897	158.93	0.310	0.0000	0.06856	8500.78
FL4	MIX40.F_I		81.45	1.27401	239.297	3083.78	223.337	3038.25	0.3303	852.12	0.482	0.0301	0.06863	17666.07
FL41	HPT41.F_I		85.89	1.27721	239.297	3003.82	191.170	2860.12	0.5994	1504.12	0.317	0.0285	0.06862	12737.20
FL44	MIX44.F_I		85.89	1.29731	67.055	2331.29	52.100	2199.58	0.6320	1401.79	0.959	0.0285	0.06862	10939.36
FL45	LPT45.F_I		90.34	1.29954	67.055	2286.95	52.095	2156.95	0.6316	1388.43	0.999	0.0270	0.06862	11392.06
FL7	Noz8.F_I		90.34	1.32172	16.788	1704.22	15.123	1661.33	0.3999	777.40	4.734	0.0270	0.06862	12491.16
BL 3	Sink39.F_I		0.89	1.35941	197.081	1346.97	0.000	0.00	0.0000	0.00	0.000	0.0000	0.00000	0.00
FL8	NozSink9.F_I		90.34	1.32172	16.537	1704.22	8.920	1463.35	1.0000	1831.54	3.000	0.0270	0.06862	8996.48
F1394	NozSink1.F_I		0.00	1.50617	14.696	0.000	0.000	0.00	0.0000	0.00	0.000	0.0000	0.00000	0.00
BURNERS														
		Ttout	eff	dPqP	LHV	wfuel	FAR							
BRN36		4304.85	0.9950	0.0400	18400	2.37670	0.05918							

**Table 4.3c Maximum power output comparison baseline and hybrid engines**

	Baseline engine	Hybrid engine
<b>Alt = 0.0 ft, M = 0.0</b>		
Thrust (lbf)	41668.8	47725.9
TSFC (1/h)	0.3238	0.3408
Mass flow rate (lbm/s)	1500	1500
T <sub>t4</sub> (R)	2900.0	3161.2
<b>Alt = 30 kft, M = 0.8</b>		
Thrust (lbf)	11483.9	13173.0
TSFC (1/h)	0.6705	0.6495
Mass flow rate (lbm/s)	779.5	754.2
T <sub>t4</sub> (R)	2882.7	3083.8

Table 4.4 shows a comparison of the fluid properties for both the baseline and hybrid engine at the entrance and exit of the combustor at SLS and cruise conditions at maximum thrust. The properties of the flow entering station 3.1 are fairly similar for the baseline and hybrid engines. The properties of the flow exiting the PDC are taken at the exit of MIX39 (station 4.0 as shown in Fig. 3.4), which combines the tube and internal bypass flows. With no internal bypass (and no mixer), the flow exiting the PDC tubes could be much higher than the 3200 R limit as seen from Tables 4.2b and 4.3b at station 3.9. MIX39 allows the flow to cool below the temperature constraint of 3200R at a cost of a reduced stagnation pressure. MIX39 is an NPSS element that, through thermodynamic analysis, drops the exit stagnation pressure due to constant area mixing (e.g., see Oates pg. 166). The burner pressure ratio of the baseline engine is 0.96 for SLS or cruise. The burner pressure ratio for the PDC ranges from 1.20 at SLS to 1.21 at cruise (M = 0.8, Alt = 30,000 ft). If the exit stagnation pressure of the flow is considered at the exit of the detonation tubes (station 3.9 in Tables 4.2b and 4.3b), the pressure ratio of the

burner is 1.47 at SLS and 1.51 at a cruise. Thus, the internal mixer causes about a 23.7% reduction in the combustor pressure ratio for SLS or cruise.

**Table 4.4 Combustor Properties at SLS and Cruise, Maximum Power (ff = 1)**

	Baseline SLS	Hybrid SLS	Baseline Cruise	Hybrid Cruise
Altitude	0.0 ft	0.0 ft	30,000 ft	30,000 ft
Flt Mach number	0.0	0.0	0.8	0.8
Eq Ratio		0.90		0.86
iBPR		0.342		0.308
Mcj		3.37		3.42
Station 3.1 flow in:				
Tt	1419.7 R	1419.7 R	1370.6 R	1347.0 R
Pt	380.2 psi	380.2 psi	212.7 psi	197.1 psi
Mass flow rate	148.3 lbm/s	148.3 lbm/s	83.2 lbm/s	79.1 lbm/s
Mach number		0.3		0.3
Station 4.0 flow out:				
Tt	2900.0 R	3161.2 R	2882.7 R	3038.8 R
Pt	365.0 psi	454.8 psi	204.2 psi	239.3 psi
Mass flow rate	152.1 lbm/s	152.9 lbm/s	85.3 lbm/s	81.5 lbm/s
Mach number		0.33		0.33

The combustor properties in Table 4.4 are calculated assuming steady flow through the PDC. Applying a 4% pressure loss in the TTSS element to account for unsteady losses yields a 0.5% reduction in thrust and a 0.5% increase in TSFC. An 8% loss would yield a 1.2% reduction in thrust and a 1.2% increase in TSFC. These losses may be low due to their application at the exit of the detonation tubes. Exit losses do not capture valve losses. In order to model the pressure losses due to the opening and closing of the valves in to the detonation tubes, unsteady affects should be included in the thermodynamics of the PDC cycle. This was not included in this work.

## Hybrid Turbofan Performance Comparison

Throttle hooks for the hybrid engine are performed at the configuration shown in Table 3.5 at maximum thrust at a fill fraction of 1.0 and compared to that of the baseline engine in Figs. 4.5a and 4.5b.

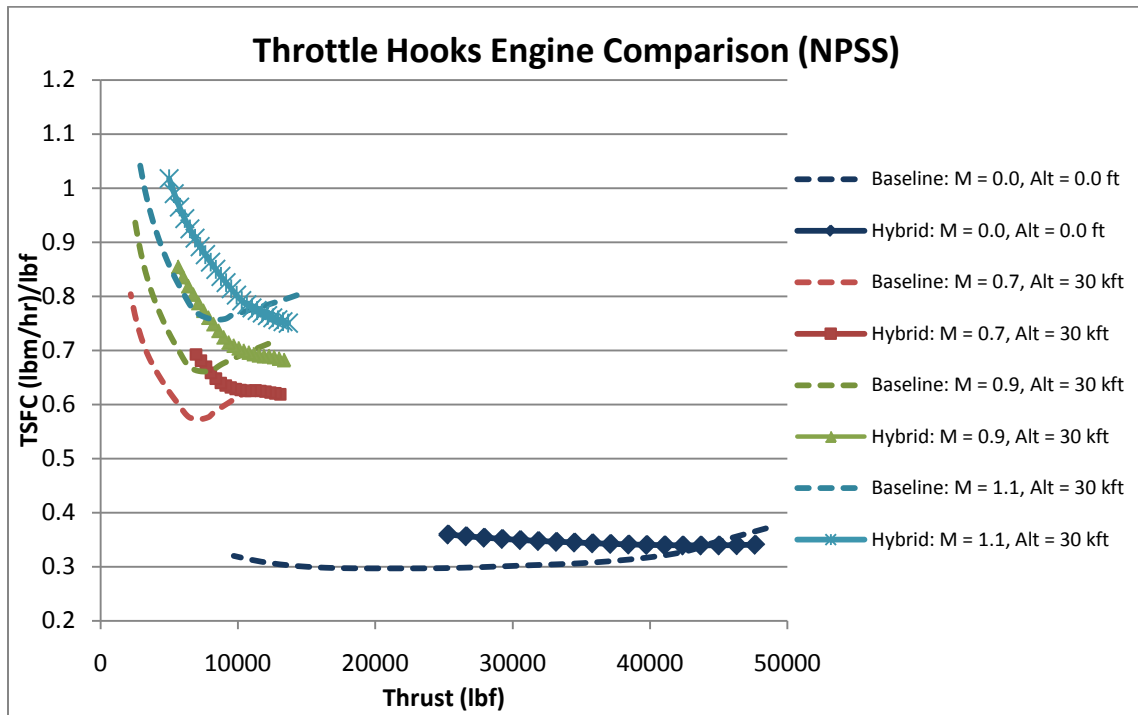


**Figure 4.5a Throttle hook comparison baseline and hybrid turbofan engines in NPSS**

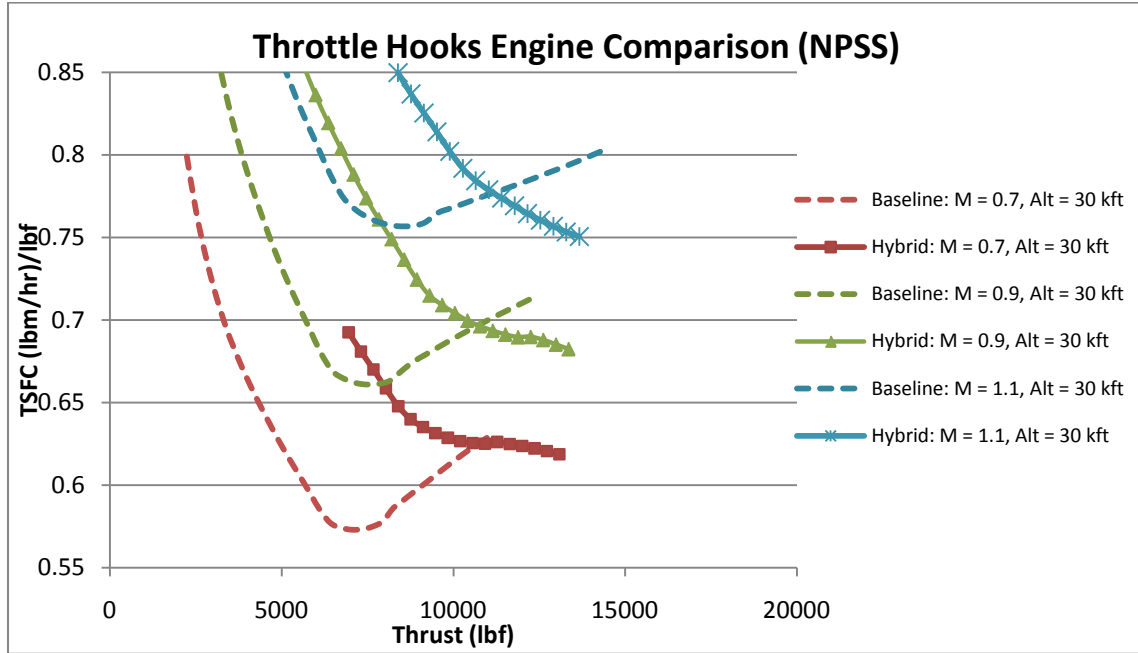


**Figure 4.5b Zoomed in view of Fig. 4.5a**

Figure 4.5b shows a comparison of the hybrid and baseline engine throttle hooks at sea level static and 30,000 ft at a variety of Mach numbers. The baseline engine yields a lower TSFC at lower thrust values for a majority of the thrust range; however, as the thrust increases, the TSFCs cross. This crossing also occurs at the higher Mach numbers. It is seen that the baseline engine has a larger thrust range. The lower hybrid range of thrust occurs since the internal bypass bleed air (BLD4) at station 3.93 (Fig. 3.2) is much greater than the air flowing through the internal bypass, due to reduced bypass flow needed to balance the static pressure at MIX39, and the solver cannot converge on a solution. The internal bypass bleed air variation with thrust is shown in Fig. 4.5c. As the thrust increases, less air is bled from the internal bypass to balance static pressures in MIX39. The thrust increases until the bleed air is zero, after which the static pressures

will not balance. If it were possible to provide additional air pumped into the mixer, one could increase the thrust. No attempts were made for this work. The internal bypass bleed is the limiting factor for the hybrid engine performance.

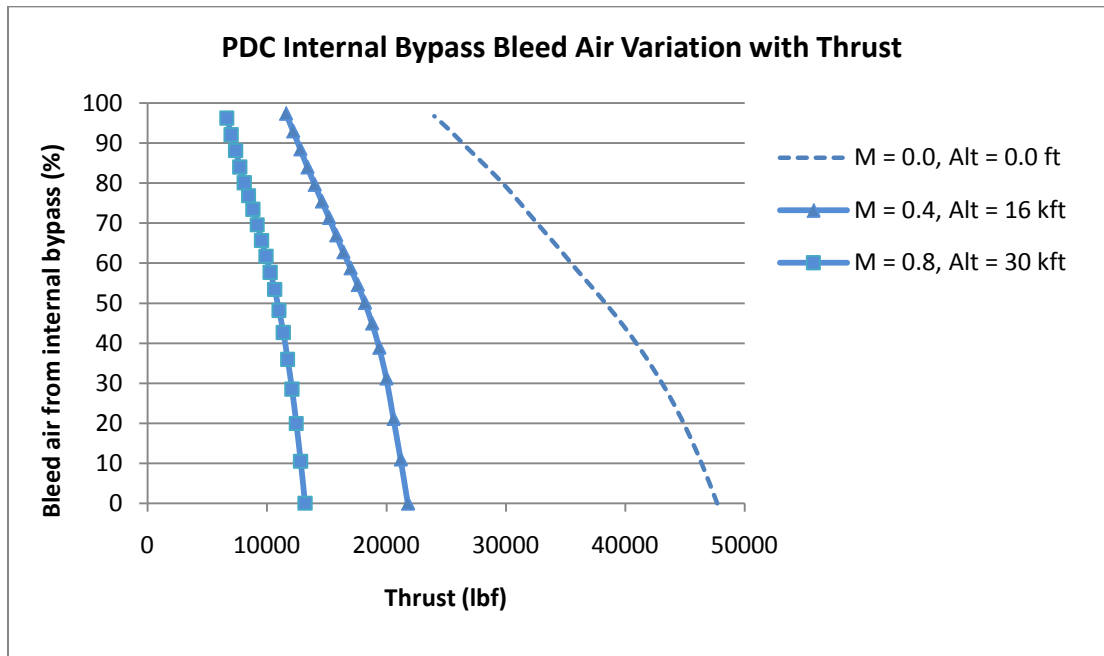


**Figure 4.5c Internal bypass bleed air variation with thrust**

Figure 4.6 shows the effects of fill fraction, with throttle hooks run at sea level static and cruise conditions at maximum thrust at the configuration shown in Table 3.5. Figure 4.6 shows that fill fraction can be adjusted to reduce the TSFC at any thrust level to roughly that of the baseline engine and perhaps slightly lower. The best results are seen at the maximum thrust level of each fill fraction shown in Figs. 4.6b and 4.6d.

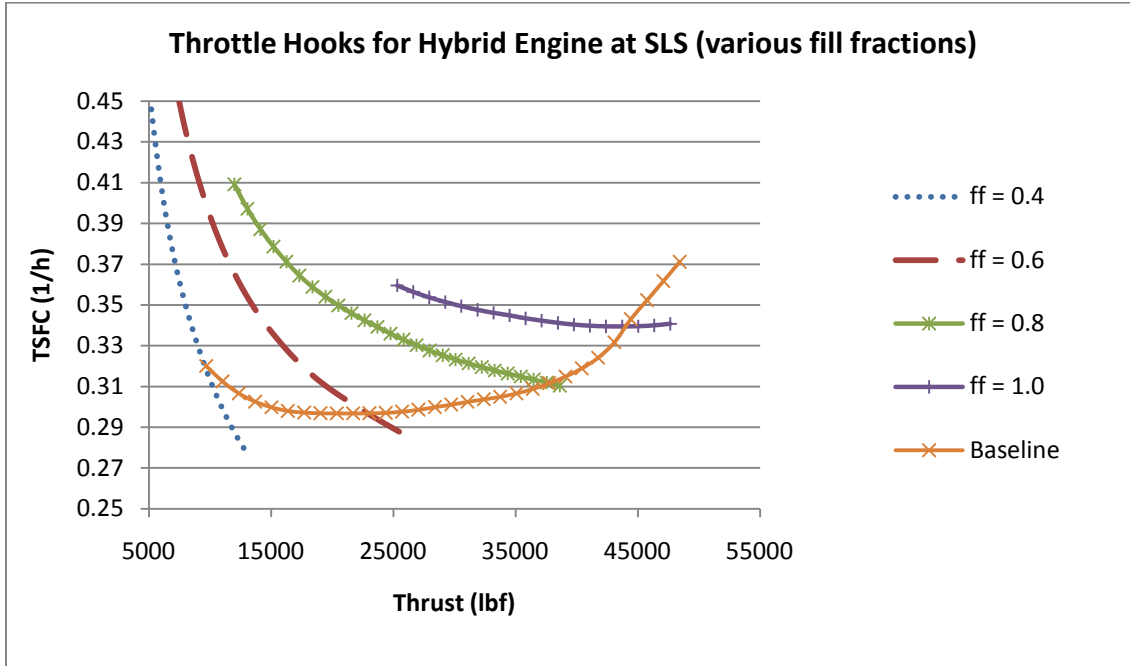


**Figure 4.6a Throttle hooks at various fill fractions at SLS**

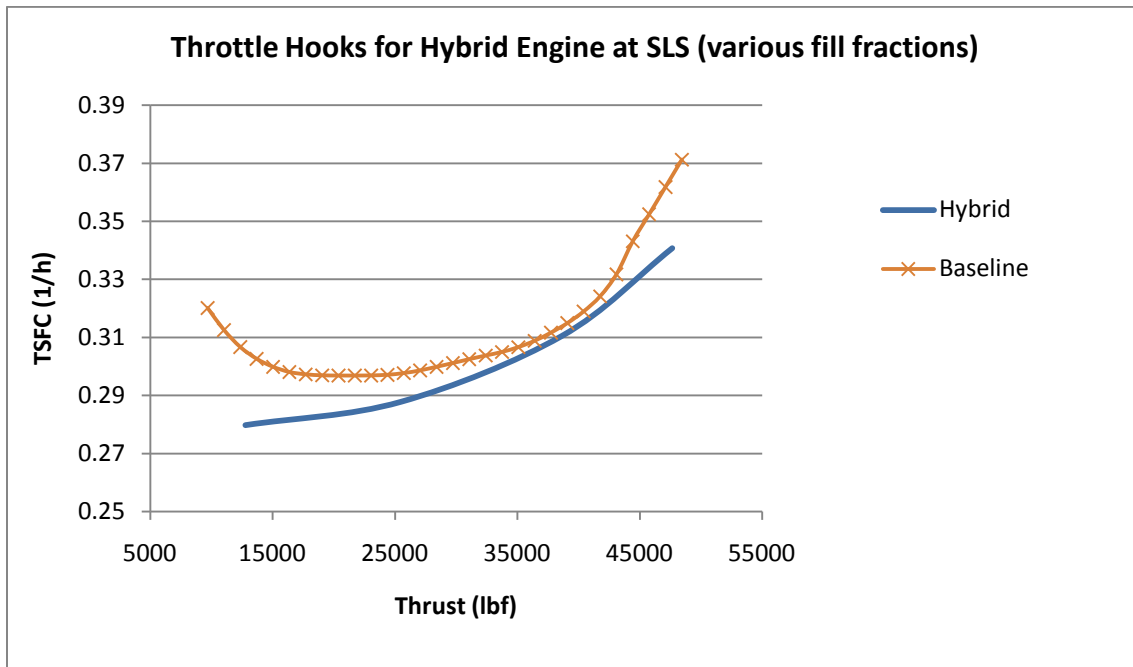


**Figure 4.6b Throttle hooks at fill fractions from 0.4 to 1.0 at maximum thrust at SLS**

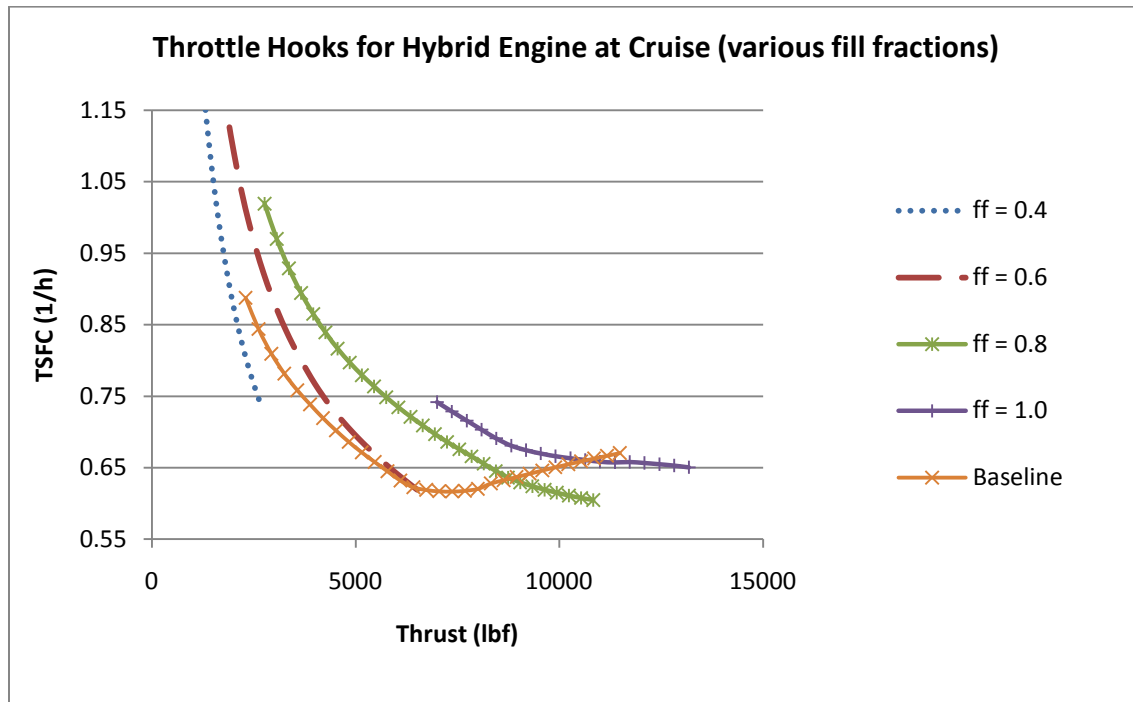


**Figure 4.6c Throttle hooks at various fill fractions at cruise ( $M = 0.8$ , Alt = 30kft)**

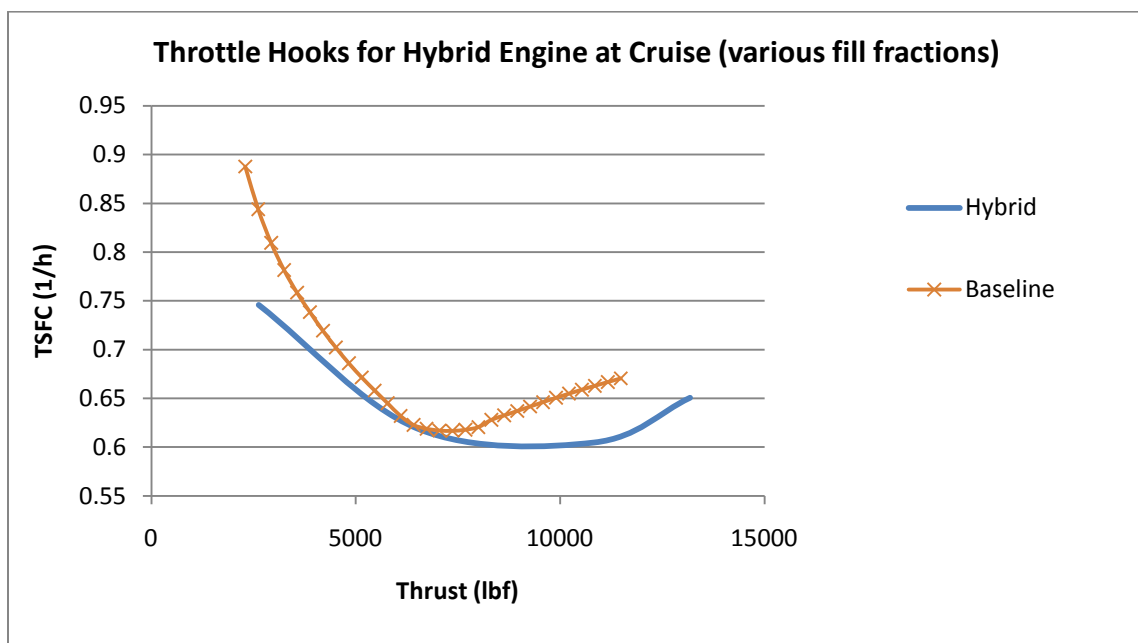


**Figure 4.6d Throttle hooks at fill fractions from 0.4 to 1.0 at maximum thrust at cruise ( $M = 0.8$ , Alt = 30kft)**



For comparison purposes, throttle hooks were run at various frequencies in Fig. 4.7 at the configuration shown in Table 3.5 at a fill fraction of 1.0. The results are very similar and indicate that frequency may be considered as an additional throttling parameter for future research.

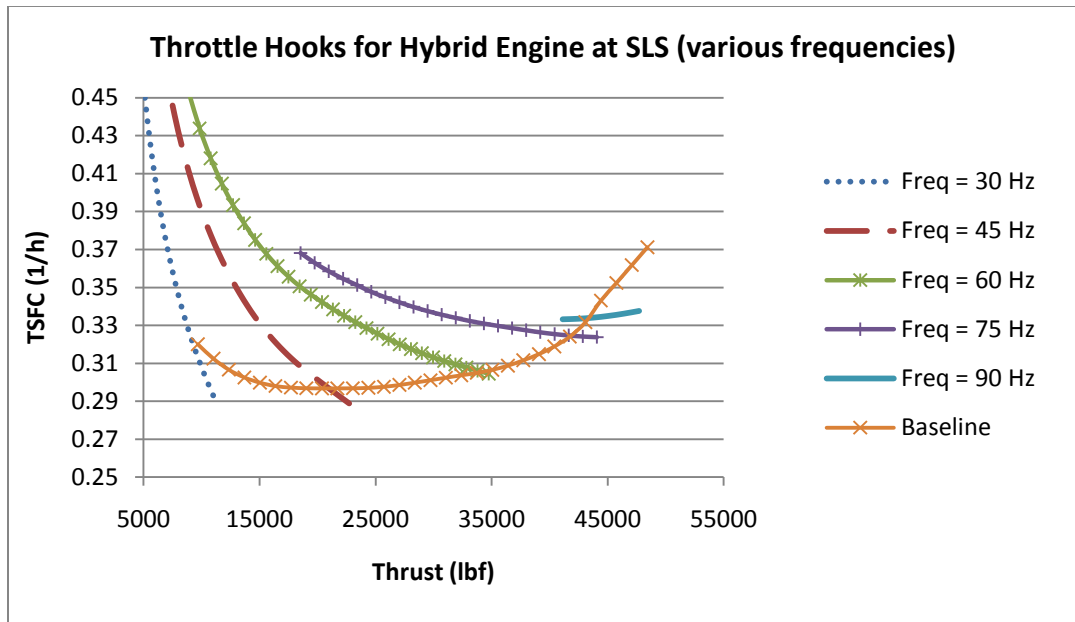


**Figure 4.7a Throttle hooks at various frequencies at SLS**

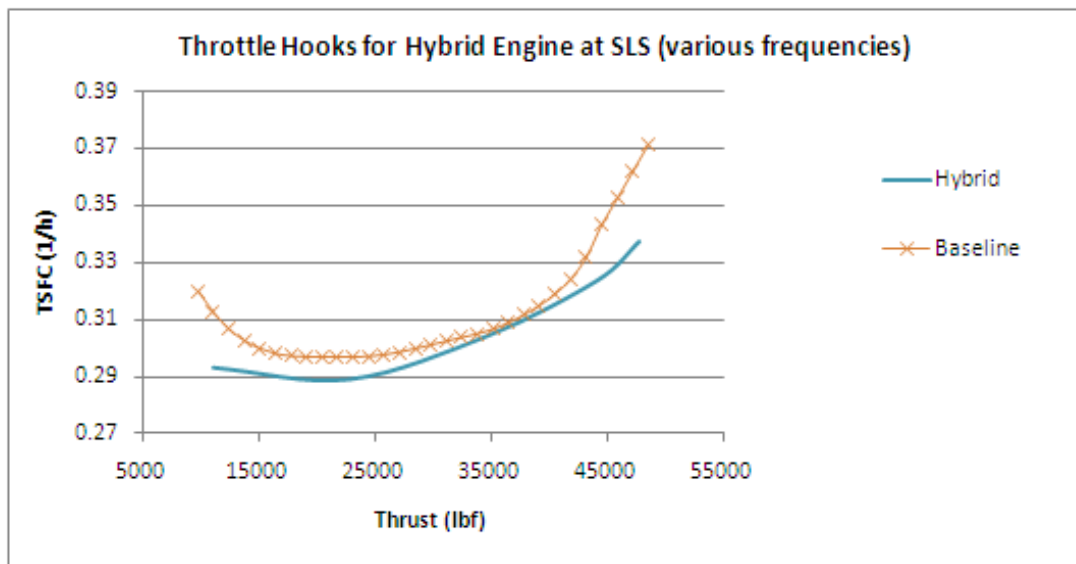


**Figure 4.7b Throttle hooks at various frequencies at maximum thrust at SLS**

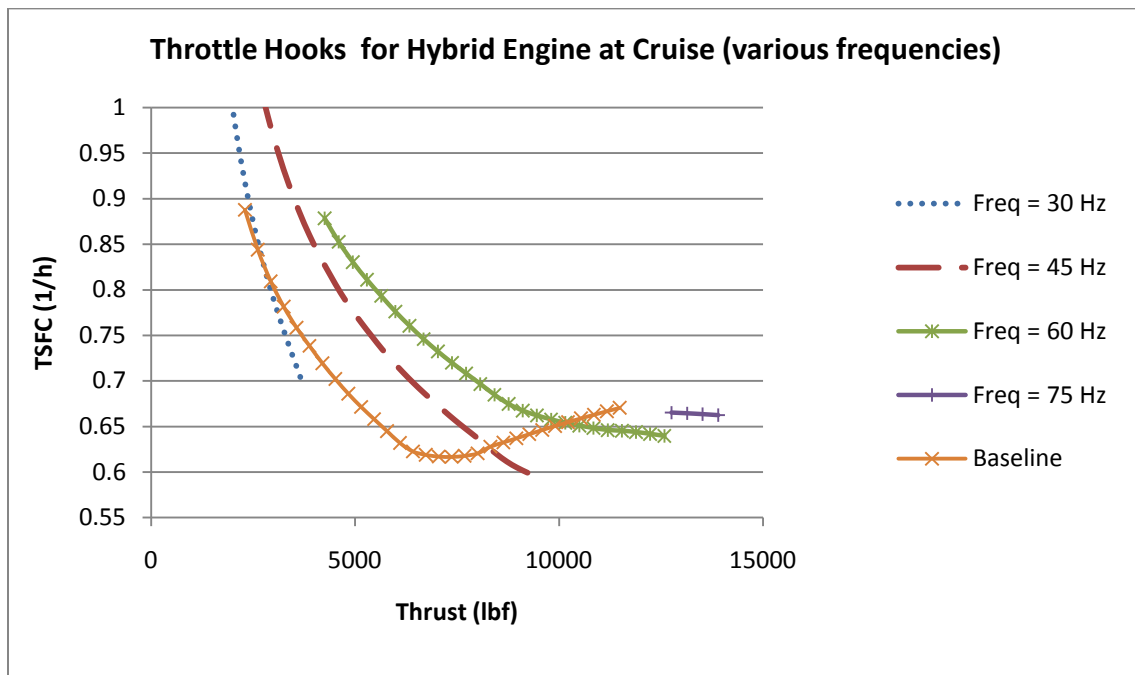


**Figure 4.7c Throttle hooks at various frequencies at cruise ( $M = 0.8$ , Alt = 30kft)**

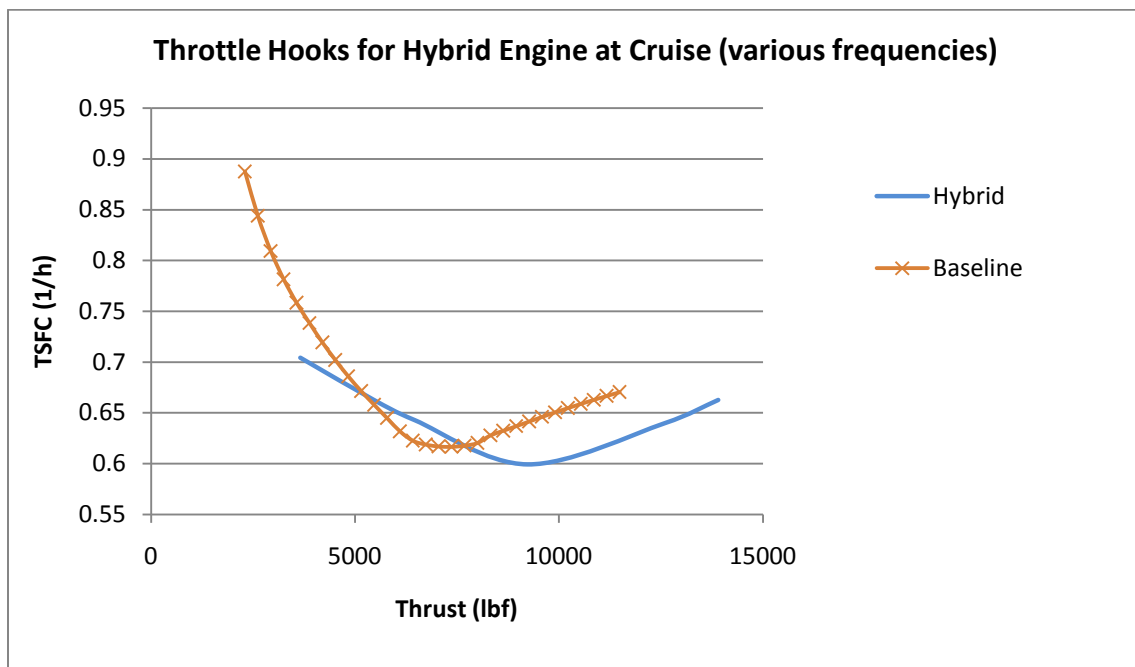


**Figure 4.7d Throttle hooks at various frequencies at maximum thrust at cruise ( $M = 0.8$ , Alt = 30kft)**

Figures 4.8a, 4.8b, and 4.8c show the effect of flight Mach number for the hybrid engine as compared to the baseline at various altitudes and fill fractions at sea level and 30,000 ft. The model is run at the configuration in Table 3.5 at maximum thrust. At higher Mach numbers the baseline engine thrust is slightly higher, except for a fill fraction of one at sea level. At cruising altitude there is a range of fill fractions where the hybrid engine can match the baseline.

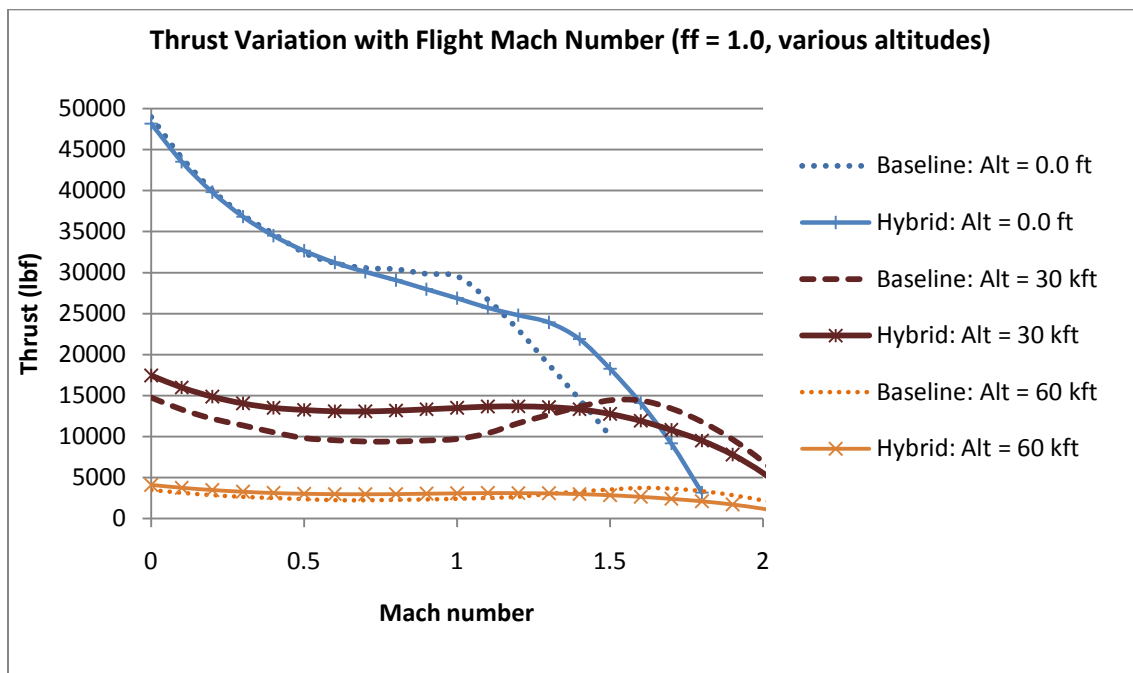


**Figure 4.8a Variation of thrust with flight Mach number comparison of the baseline and hybrid engines in NPSS at 0.0 ft, 30,000 ft, and 60,000 ft (maximum thrust)**

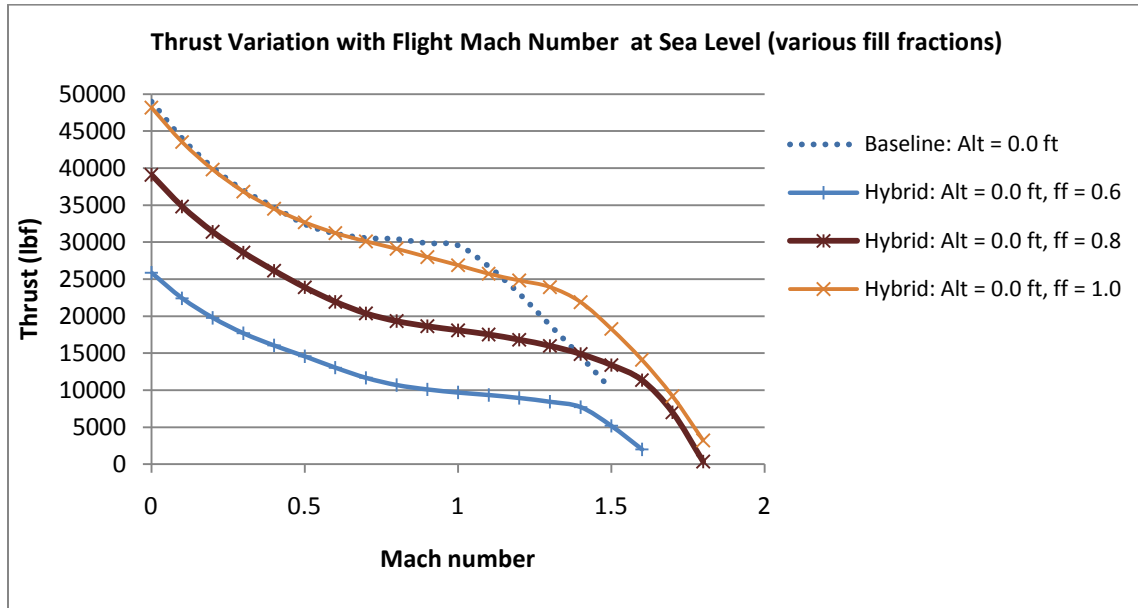


**Figure 4.8b Variation of thrust with flight Mach number comparison of the baseline and hybrid engines in NPSS at fill fractions of 0.6, 0.8, and 1.0 at sea level (maximum thrust)**

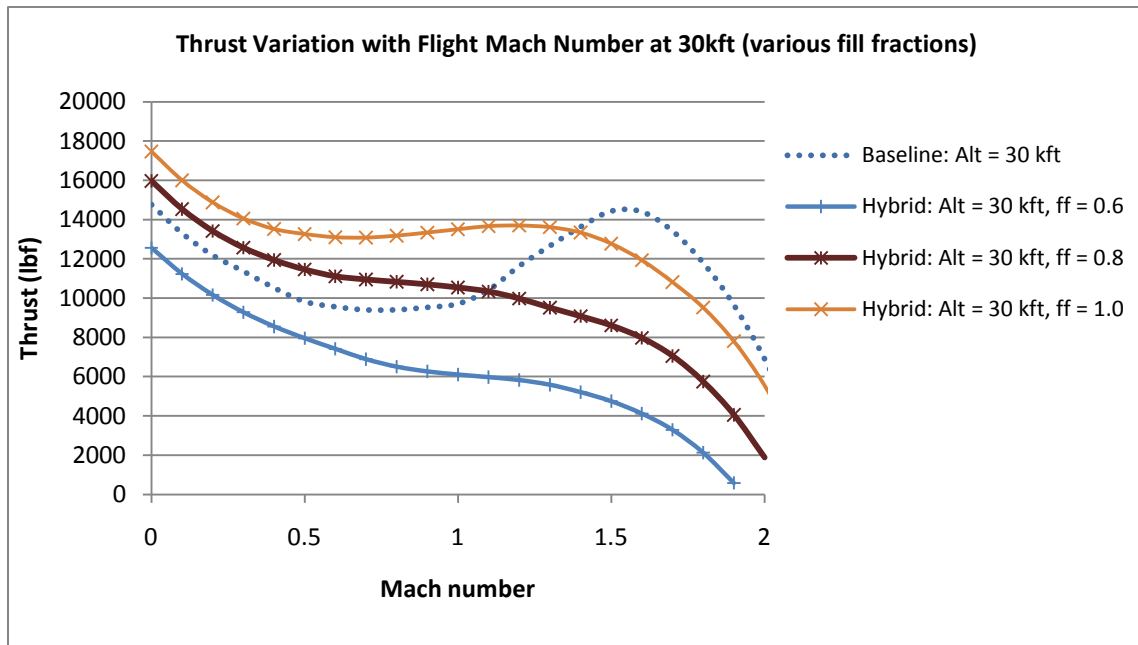


**Figure 4.8c Variation of thrust with flight Mach number comparison of baseline and hybrid engines at fill fractions of 0.6, 0.8, and 1.0 at 30,000 ft (maximum thrust)**

The effects of fill fraction on thrust are plotted at SLS and cruise conditions in Fig. 4.8d. For the configuration listed in Table 3.5 and at maximum thrust, in general, a lower fill fraction corresponds to a lower thrust.

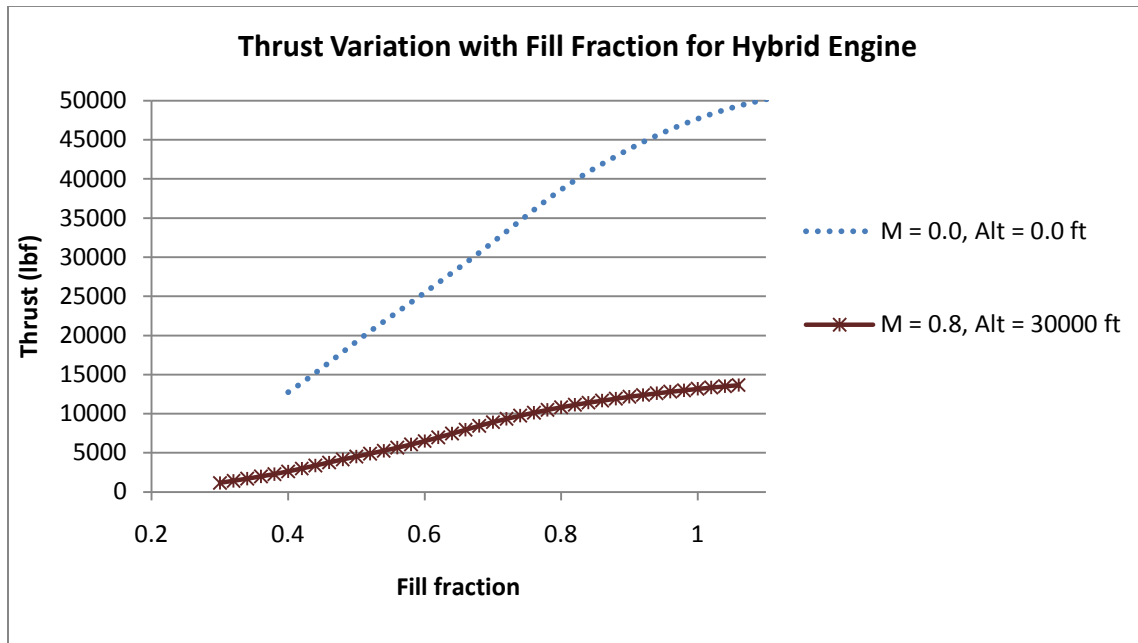


**Figure 4.8d Thrust variation with fill fraction for the hybrid engine at SLS and cruise (maximum thrust)**

The thrust is divided by the freestream pressure to determine the effects of altitude on the engine. As shown in Fig. 4.8e, the altitude has a significant effect on thrust as the curves at SLS and cruise conditions are nearly identical.

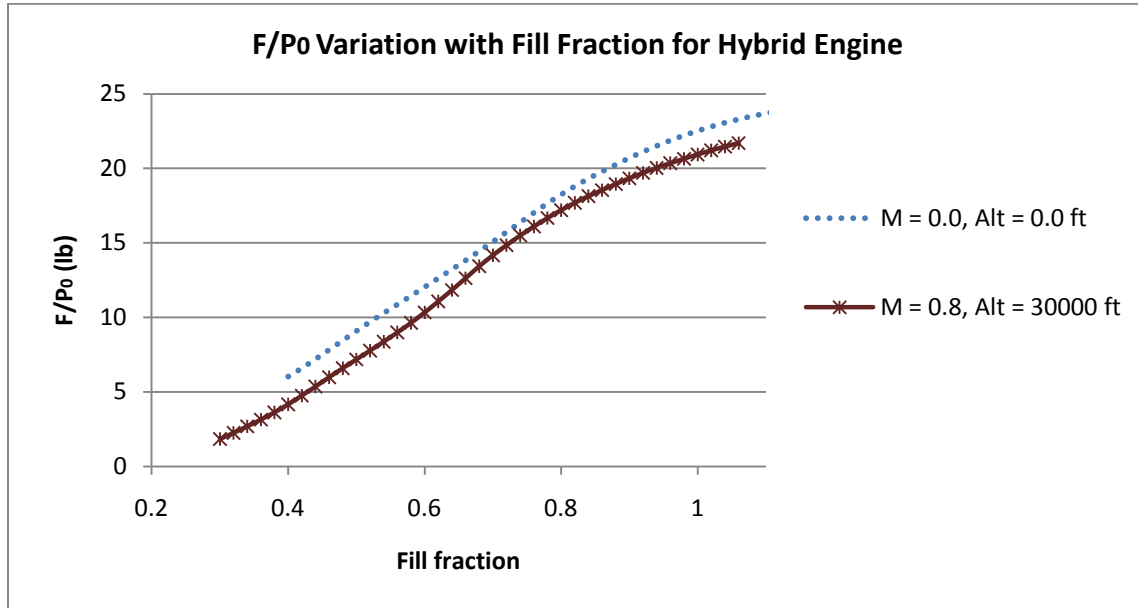


**Figure 4.8e Thrust divided by free stream pressure variation with fill fraction for the hybrid engine as SLS and cruise (maximum thrust)**

Fill fraction is also varied in Fig. 4.9 to determine the effects on TSFC at SLS and cruise conditions. The model is run at maximum thrust at the configuration in Table 3.5. Results indicate that at cruise conditions the lowest TSFC is found at a fill fraction of 0.7. The two curves are at different thrusts. At a thrust of 13,000 lbs, TSFC at cruise is 0.6468 and TSFC at SLS is 0.2794.

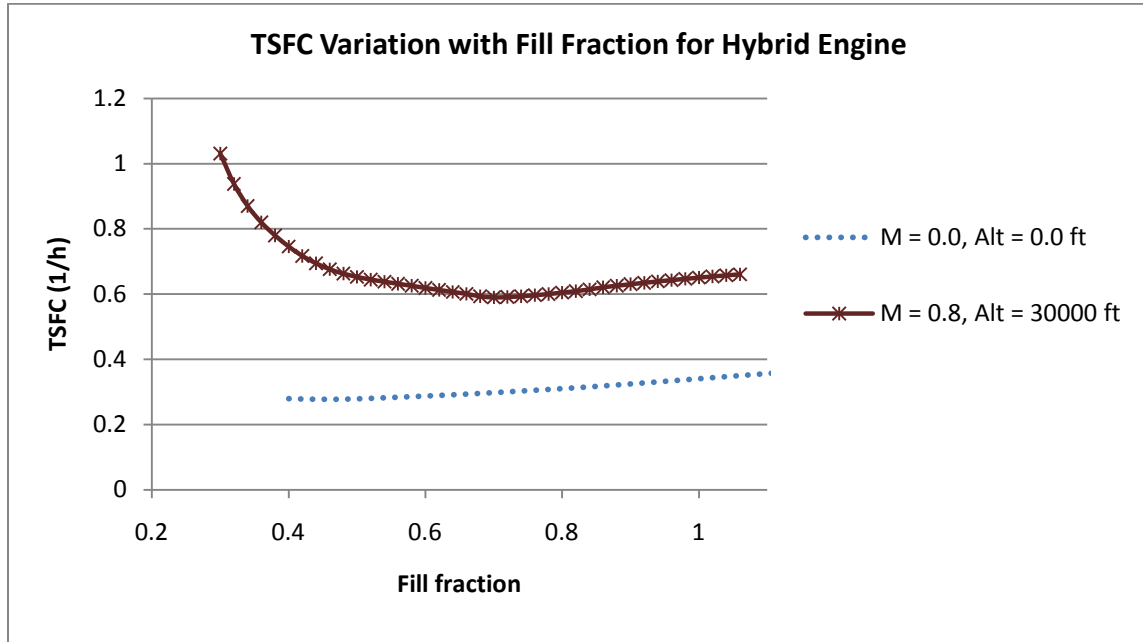


**Figure 4.9 TSFC variation with fill fraction for the hybrid engine at SLS and cruise (maximum thrust)**

The mass flow rate variation with thrust is shown in Figs. 4.10a, 4.10b, and 4.10c. The model is run at the configuration in Table 3.5 at maximum power at SLS and cruise conditions and fill fractions of 0.6, 0.8, and 1.0. The baseline engine has a higher mass flow rate at all thrusts than the hybrid. The fill fraction affects the mass flow rate only by the range of thrust it covers.

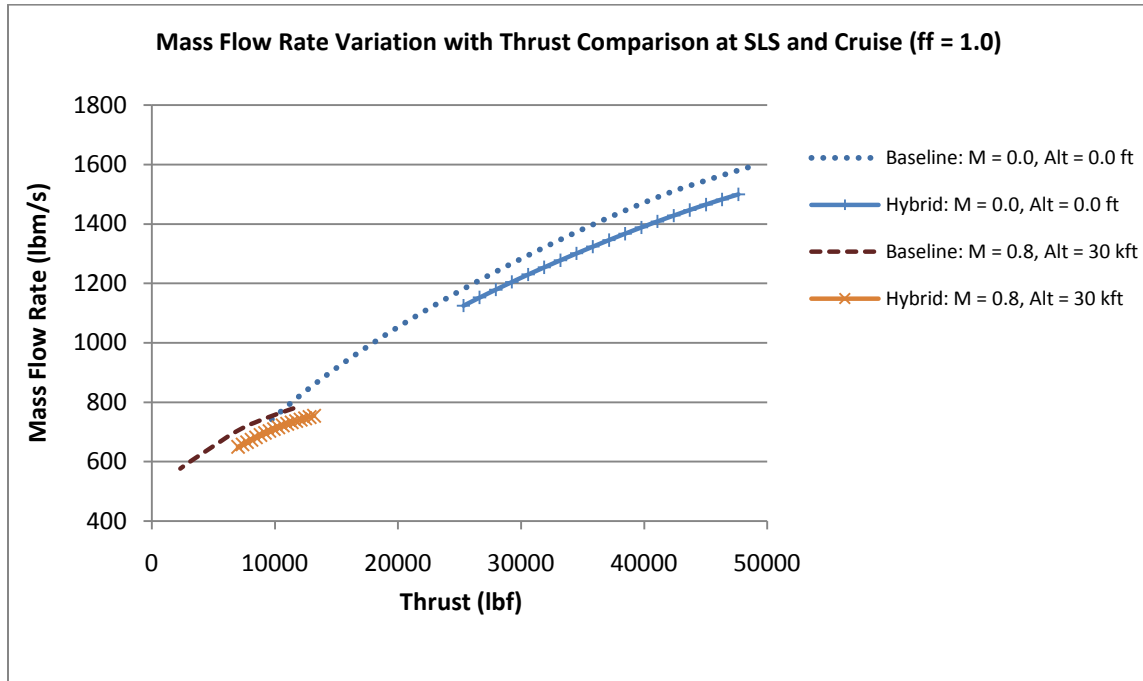


**Figure 4.10a Mass flow rate variation with thrust comparison of the baseline and hybrid engines at SLS and cruise conditions (maximum thrust)**

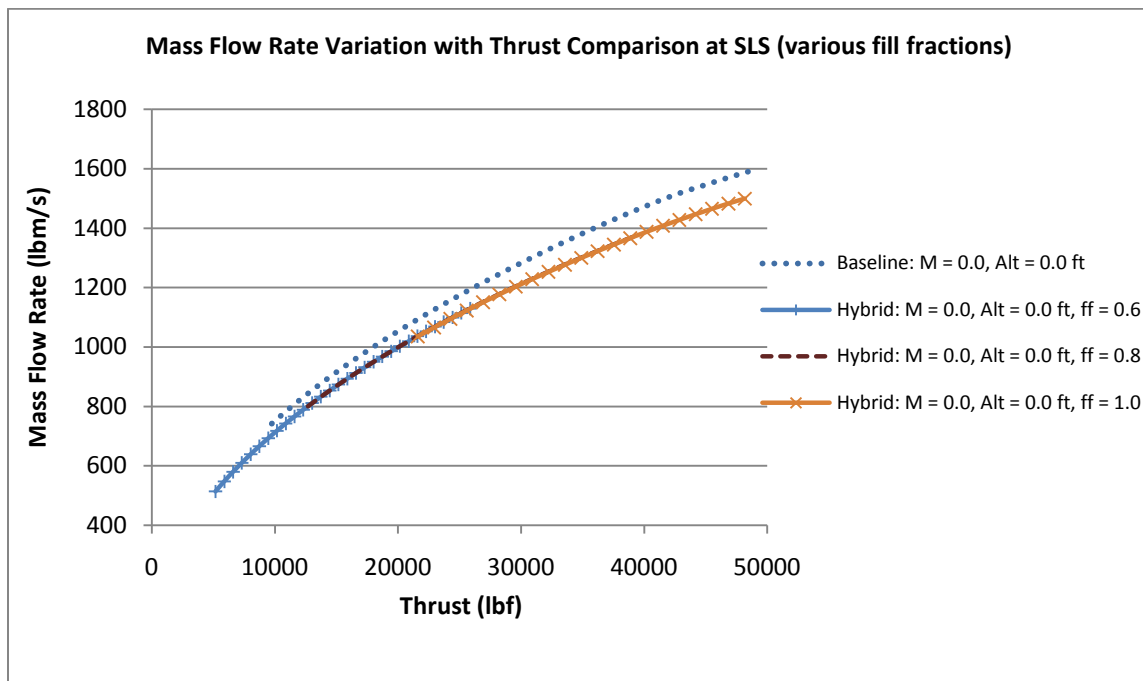


**Figure 4.10b Mass flow rate variation with thrust comparison of the baseline and hybrid engines at SLS at fill fractions of 0.6, 0.8, and 1.0 (maximum thrust)**



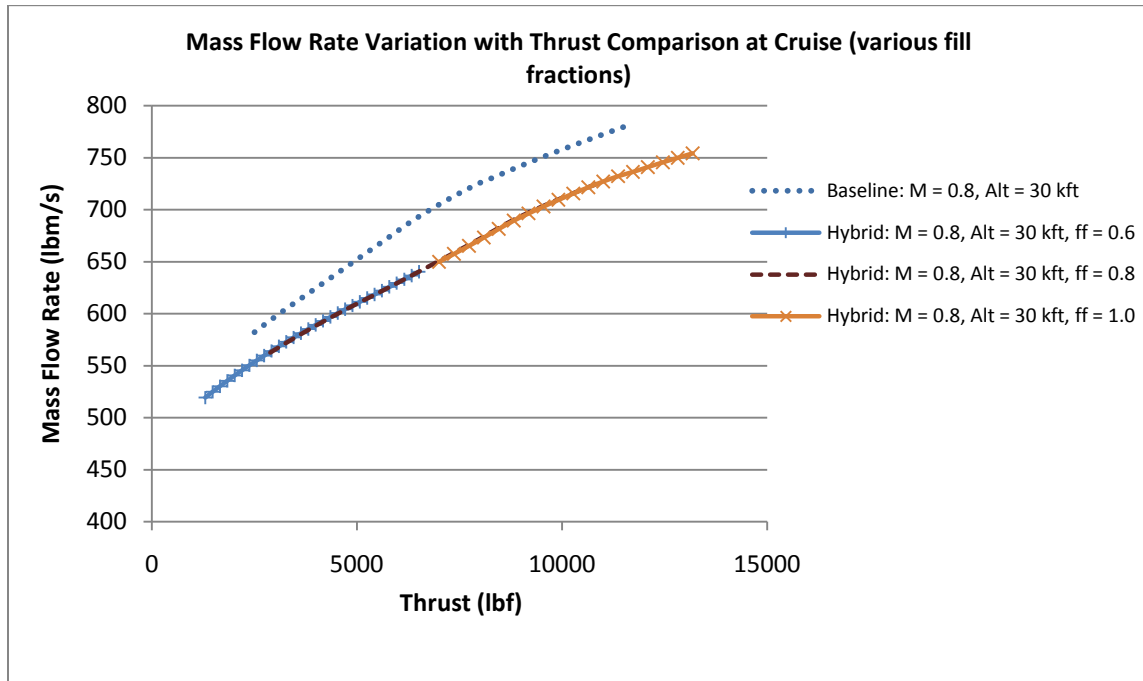


**Figure 4.10c Mass flow rate variation with thrust comparison of the baseline and hybrid engines at 30,000 ft at fill fractions of 0.6, 0.8, and 1.0 (maximum thrust)**

### Component Performance

The fan, high pressure compressor (HPC), low pressure turbine (LPT), and turbofan bypass ratio variation with  $T_{t2}/T_0$  are shown in Figs. 4.11- 4.14. The model is run at the configuration in Table 3.5 at maximum power at a fill fraction of 1.0 at SLS and 30,000 ft. For the baseline model, the fan and HPC pressure ratios break at 1.0 at 30,000 ft. The hybrid model is already past the break point in the plots shown. The LPT is choked for both models. The bypass ratio is shown to steadily increase for both the baseline and hybrid engines.

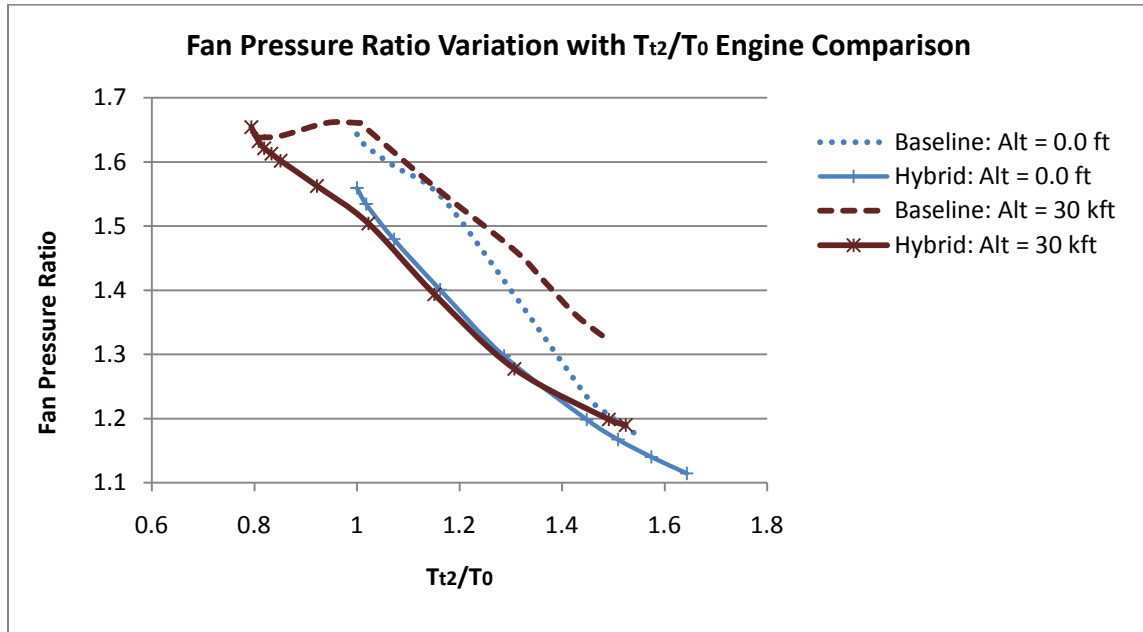


**Figure 4.11** Fan pressure ratio variation with  $T_{t2}/T_0$  comparison of the baseline and hybrid engines at SLS and cruise (maximum thrust)

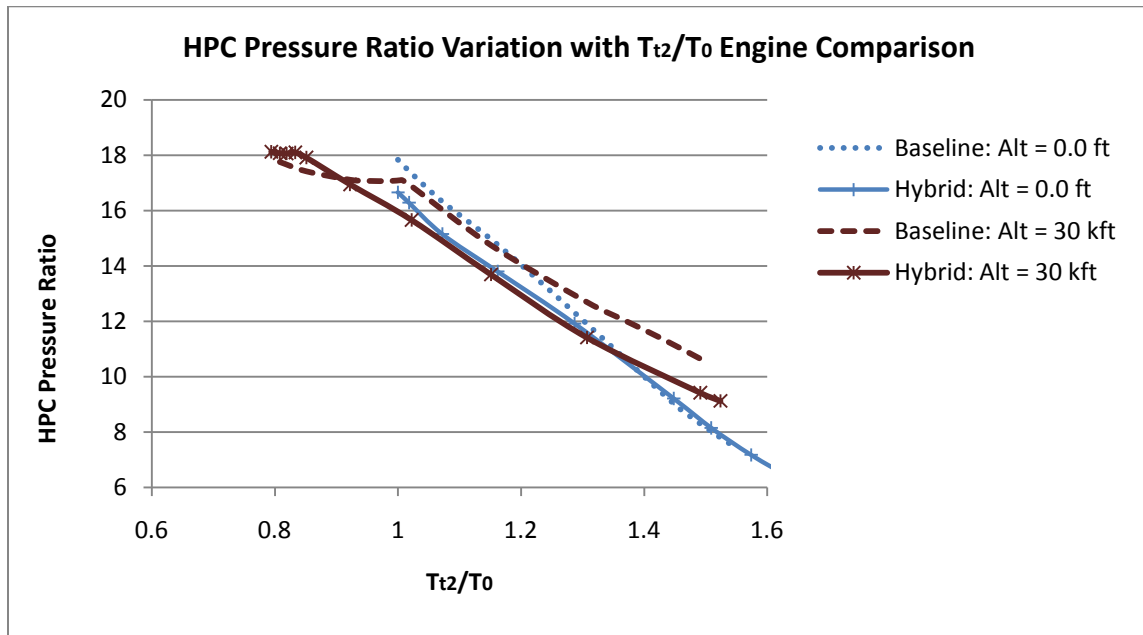


**Figure 4.12** High pressure compressor ratio variation with  $T_{t2}/T_0$  comparison of the baseline and hybrid engines at SLS and cruise (maximum thrust)

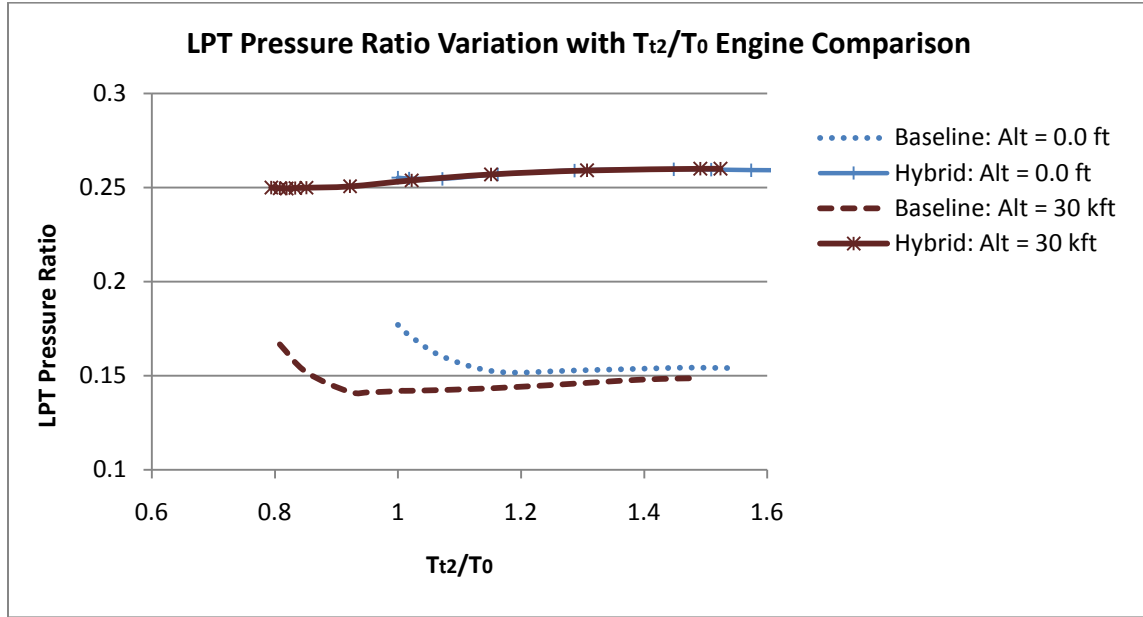


Figure 4.13 Low pressure turbine pressure ratio variation with  $T_{t2}/T_0$  comparison of the baseline and hybrid engines at SLS and cruise (maximum thrust)

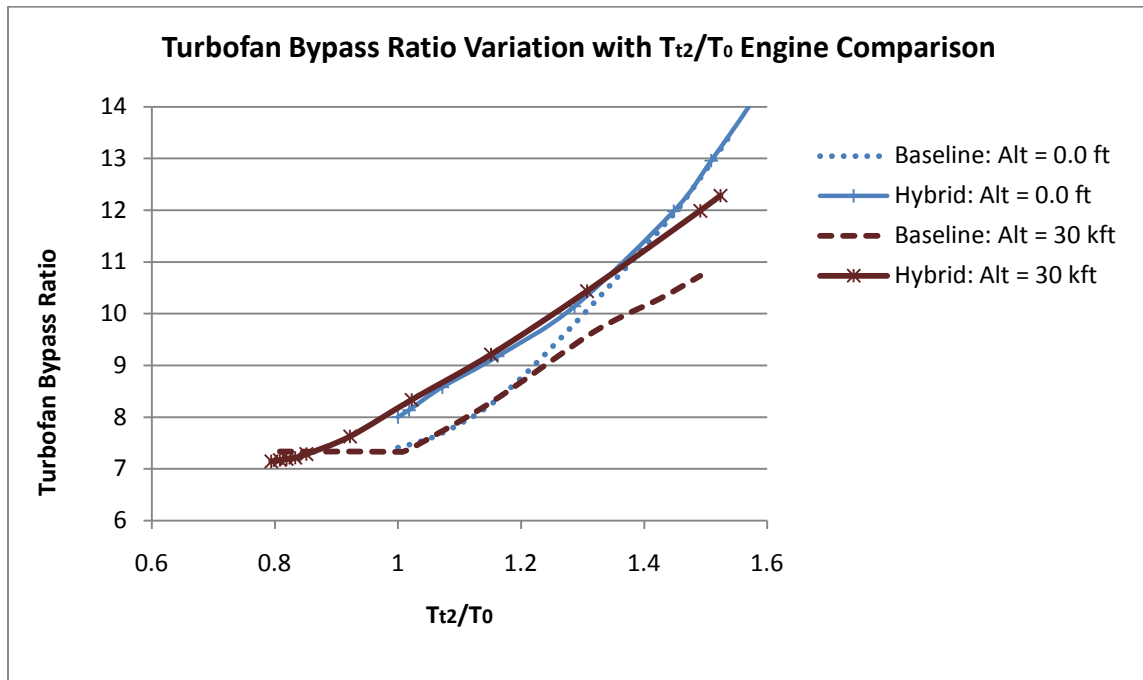
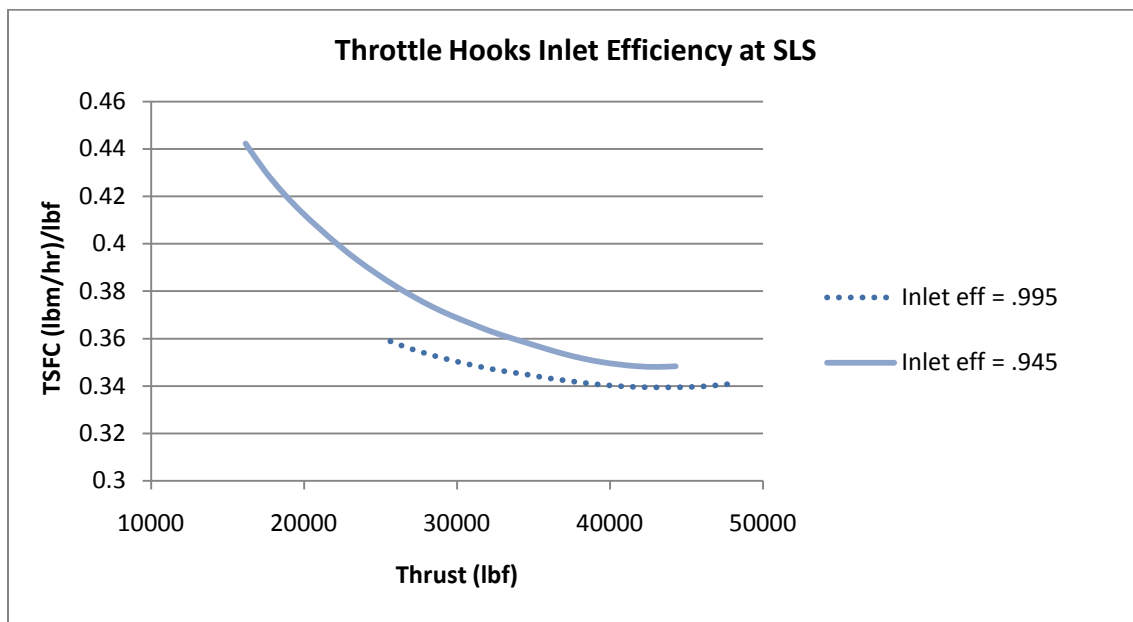


Figure 4.14 Turbofan bypass ratio variation with  $T_{t2}/T_0$  comparison of the baseline and hybrid engines at SLS and cruise (maximum thrust)

## Component Adiabatic Efficiencies

It was of interest to determine how changing the adiabatic efficiencies of various components affected the performance of the hybrid engine. Changes in the inlet, fan, turbine, compressor, and burner efficiencies were evaluated via throttle hooks shown in Figs. 4.16 - 4.21, respectively. The dotted lines represent the on-design efficiencies. The model was run at maximum thrust at the configuration shown in Table 3.5. With a 5% decrease in efficiency, each component resulted in an average of 1.2% to 1.5% increase in TSFC with the exception of the burner. The burner efficiency is used to calculate the heat addition into the system as shown in Eq. 2.11. Decreasing the efficiency of the burner in Fig. 4.21 less than 97.5% leads to choking, in which case the solver cannot converge to a solution. Decreasing burner efficiency from its original value of 99.5% to 97.5% resulted in a 3.4% average decrease in TSFC.



**Figure 4.15 Throttle hooks for inlet efficiency of the hybrid engine (maximum thrust)**

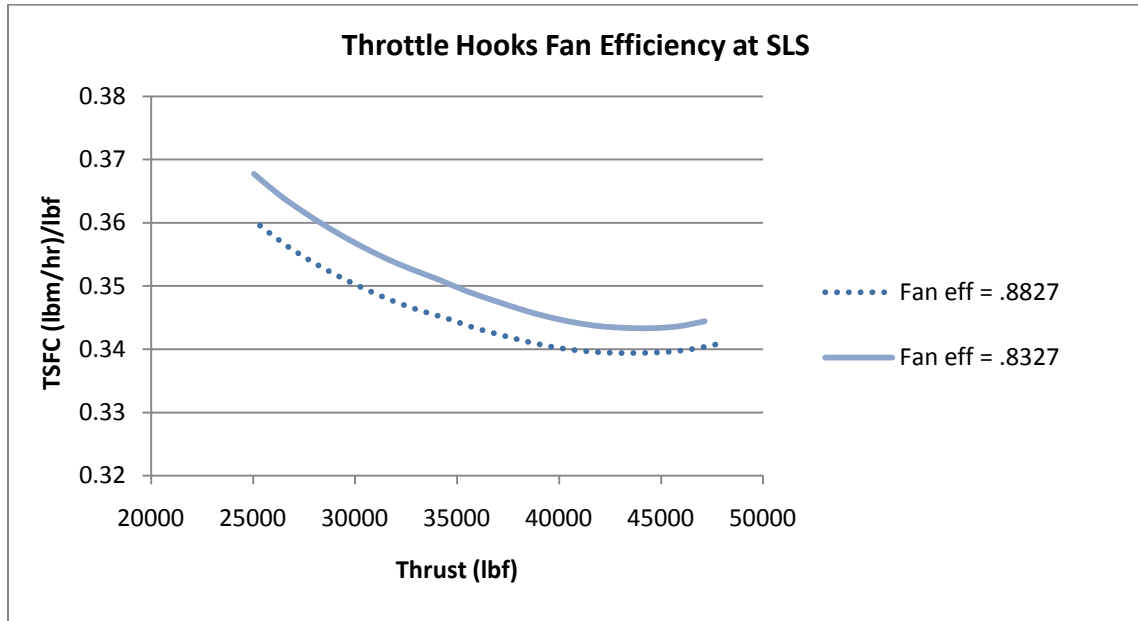


**Figure 4.16 Throttle hooks for fan efficiency of the hybrid engine (maximum thrust)**

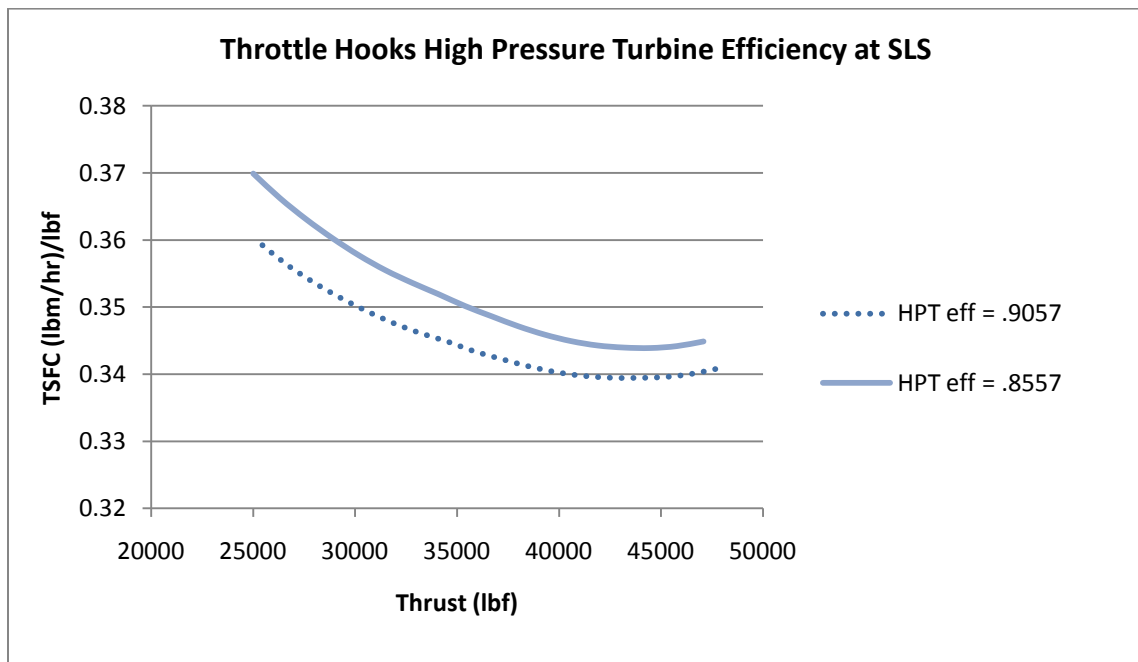


**Figure 4.17 Throttle hooks for high pressure turbine efficiency of the hybrid engine (maximum thrust)**

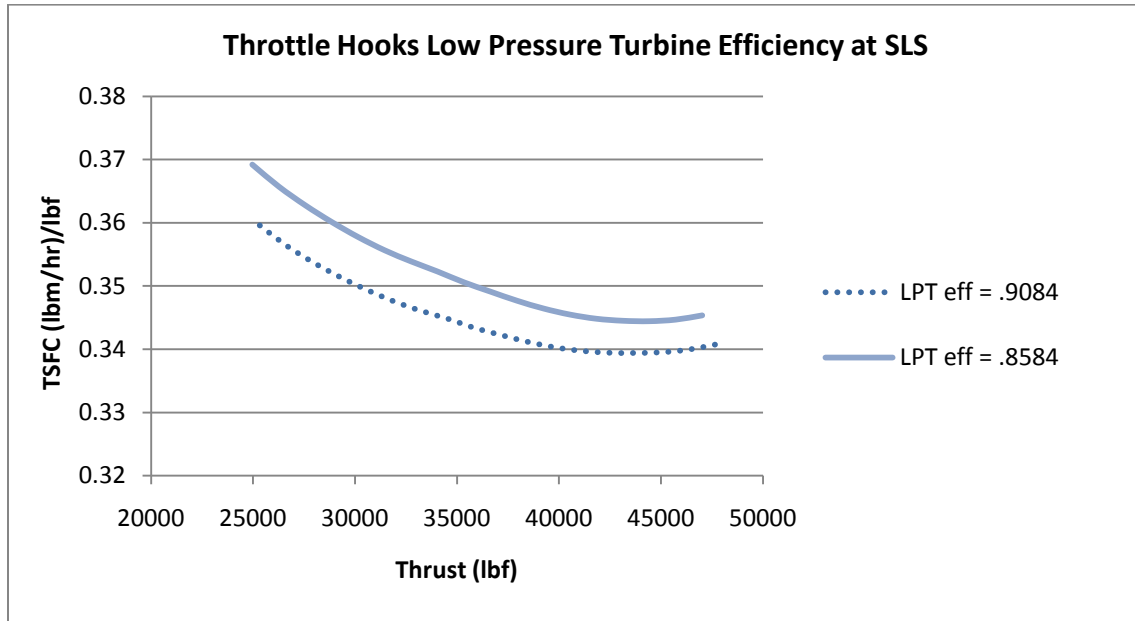


**Figure 4.18 Throttle hooks for low pressure turbine efficiency of the hybrid engine (maximum thrust)**

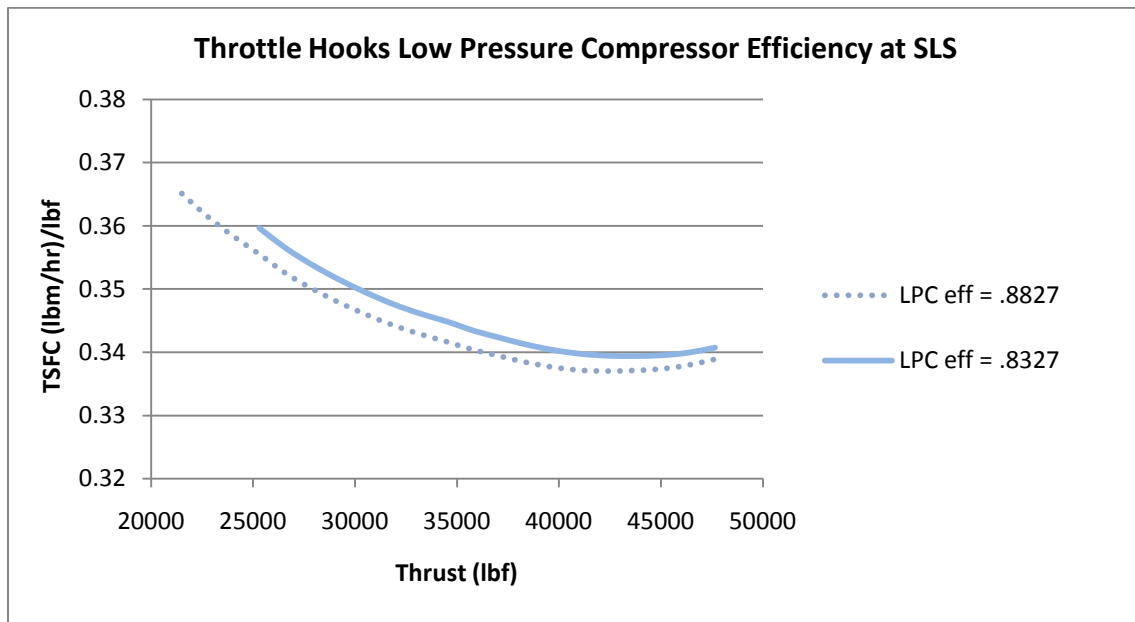


**Figure 4.19 Throttle hooks for low pressure compressor efficiency of the hybrid engine (maximum thrust)**

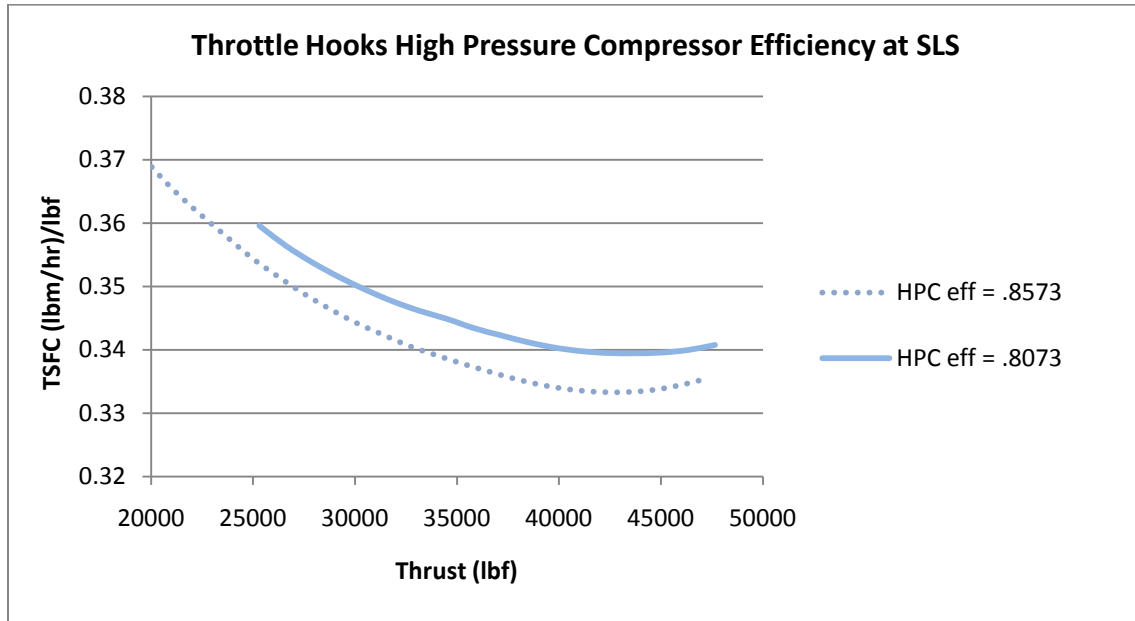


**Figure 4.20 Throttle hooks for high pressure compressor efficiency of the hybrid engine (maximum thrust)**

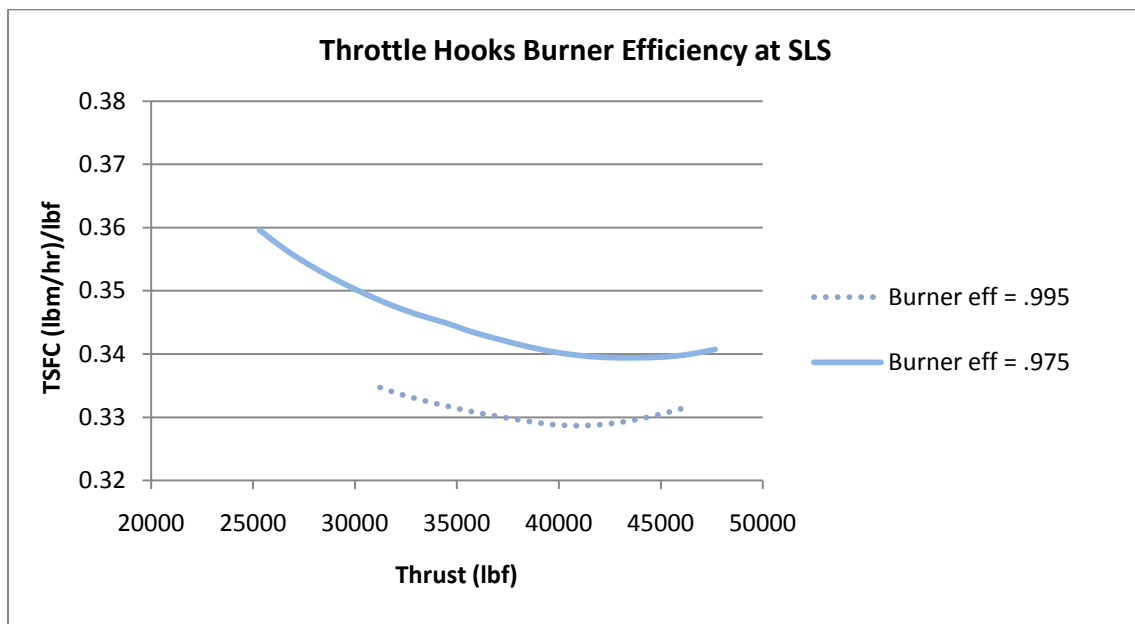


**Figure 4.21 Throttle hooks for burner efficiency of the hybrid engine (maximum thrust)**

## Parameter On-Design Choices

The design choices listed in Table 3.5 used for the analysis above are based on a parametric study performed with the turbofan model at design conditions. Since the current model was modified for off-design performance, changes in these design parameters may improve engine performance at design and/or off-design conditions.

Throttle hooks were run at SLS and cruise conditions for various on-design frequencies, purge fractions, and equivalence ratios shown in Figs. 4.22 - 4.24, respectively, to determine if changing these parameters could improve performance. Figure 4.22 indicates that a lower design frequency may improve TFSC, but at the expense of thrust range. A lower equivalence ratio yields TSFC improvements similar to that of frequency; however, a design equivalence ratio below 0.88 chokes the burner inlet and a solution cannot be converged in Fig. 4.23. The design purge fraction may yield a lower TSFC as a purge fraction of 0.75 yields a 2.2% decrease in TSFC below design value of 0.5 with the same thrust range shown in Fig. 4.24. As seen from Eq. 3.6, the mass of the purge air increases as the purge fraction increases. The increased purge fraction increases the mass flow through the tubes while decreasing the flow through the internal bypass. This results in an increase in thrust as well as TSFC, however, thrust increases more than TSFC. A thorough parametric study should be conducted to identify such design parameters as number of tubes, tube geometry, etc., that may yield better performance at design and off-design conditions.



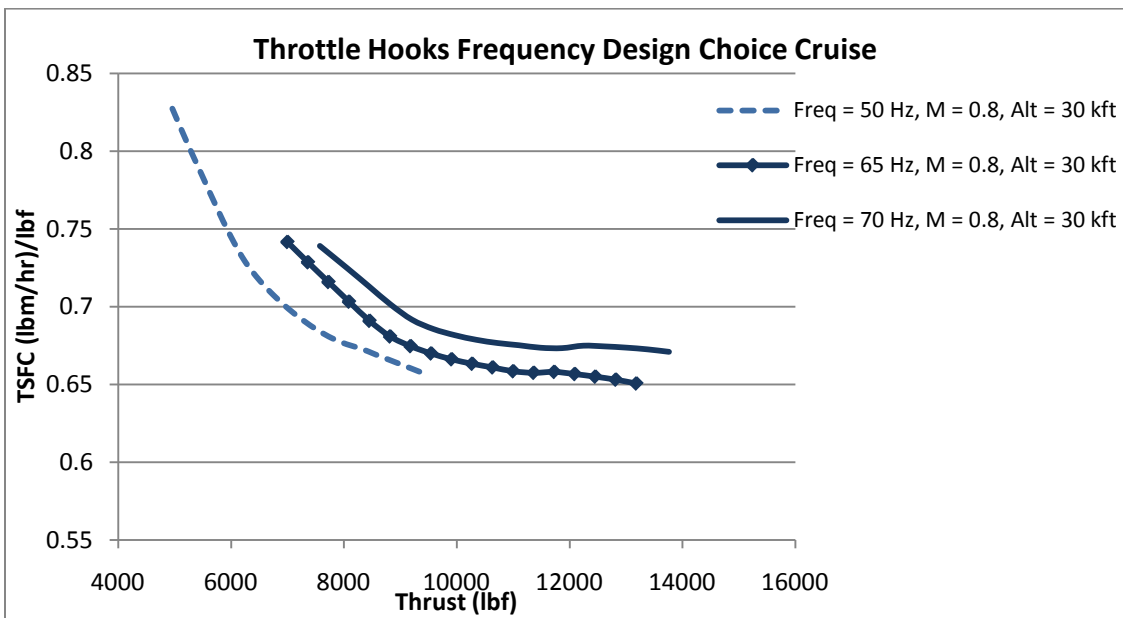
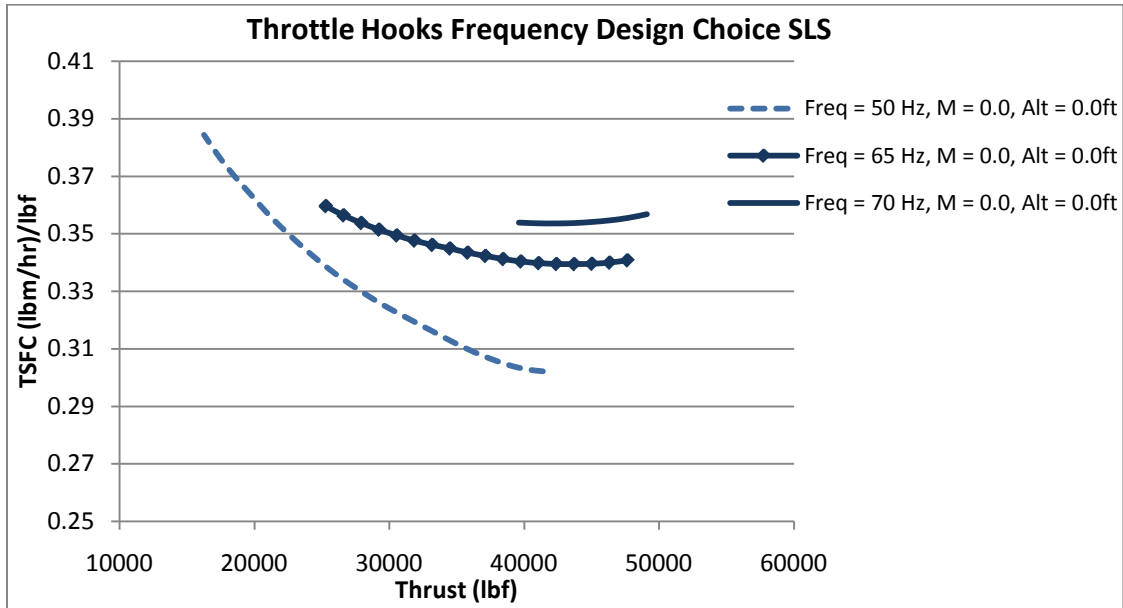


**Figure 4.22 Throttle hooks at various design frequencies at SLS and cruise (M = 0.8, Alt = 30,000 ft)**

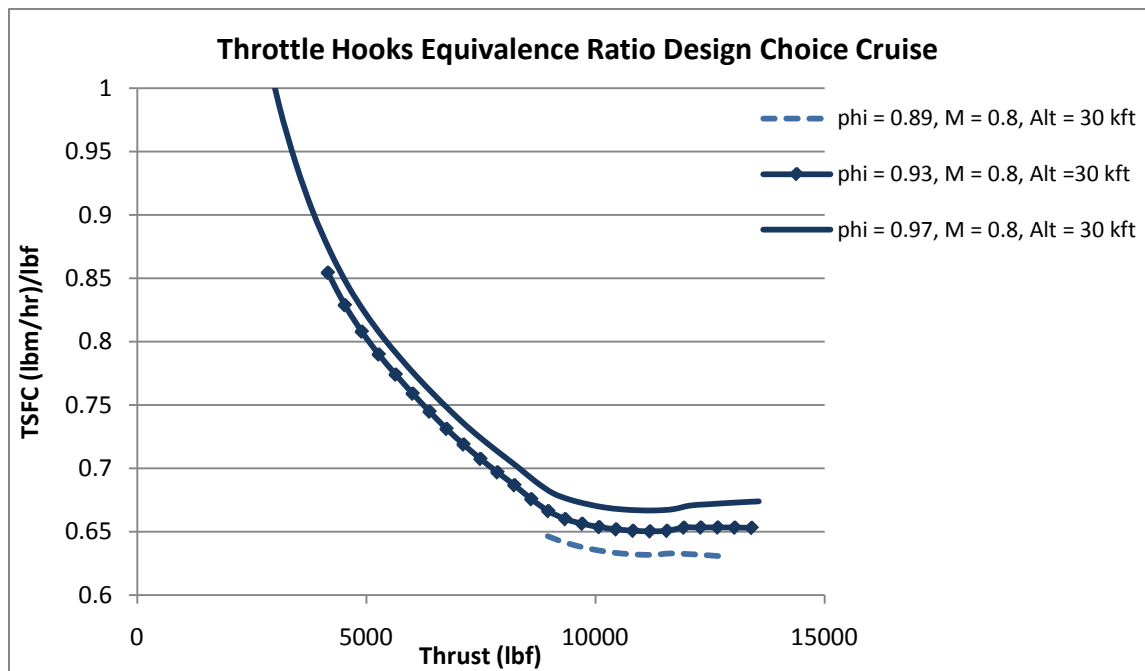
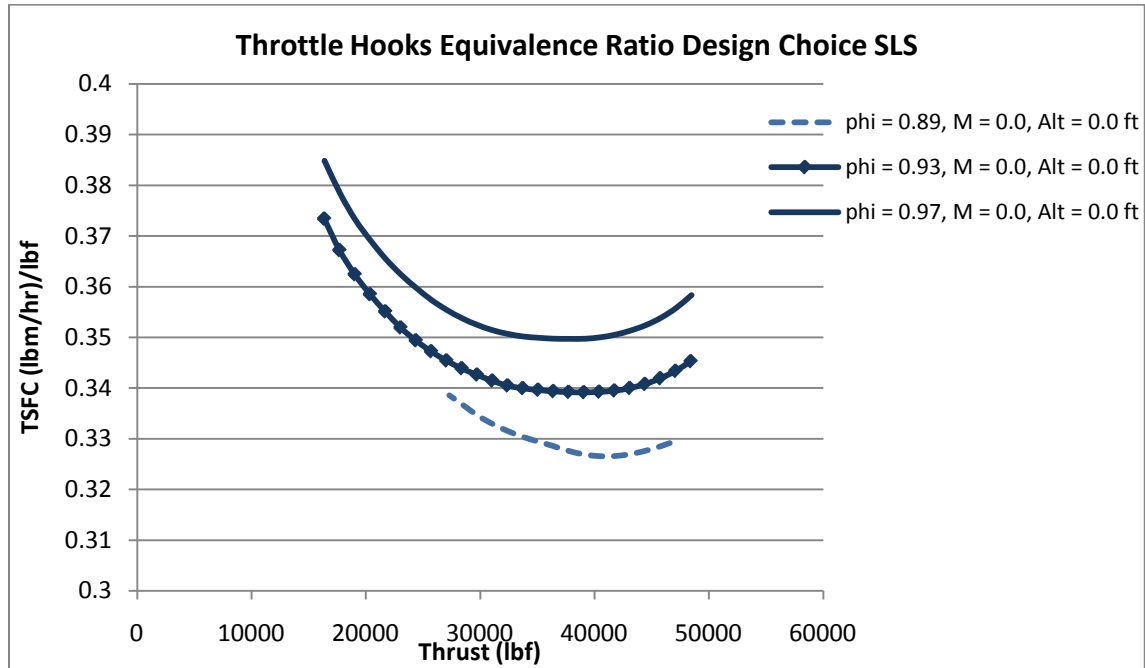


**Figure 4.23 Throttle hooks at various design equivalence ratios at SLS and cruise ( $M = 0.8$ ,  $Alt = 30,000$  ft)**

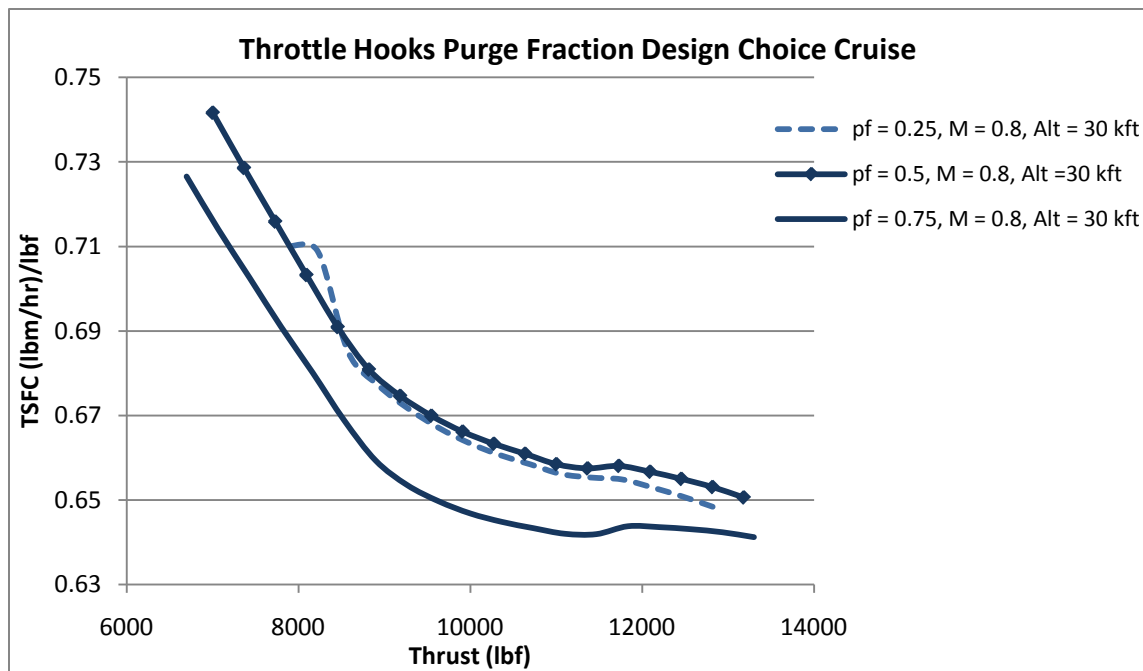
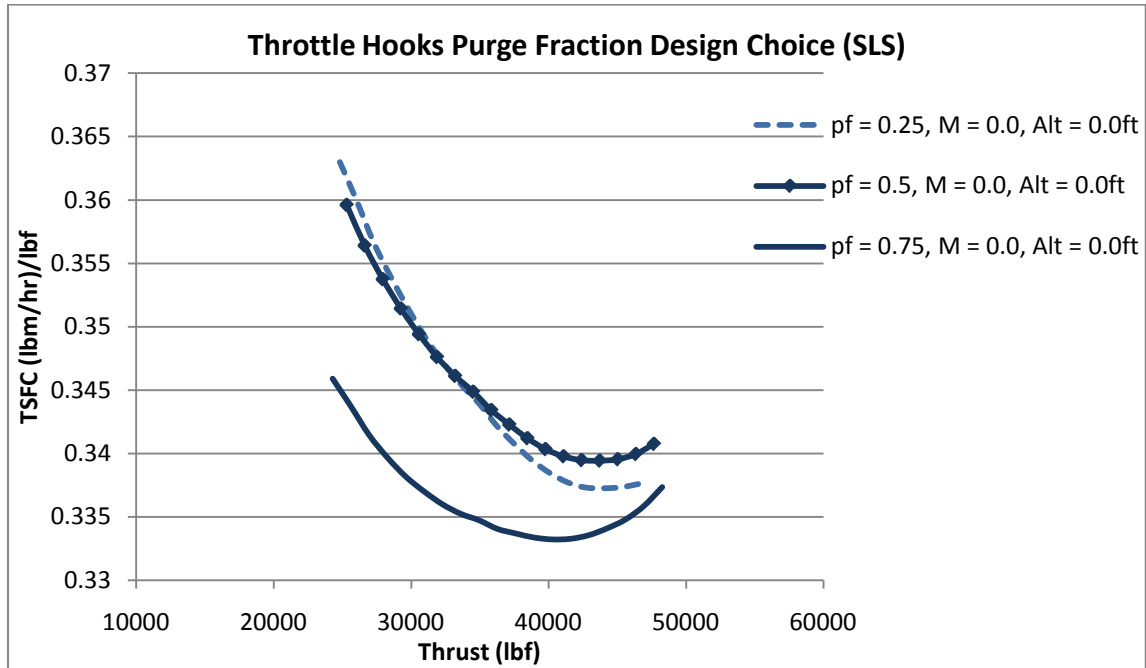


**Figure 4.24 Throttle hooks at various design purge fractions at SLS and cruise ( $M = 0.8$ ,  $\text{Alt} = 30,000\text{ ft}$ )**

## **V. Conclusions and Recommendations**

### **Introduction**

A turbofan engine with a pulsed detonation combustor may have performance gains over a conventional turbofan, specifically in the areas of thrust and thrust specific fuel consumption. Research (Andrus, 2007) has shown that at design conditions, the hybrid engine may allow an 8.0% decrease in TSFC while maintaining thrust. The objective of this work was to develop a hybrid engine model with a pulsed detonation combustor to run off-design in NPSS, and to evaluate the performance of the hybrid engine at various off-design conditions.

### **Hybrid Turbofan Engine Off-Design Performance**

To determine the performance of the hybrid turbofan engine, the model was run over a range of off-design conditions, at various Mach numbers, altitudes, and fill fractions, and compared to that of the baseline engine. Equivalence ratio, frequency, and fill fraction were all potential parameters to be used to throttle the hybrid engine. After performing an operating limit analysis on the hybrid engine, it was discovered that at constant equivalence ratio, the aircraft has a maximum operating altitude of 13,000 ft. In order for the hybrid engine to operate at realistic cruising altitudes, the equivalence ratio was adjusted until the maximum thrust for the given operating condition was reached. This allowed for a maximum engine operating envelope of  $M = 2.2$ , and  $Alt = 80,000$  ft.

The estimated aircraft flight envelope resulted in a maximum altitude of 38,000 ft. This is less than that of an aircraft with a conventional burner, but acceptable for flight.

Frequency or fill fraction could have been chosen as the independent throttling parameter, but it was decided that frequency would remain fixed and that fill fraction would be throttled for this model. Results indicate that adjusting either of these parameters can reduce the TSFC at any thrust level to roughly that of the baseline engine and slightly lower at some thrust levels, particularly at cruise conditions. These results are significant as incorporating hybrid PDEs into aircraft may save fuel costs.

## **Recommendations**

The hybrid model described in this research has shown to yield performance gains over a conventional engine, but not without limitations. The engine yields its lowest TSFC at maximum thrust which occurs when the internal bypass bleed is zero. The thrust range is limited due to the internal bypass of the PDC. The model could also not be run at fill fractions greater than one due to limitations of the internal bypass. Modifying the burner architecture to eliminate the internal bypass to accommodate fill fractions greater than one may be considered. This modification would also eliminate the need for an internal mixer, thus increasing the pressure of the flow exiting the PDC. Should the internal bypass remain in the PDC, the static pressure entering MIX39 can be controlled by decreasing the area of the duct into the mixer. Such a valve could allow for better engine performance as all flow would be maintained within the PDC. Throttling frequency as well as fill fraction may result in gains. Additionally, distributing all of the

bleed flow from the internal bypass into MIX 40 immediately preceding the high pressure turbine may result in better performance than splitting the bleed flow equally between MIX40 and MIX44. A boost pump should also be implemented to increase the pressure of the internal bleed flow into MIX40 due to the pressure increase of the flow exiting the PDC. Design parameters such as frequency, purge fraction, equivalence ratio, and tube geometry affect off-design performance and a complete parametric study should be performed to obtain the design parameters which yield the optimal design and off-design performance.

## Appendix A. Derivation for Ideal PDE Cycle Thermodynamics

This is a derivation of the entropy rise, thermal efficiency, and Chapman-Jouguet Mach number according to the Heiser and Pratt thermodynamics used in this thesis (Shapiro, 1953:193).

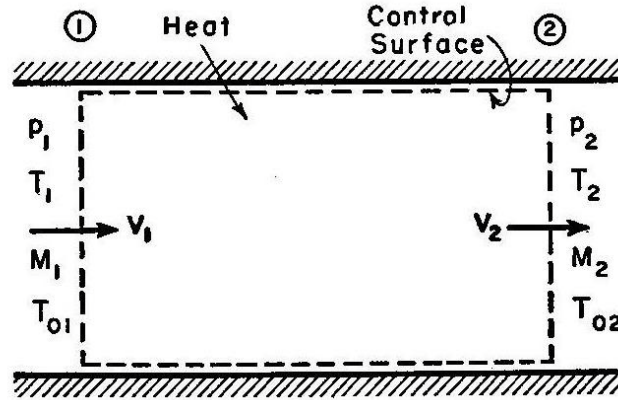


Figure A.1

Consider the flow through a control volume of Fig A.1. The continuity equation for constant area is

$$\frac{\rho_2}{\rho_1} = \frac{V_1}{V_2} \quad (\text{A.1})$$

The momentum equation is

$$p_1 - p_2 = \dot{m} / A (V_2 - V_1)$$

and noting for a perfect gas  $\rho V^2 = \gamma p M^2$ , this may be arranged to give

$$\frac{p_2}{p_1} = \frac{1 + \gamma M_1^2}{1 + \gamma M_2^2} \quad (\text{A.2})$$

From the perfect-gas law

$$\frac{p_2}{p_1} = \frac{\rho_2}{\rho_1} \frac{T_2}{T_1} \quad (\text{A.3})$$

Inserting equations A.1 and A.2 into A.3 yields

$$\frac{T_2}{T_1} = \frac{1 + \gamma M_1^2}{1 + \gamma M_2^2} \frac{V_2}{V_1} \quad (\text{A.4})$$

From the definition of the Mach number and perfect gas

$$\frac{M_2}{M_1} = \frac{V_2}{V_1} \frac{c_1}{c_2} = \frac{V_2}{V_1} \sqrt{\frac{T_1}{T_2}} \quad (\text{A.5})$$

Using the value of  $V_2/V_1$  from Eq. A.5, Eq. A.4 becomes

$$\frac{T_2}{T_1} = \frac{M_2^2}{M_1^2} \frac{(1 + \gamma M_1^2)^2}{(1 + \gamma M_2^2)^2} \quad (\text{A.6})$$

From the energy equation

$$T_0 = T + \frac{V^2}{2c_p} = T \left( 1 + \frac{V^2}{2c_p T} \right) = T \left( 1 + \frac{\gamma - 1}{2} M^2 \right)$$

or

$$\frac{T_{02}}{T_{01}} = \frac{T_2}{T_1} \frac{1 + \frac{\gamma - 1}{2} M_2^2}{1 + \frac{\gamma - 1}{2} M_1^2} \quad (\text{A.7})$$

Elimination of  $T_2/T_1$  from Eqs. A.6 and A.7 yields



$$\frac{T_{02}}{T_{01}} = \frac{M_2^2}{M_1^2} \frac{(1 + \gamma M_1^2)^2}{(1 + \gamma M_2^2)^2} \frac{1 + \frac{\gamma-1}{2} M_2^2}{1 + \frac{\gamma-1}{2} M_1^2} \quad (\text{A.8})$$

Setting  $M_1=1$  and  $M_2=M_{CJ}$  (Shapiro, 1953:195), Eq. A.6 becomes

$$\frac{T_2}{T_1} = \frac{(1 + \gamma)^2 M_{CJ}^2}{(1 + \gamma M_{CJ}^2)^2} \quad (\text{A.9})$$

Eq. A.8 becomes

$$\frac{T_{02}}{T_{01}} = \frac{2(\gamma+1)M_{CJ}^2 \left(1 + \frac{\gamma+1}{2} M_{CJ}^2\right)^2}{(1 + \gamma M_{CJ}^2)^2}$$

Similarly,

$$\begin{aligned} \frac{V_2}{V_1} &= \frac{\rho_1}{\rho_2} = \frac{(\gamma+1)M_{CJ}^2}{1 + \gamma M_{CJ}^2} \\ \frac{p_2}{p_1} &= \frac{\gamma+1}{1 + \gamma M_{CJ}^2} \end{aligned} \quad (\text{A.10})$$

From the definition of isentropic stagnation pressure

$$\frac{p_0}{p} = \left(1 + \frac{\gamma-1}{2} M^2\right)^{\frac{\gamma}{\gamma-1}}$$

thus,

$$\frac{p_{02}}{p_{01}} = \frac{p_2}{p_1} \frac{\left(1 + \frac{\gamma-1}{2} M_2^2\right)^{\frac{\gamma}{\gamma-1}}}{\left(1 + \frac{\gamma-1}{2} M_1^2\right)^{\frac{\gamma}{\gamma-1}}} \quad (\text{A.11})$$

Substituting Eq. A.10 and  $M_1=1$  and  $M_2=M_{CJ}$  into Eq. A.11 yields

$$\frac{p_{02}}{p_{01}} = \frac{\gamma+1}{1+\gamma M_{CJ}^2} \frac{2 \left(1 + \frac{\gamma-1}{2} M_{CJ}^2\right)^{\frac{\gamma}{\gamma-1}}}{\gamma+1}$$

Defining the change in entropy as

$$\frac{s_2 - s_1}{c_p} = \ln \left( \frac{T_2 / T_1}{\left(p_2 / p_1\right)^{\frac{\gamma-1}{\gamma}}} \right) \quad (\text{A.12})$$

and substituting Eq. A.9 and A.10 into Eq. A.12 yields the Heiser and Pratt change in entropy:

$$\frac{s_4 - s_3}{c_p} = -\ln \left[ M_{CJ}^2 \left( \frac{\gamma+1}{1+\gamma M_{CJ}^2} \right)^{\frac{\gamma+1}{\gamma}} \right]$$

Deriving thermal efficiency

$$\begin{aligned}
 q_{rej} &= h_{10} - h_0 = c_p (T_{10} - T_0) = c_p T_0 \left[ \exp\left(\frac{s_{10} - s_0}{c_p}\right) - 1 \right] \\
 &= c_p T_0 \left[ \exp\left(\frac{s_4 - s_3}{c_p}\right) - 1 \right] \\
 &= c_p T_0 \left[ \frac{1}{M_{CJ}^2} \left( \frac{1 + \gamma M_{CJ}^2}{\gamma + 1} \right)^{\frac{\gamma+1}{\gamma}} - 1 \right]
 \end{aligned}$$

and since

$$\eta_{th} = 1 - \frac{q_{rej}}{q_{add}} \quad \text{and} \quad \bar{q} = \frac{q_{add}}{c_p T_0}$$

the thermal efficiency becomes

$$\eta_{th} = 1 - \left[ \frac{1}{M_{CJ}^2} \left( \frac{1 + \gamma M_{CJ}^2}{\gamma + 1} \right)^{\frac{\gamma+1}{\gamma}} - 1 \right] / \bar{q}$$

To define  $M_{CJ}$  we first rearrange the mass and momentum equations

$$p_1 + \rho_1 V_1^2 = p_2 + \frac{\rho_1^2}{\rho_2} V_1^2$$

to yield

$$\begin{aligned}
 V_1^2 &= v_1^2 \left( \frac{p_2 - p_1}{v_1 - v_2} \right) \\
 V_2^2 &= v_2^2 \left( \frac{p_2 - p_1}{v_1 - v_2} \right)
 \end{aligned}$$

The energy equation  $h_1 + \frac{1}{2} V_1^2 = h_2 + \frac{1}{2} V_2^2$  may be rearranged with the momentum

equation to yield

$$h_2 - h_1 = \frac{1}{2}(V_1^2 - V_2^2)$$

Substituting the mass balance equation we get the Hugoniot relation:

$$h_2 - h_1 = \frac{1}{2}(p_2 - p_1)(v_1 + v_2) \quad (\text{A.13})$$

Assuming a perfect gas and  $h_1 = c_p T$ ,  $h_2 = c_p T_2 - q_{add}$  we get

$$\frac{\gamma}{\gamma - 1}(p_2 v_2 - p_1 v_1) - q_{add} = \frac{1}{2}(p_2 - p_1)(v_2 + v_1) \quad (\text{A.14})$$

The expression for the Mach number of the Rayleigh process at station 1 can be written as

$$M_1^2 = \frac{v_1}{\gamma p_1} \left( \frac{p_2 - p_1}{v_1 - v_2} \right) \quad (\text{A.15})$$

Solving eqs. A.13 and A.14 to determine the volume and pressure ratios in terms of approaching Mach number yields

$$\frac{V_2}{V_1} = \frac{1 + \gamma M_1^2 \pm \sqrt{(M_1^2 - 1)^2 - 2(\gamma + 1)(\gamma - 1)M_1^2 q_{add} / a_1^2}}{(\gamma + 1)M_1^2}$$

$$\frac{p_2}{p_1} = \frac{1 + \gamma M_1^2 \mp \sqrt{(M_1^2 - 1)^2 - 2(\gamma + 1)(\gamma - 1)M_1^2 q_{add} / a_1^2}}{(\gamma + 1)}$$

For any  $M_1$  the value of  $q_{add}$  is found by setting the quantity under the radical equal to zero. This yields

$$\frac{\gamma - 1}{a_1^2} q_{add} = \frac{(M_{CJ}^2 - 1)^2}{2(\gamma + 1)M_{CJ}^2}$$

Solving for  $M_{CJ}$  with  $\tilde{q} = c_p T_0$  and  $\psi = q_{rej} / q_{add}$  yields

$$M_{CJ}^2 = (\gamma + 1)(\tilde{q} / \psi) + 1 + \sqrt{[(\gamma + 1)(\tilde{q} / \psi) + 1]^2 - 1} \quad (\text{A.16})$$

## Appendix B. Model File for Baseline Turbofan Engine

```
//
//-----
// TURBOJET ENGINE BUILD          |
//                                |
// BUILD AND VERIFY TURBOJET      |
//                                |
// DESIGN POINT ONLY              |
//                                |
//-----
// TURBOJET CONFIGURATION
//-----

cout << "\t-----\n"
    << "\t Baseline High Bypass Turbofan built to match AEDsys \n"
    << "\t-----\n\n";

// Set model name
MODELNAME = "Baseline HBTF CmpareAEDsys.mdl with mixers";
//-----
// set the thermo package
//-----
    setThermoPackage("GasTb1");
// setThermoPackage("Janaf");

//-----
// include the standard interpreted things
//-----
#include <InterpIncludes.ncp>
#include "ncp.view"
// #include "bleed_macros.fnc"
// #include "NewDuct.int"

//-----
// #include the definition file for the user defined engine
// performance component
//-----
#include "EngPerf.cmp" ;

//-----
// MODEL DEFINITION
```

```

//-----
// ##### FLIGHT CONDITIONS #####
Element FlightConditions AMBIENT {
    // Specify Design conditions
    alt = 0.0;           // design altitude (ft)
    MN = 0.01;          // design Mach number
    // Ps = 14.696;      // ambient pressure (psia)
    // Ts = 59.0;        // ambient temperature (F)
    W = 1500.00;         // design mass flow (lbm/s)
}

//##### Inlet #####
Element Inlet INLET {

    eRamBase = 0.995; //Ram Recovery Factor?
}

// ##### Splitter #####
Element Splitter SPLIT {
    BPR = 8.0; // Bypass Ratio

}

// ##### FAN #####
// here the fan represents the outer portion of the Low pressure
// compressor spool
Element Compressor Fan21 {
    // // use these lines if no compressor map is imlemented
    // effDes = 0.88042; //0.882886;
    // PRdes = 1.56;

    // use these lines if compressor map is used...
    #include "fan.map" ; //Compressor sub-element map
    S_map.effDes = 0.8827; //0.88289;
    S_map.PRdes = 1.56;
}

// ##### Bypass Duct/ Nozzle/ Sink #####
Element Duct Bypass13 {
    // AEDsys assumes flow in bypass duct is isentropic
    // dPqPbase = 0.015; // pressure loss through the bypass duct
}

```

```

Element Nozzle Noz18 {
    // Cfg = 0.995;
    dPqP = 1.0-0.98; // pressure loss from nozzle inlet to throat
    PsExhName = "AMBIENT.Fl_O.Ps";

    // AEDsys uses a fixed convergent nozzle for bypass exit
    switchType = "CONIC";
}

Element FlowEnd NozSink19 {

}

// ##### Low Pressure Compressor #####
Element Compressor LPC20 {
    // // use these lines if no compressor map is implemented
    // effDes = 0.88042; // set the design point isentropic efficiency
    // PRdes = 1.56;

    // use these lines if compressor map is used...
    #include "lpc.map";
    S_map.effDes = 0.8827; // set design point isentropic efficiency
    S_map.PRdes = 1.56;

}

// ##### High Pressure Compressor #####
Element Compressor HPC25 {
    // // use these lines if no compressor map is implemented
    // effDes = 0.85755; // set the design point isentropic efficiency
    // PRdes = 16.66667;

    // use these lines if compressor map is used...
    #include "hpc.map" ; // Compressor sub element map
    S_map.effDes = 0.8573 ; // design point isentropic efficiency
    S_map.PRdes = 16.66667 ; // Set the pressure ratio at design

}

// ##### Bleed starting point #####
Element Bleed BLD3 {
    // ===== BLEEDS =====

```



```

// Three Bleeds are taken off of the back side of the
// High pressure Compressor
BleedOutPort BL_Cool_301 {
    fracW = 0.05; // mass flow (5% for cooling turbine)
}
BleedOutPort BL_Cool_302 {
    fracW = 0.05; // mass flow (5% for cooling turbine)
}
BleedOutPort BL_Env_303 {
    fracW = 0.01; // mass flow fraction (1% bleed)
}
}

// ##### Fuel #####
Element FuelStart FUEL32{
    LHV = 18400; // BTU/lbm - Lower Heating Value of the fuel -
    // default is 18400 BTU/lbm
}

// ##### Burner #####
Element Burner BRN36{
    effBase = 0.995; // component efficiency
    dPqPBase = 1.0 - 0.96; //pi b = 1.0-(dP/P) pressure drop across burner

    // Change from burner default of FAR to TEMPERATURE
    switchBurn = TEMPERATURE;

    // Total temp. at exit (degrees Rankine) || not to be used with FAR
    TtCombOut = 2900.0;
}

// ##### Bleed Mixer/IGV #####
Element Bleed MIX40 {
    BleedInPort BIn40{
        Pscale = 0.88;
    }
}

// ##### HP Turbine #####

```

```

Element Turbine HPT41 {
    #include "hpt.map"; //High Pressure Turbine Map
    S_map.effDes = 0.9057;//0.90555;0.91075;

// InterStageBleedInPort BIIIn41 {
//         Pfract = 1;    //force the bleed to come in at entrance
// }

}
// ##### Bleed Mixer #####
Element Bleed MIX44 {
    BleedInPort BIIIn44{
        Pscale = 0.68;
    }

    //         FI_I1.MN = .29;
// BI_I1.Pscale = 0.92; // Scale pressure so that the pressure ratio across mixer = 1
// BI_I1.MN = 0.31;
}

// ##### LP Turbine #####
Element Turbine LPT45 {
    #include "lpt.map" //Low Pressure Turbine Map
    S_map.effDes = 0.9084;//0.90836;0.90906;

// InterStageBleedInPort BIIIn44 {
//         Pfract = 1.;    // force bleed to come in at turbine entrance
// }

}

// ##### Nozzle #####
Element Nozzle Noz8 {
    //Cfg = 0.995;
    //Cv = 0.985;
    dPqP = 1.0-0.985;
    PsExhName = "AMBIENT.FI_O.Ps";
    switchType = "CONIC"; // AEDsys uses a fixed convergent nozzle for core exit
}

// ##### Terminate Flow #####

```

```

Element FlowEnd Sink39 {
// BleedInPort BIn44{
//          Pscale = 0.96;
// }
// sink for the environmental bleed...
}

Element FlowEnd NozSink9 {
// sink for the core airflow
}

//
%%%%%%%%%%%%%%
%%%%%%%%%%%%%%
// Put shafts in the model
//
%%%%%%%%%%%%%%
%%%%%%%%%%%%%%

##### Low-Pressure Shaft #####
Element Shaft LPShf {
    ShaftInputPort LPC, FAN, LPT ;
    Nmech = 2000.0;
    inertia = 1.0; // inertia is only needed for transient analysis
    HPX = 0.0 ;// +131.; //+92.30; // Horsepower extracted from the shaft hp ( = 325.7
kW)
    fracLoss = 1.0 - 0.99; // Fractional loss on positive port torque (1.0 - eta_m)
}

##### High Pressure Shaft #####
Element Shaft HPShf {
    ShaftInputPort HPT, HPC ;
    Nmech = 11000.0;
    inertia = 1.0;
    HPX = 143.178 ;//+372; // +415.; // +400.0; // Horsepower extracted from the shaft hp
( = 105.7 kW)/ eta m ( = 0.99)
    fracLoss = 1.0 - 0.99; // Fractional loss on positive port torque (1.0 - eta_m)
//cout << inertia.unitsunits <<endl;
//quit();
}

##### Engine Performance #####
Element EngPerf PERF{

```

```

}

//
// -----
//           Flow Connections           //
//                                     //
//           This is where the flow is defined for the engine //
// -----
//

##### Ambient to Splitter #####
linkPorts( "AMBIENT.Fl_O",      "INLET.Fl_I",      "FL0" );
linkPorts( "INLET.Fl_O",      "SPLIT.Fl_I", "FL1" );

##### Bypass air #####
linkPorts( "SPLIT.Fl_O2",      "Fan21.Fl_I",      "FLb2" );
linkPorts( "Fan21.Fl_O",      "Bypass13.Fl_I",      "FLb3" );
linkPorts( "Bypass13.Fl_O",    "Noz18.Fl_I",      "FLb7" );
linkPorts( "Noz18.Fl_O",      "NozSink19.Fl_I",      "FLb8" );

##### Core Air Flow #####
linkPorts( "SPLIT.Fl_O1",      "LPC20.Fl_I",      "FL2" );
linkPorts( "LPC20.Fl_O",      "HPC25.Fl_I",      "FL25" );
linkPorts( "HPC25.Fl_O",      "BLD3.Fl_I",      "FL3" );
linkPorts( "BLD3.Fl_O",      "BRN36.Fl_I",      "FL31" );
##### Fuel Flow #####
linkPorts( "FUEL32.Fu_O",      "BRN36.Fu_I",      "Fu3" );
linkPorts( "BRN36.Fl_O",      "MIX40.Fl_I",      "FL4");
linkPorts( "MIX40.Fl_O",      "HPT41.Fl_I",      "FL41" );
linkPorts( "HPT41.Fl_O",      "MIX44.Fl_I",      "FL44");
linkPorts( "MIX44.Fl_O",      "LPT45.Fl_I",      "FL45" );
linkPorts( "LPT45.Fl_O",      "Noz8.Fl_I",      "FL7");
linkPorts( "Noz8.Fl_O",      "NozSink9.Fl_I",      "FL8" );

##### Bleed port linkage #####
//linkBleedCB("BLD3", "MIX40", 0.05, 1.0, 1.0, "BL 1");
//linkBleedCB("BLD3", "MIX44", 0.05, 1.0, 1.0, "BL 2");
//linkBleedCB("BLD3", "Sink39", 0.01, 1.0, 1.0, "BL 3");
linkPorts( "BLD3.BL_Cool_301",  "MIX40.BIn40",      "BL 1");
linkPorts( "BLD3.BL_Cool_302",  "MIX44.BIn44",      "BL 2");
linkPorts( "BLD3.BL_Env_303",    "Sink39.Fl_I", "BL 3");

$$$$$$$$$$$$$$$$$$$$$$$$$$$$$$$$$$$$$$$$$$$$$$$$$$$$$$$$$$$$$$$$
//           Mechanical (Shaft) connections

```



## Appendix C. Model File for Hybrid Turbofan Engine

```
//
//-----
//  HYBRID TURBOFAN ENGINE |
//                          |
//-----
//  CONFIGURATION
//-----

cout << "\t-----\n"
      << "\t Hybrid Pulsed Detonation Combustor High Bypass Turbofan ... \n"
      << "\t-----\n\n";
// Set model name
MODELNAME = "PDC HBTF"; //Pulsed Detonation Combustor High Bypass
Turbofan";
//-----
// set the thermo package
//-----
setThermoPackage("GasTb1");
// setThermoPackage("FPT");

//-----
// include the standard interpreted things
//-----
#include <InterpIncludes.ncp>
#include "ncp.view"

//-----
// #include the definition file for the user defined engine
// performance component
//-----
#include "EngPerf.cmp" ;

//-----
// MODEL DEFINITION
//-----
// ##### FLIGHT CONDITIONS #####
Element FlightConditions AMBIENT {
    // Specify Design conditions
    alt = 0.0;    // design altitude (ft)
    MN = 0.01;    // design Mach number
```

```

// Ps = 14.696;      // ambient pressure (psia)
// Ts = 59.0; // ambient temperature (F)
W = 1500.00;          // design mass flow (lbm/s)
}

##### Inlet #####
Element Inlet INLET {

    eRamBase = .995; //Ram Recovery Factor? //.995
}

// ##### Splitter #####
Element Splitter SPLIT {
    BPR = 8.0; // Bypass Ratio

}

// ##### FAN #####
// here the fan represents the outer portion of the Low pressure
// compressor spool
Element Compressor Fan21 {
// // use these lines if no compressor map is implemented
// effDes = 0.88042; //0.882886;
// PRdes = 1.56;

    // use these lines if compressor map is used...
    #include "fan.map" ; //Compressor sub-element map
    S_map.effDes = 0.8827; //0.88289; //.8827
    S_map.PRdes = 1.56;
}

// ##### Bypass Duct/ Nozzle/ Sink #####
Element Duct Bypass13 {
    // AEDsys assumes flow in bypass duct is isentropic (p109, #9)
    // dPqPbase = 0.015;      // pressure loss through the bypass duct
}

Element Nozzle Noz18 {
    // Cfg = 0.995;
    dPqP = 1.0-0.98; // pressure loss from nozzle inlet to throat
    PsExhName = "AMBIENT.Fl_O.Ps";
}

```

```

    switchType = "CONIC"; // AEDsys uses a fixed convergent nozzle for bypass exit
}

Element FlowEnd NozSink19 {

}

// ##### Low Pressure Compressor #####
Element Compressor LPC20 {
// // use these lines if no compressor map is implemented
// effDes = 0.88042; // set the design point isentropic efficiency
// PRdes = 1.56;

// use these lines if compressor map is used...
#include "lpc.map";
S_map.effDes = 0.8827; // 0.88289;    set the design point isentropic
//efficiency//.8827
S_map.PRdes = 1.56;

}

// ##### High Pressure Compressor #####
Element Compressor HPC25 {
// // use these lines if no compressor map is implemented
// effDes = 0.85755; //0.8855338;    // set the design point isentropic efficiency
// PRdes = 16.66667;

// use these lines if compressor map is used...
#include "hpc.map" ; // Compressor sub element map
S_map.effDes = 0.8573 ; //0.857535 ; set the maps design point
//isentropic efficiency//.8573
S_map.PRdes = 16.66667 ; // Set the pressure ratio at design

}

// ##### Bleed starting point #####

Element Bleed BLD3 {
// ===== BLEEDS
=====
// Three Bleeds are taken off of the back side of the High pressure Compressor
BleedOutPort BL_Cool_301 {

```



```

        //fracBldWork = 1.0; // work fraction where bleed is taken
        //fracBldP = 1.0;    // Pressure fraction where bleed is taken
        fracW = 0.05;      // mass flow (5% for cooling turbine)
    }
    BleedOutPort BL_Cool_302 {
        //fracBldWork = 1.0; // work fraction (dhb/dh)
        //fracBldP = 1.0;    // Pressure fraction (dPb/dP)
        fracW = 0.05; // mass flow (5% for cooling turbine)
    }
    BleedOutPort BL_Env_303 {
        //fracBldWork = 1.0; // (dhb/dh) work fraction - closely tied with
pressure fraction...
        //fracBldP = 1.0;    // Pressure Fraction (dPb/dP)
        fracW = 0.01; // mass flow fraction (1% bleed)
    }
}

// ##### Fuel #####

Element FuelStart FUEL32{

    LHV = 18400;    // BTU/lbm - Lower Heating Value of the fuel -
        // default is 18400 BTU/lbm

}

// ##### Burner #####

// Element Burner BRN36{
//   effBase = 0.995; // component efficiency ... ??
//   dPqPBase = 1.0 - 0.96; //0.04;    // pi b - pressure drop across burner... ?? (dP/P)
//
//   switchBurn = TEMPERATURE; // Change from burner defaults using Fuel-air Ratio
(FAR) to TEMPERATURE
//   TtCombOut = 2900.0;    // Total temperature at exit (degrees Rankine) || not to be
used with FAR
//
//   // or use the default FAR and define what the FAR is...
//   // FAR = 0.02282;    // Fuel-to-Air ratio; not to be used with TtCombOut,
Wfuel, etc.
//
// }
#include "PDC_burner_bleed.int"

```

```

Element PulseDetonationCombustor BRN36{
    effBase = .995;    // burning efficiency//.995
    dPqPBase = 1.0-0.96;    // pressure loss across valves/through bypass
    switchBurn = FAR;    // set fuel-air ratio (vs equivalence ratio)
    FAR = (0.0683 * 1.00); //approximately 85% of stoichiometric conditions
    purgeFrac = 0.2;    // designate purge fraction
    fillFrac = 0.8;    // designate fill fraction
    lTube = 36;    // length of tube in inches
    n_tubes = 24;    // number of tubes
    dTube = 2.0;    // inside diameter of tubes
    tCycle = .016776271641; // cycle time
    flowby = 1;    // percentage of internal bypass flow into mixer39
}
// ##### Wall heat exchange #####
// *** not uses in the current model ***
//Element Wall WALL38{
// Ahx1 = PI*36; // area of wall inside PDT
// Ahx2 = PI*36*1.02; // area that bypass flow sees
// ChxDes1 = 0.7; // heat transfer film coefficient - blind guess...
// ChxDes2 = 0.7; //
// CpMat = 0.1481; //specific heat of material (titanium @ 2160 R)
// // # tubes pi/4 length oD iD(in) rho(lbm/ft^3) Titanium
// massMat = 36.*(PI/4.*(36./12.)*(2.25**2-2.**2)/144.)*280.93; //mass of material in
lbm
//
//}

// ##### Internal Bypass Bleed #####

Element Bleed BLD4 {
    // ===== BLEEDS
    =====
    // Three Bleeds are taken from the internal bypass of the PDC
    BleedOutPort BL_Cool_304 {
        //fracBldWork = 1.0; // work fraction where bleed is taken
        //fracBldP = 1.0;    // Pressure fraction where bleed is taken
        fracW = 0.499;    // mass flow (50% for cooling turbine)
    }
    BleedOutPort BL_Cool_305 {
        //fracBldWork = 1.0; // work fraction (dhb/dh)
        //fracBldP = 1.0;    // Pressure fraction (dPb/dP)
        fracW = 0.499;    // mass flow (50% for cooling turbine)
    }
}

```

```

}

// ##### PDC bypass mixer/Transition to steady-state device #####
Element Mixer MIX39{
    Fl_I1.MN = .95; // Rather high MN, but it works where lower
                    // values do not...
}
// ##### Bleed Mixer/IGV #####
Element Bleed MIX40 {
    BleedInPort BIn40{
        Pscale = 0.88;
    }
    BleedInPort BIn41{
        Pscale = .88;
    }
}

// ##### HP Turbine #####
Element Turbine HPT41 {
    #include "hpt.map"; //High Pressure Turbine Map
    S_map.effDes = 0.9057;//0.90555;0.91075;//.9057

}
// ##### Bleed Mixer #####
Element Bleed MIX44 {
    BleedInPort BIn44{
        Pscale = 0.68;
    }
    BleedInPort BIn45{
        Pscale = .68;
    }
}

// ##### LP Turbine #####
Element Turbine LPT45 {
    #include "lpt.map" //Low Pressure Turbine Map
    S_map.effDes = 0.9084;//0.90836;0.90906;//.9084

```

```

}

// ##### Nozzle #####
Element Nozzle Noz8 {
    //Cfg = 0.995;
    //Cv = 0.985;
    dPqP = 1.0-0.985; // pressure loss across the nozzle
    PsExhName = "AMBIENT.FI_O.Ps";
    switchType = "CONIC"; // AEDsys uses a fixed convergent nozzle for core exit
}

// ##### Terminate Flow #####
Element FlowEnd Sink39 {
    // sink for the environmental bleed...
}

Element FlowEnd NozSink9 {
    // sink for the core airflow
}

Element FlowEnd NozSink1 {
    // sink for the ibypass bleed airflow
}

//
%%%%%%%%%%%%%%
%%%%%%%%%%%%%%
// Put shafts in the model
//
%%%%%%%%%%%%%%
%%%%%%%%%%%%%%

//##### Low-Pressure Shaft #####
Element Shaft LPShf {
    ShaftInputPort LPC, FAN, LPT ;
    Nmech = 2000.0;
    inertia = 1.0; // inertia is only needed for transient analysis
    HPX = 0.0 ; //+92.30; // Horsepower extracted from the shaft hp ( = 325.7 kW)
    fracLoss = 1.0-.99; // Fractional loss on positive port torque (1.0
    // - etam)1.0-.99
}

```

```

##### High Pressure Shaft #####
Element Shaft HPShf {
    ShaftInputPort HPT, HPC ;
    Nmech = 11000.0;
    inertia = 1.0; // inertia is only needed for transient analysis
    HPX = 143.178 ; // +400.0; // Horsepower extracted from the shaft hp ( = 105.7 kW)/
    eta m ( = 0.99)
    fracLoss = 1.0 - .99; // Fractional loss on positive port torque (1.0 - eta_m)
    //1.0-.99
}

##### Engine Performance #####
Element EngPerf PERF{
}

//
// _____
//          Flow Connections          //
//                               //
//    This is where the flow is defined for the engine //
// _____ //
//

##### Ambient to Splitter #####
linkPorts( "AMBIENT.Fl_O",      "INLET.Fl_I",      "FL0" );
linkPorts( "INLET.Fl_O",      "SPLIT.Fl_I", "FL1" );

##### Bypass air #####
linkPorts( "SPLIT.Fl_O2",      "Fan21.Fl_I",      "FLb2" );
linkPorts( "Fan21.Fl_O",      "Bypass13.Fl_I",      "FLb3" );
linkPorts( "Bypass13.Fl_O",    "Noz18.Fl_I",      "FLb7" );
linkPorts( "Noz18.Fl_O",      "NozSink19.Fl_I",      "FLb8" );

##### Core Air Flow #####
linkPorts( "SPLIT.Fl_O1",      "LPC20.Fl_I",      "FL2" );
linkPorts( "LPC20.Fl_O",      "HPC25.Fl_I",      "FL25" );
linkPorts( "HPC25.Fl_O",      "BLD3.Fl_I",      "FL3" );
linkPorts( "BLD3.Fl_O",      "BRN36.Fl_I",      "FL31" );
##### Fuel Flow #####
linkPorts( "FUEL32.Fu_O",      "BRN36.Fu_I",      "Fu3" );
//linkPorts( "BRN36.Fl_O1", "WALL38.Fl_I1",      "Wa1" );
//linkPorts( "BRN36.Fl_O2", "WALL38.Fl_I2",      "Wa2" );
//linkPorts( "WALL38.Fl_O1",      "MIX39.Fl_I1",      "Fl39");
//linkPorts( "WALL38.Fl_O2",      "MIX39.Fl_I2",      "Fl392");

```



## Appendix D. Pulsed Detonation Combustor Code

```
#ifndef __PDC__
#define __PDC__

//*****
// * Air Force Institute of Technology
// * 2950 Hobson Way, Bldg 641
// * Wright Patterson AFB, OH 45433
// *
// * Written by Ionio Q. Andrus, Capt., USAF
// * Modified by Caitlin R. Thorn, Capt., USAF

// BASED ON "Burner.int" included in NPSS, written by~~
// * NASA Glenn Research Center
// * 21000 Brookpark Rd
// * Cleveland, OH 44135
// *
//*****

#include <InterpIncludes.ncp>

class PulseDetonationCombustor extends Element {

//-----
// ***** DOCUMENTATION *****
//-----

title = "";

description = isA() + " will calculate performance for
pulsed detonation combustor.";

usageNotes = "

The burner element performs high level burner performance
calculations. This element works with an entrance fluid and
fuel stream. It mixes the two flows together and then
performs the burn calculations. Please note that the burner
has no control over the actual fuel stream conditions--fuel type,
LHV, etc. These values are properties of the fuel flow itself
and are usually set in the FuelStart element.
```

There are two ways to specify the burner exit conditions. The first way is specify the burner fuel-to-air ratio. The second way is to set equivalence ratio. The type of input used is controlled by an option switch.

The burner tracks several different pressure losses. The first,  $dP_{qP}$ , accounts for duct friction pressure drops and approximates the pressure loss through valves. The second,  $dP_{qP}Rayleigh$ , accounts for the Rayleigh pressure drop.  $dP_{qP}Rayleigh$  is input or calculated - see switchHotLoss, an iteration is necessary since the pressure loss itself is a function of the exit conditions.

The burner also allow two efficiencies to be input. The first efficiency,  $eff$ , refers to the efficiency based on enthalpy change. The second efficiency,  $eff_{Chem}$ , refers to the efficiency based on temperature change. Both terms can be input. However, the enthalpy efficiency is always applied first.

Additionally,

The user can request a pre burner pressure loss  $dP_{qP}$ . The pressure loss calculations are performed before all the other calculations are done. This means that the combustion entrance pressure will not match the value indicated by the burner entrance.

The user can request a heat transfer  $Q_{hx}$ . The heat transfer calculations are performed after all the other calculations are done. This means that if heat transfer is being used, the exit temperature will not match the value indicated by the burner calculations.

";

background = "";

```
//-----
//  ***** SETUP VARIABLES *****
//-----
```

```
real a_dPqP {
  value = 0.0; IOstatus = "input"; units = "none";
  description = "Duct friction pressure drop adder";
}
```



```

real a_dPqPAud {
    value = 0.0; IOstatus = "unset"; units = "psia";
    description = "Audit factor adder applied to pressure ratio";
}
real a_eff {
    value = 0.0; IOstatus = "input"; units = "none";
    description = "Adiabatic efficiency adder";
}

real a_effChem {
    value = 0.0; IOstatus = "input"; units = "none";
    description = "Chemical efficiency adder";
}
real ARvalve {      // Added 15Feb2007 - IA
    value = 0.5; IOstatus = "input"; units = "none";
    description = "Ratio of valve throat area to tube cross section area";
}
real deltaS {      //Added 17Jan2007 - IA
    value = 0.0; IOstatus = "output"; units = "none";
    description = "Change in entropy due to detonation";
}
real DDT {      //Added 17Jan2007 - IA
    value = 0.0005; IOstatus = "input"; units = "none"; //seconds
    description = "Detonation to deflation time in seconds";
}
real dPqP {
    value = 0.0; IOstatus = "output"; units = "none";
    description = "Adjusted duct friction pressure drop";
}
real dPqPBase {
    value = 0.0; IOstatus = "input"; units = "none";
    description = "Duct friction pressure drop ";
}
real dPqPRayleigh {
    value = 0.0; IOstatus = "input"; units = "none";
    description = "Adjusted Rayleigh pressure drop";
}
real dTube {      //Added 17Jan2007 - IA
    value = 2.0; IOstatus = "input"; units = "none"; // inches...
    description = "Inside diameter of the detonation tube";
}
real eff {
    value = 1.0; IOstatus = "output"; units = "none";

```

```

    description = "Adjusted adiabatic burner efficiency";
}
real effBase {
    value = 1.0; IOstatus = "input"; units = "none";
    description = "Adiabatic burner efficiency, from socket ";
}
real effChem {
    value = 1.0; IOstatus = "input"; units = "none";
    description = "Adjusted chemical efficiency";
}
real effChemBase {
    value = 1.0; IOstatus = "input"; units = "none";
    description = "Chemical efficiency, from socket";
}
real eqRatio {
    value = 1.0; IOstatus = "input"; units = "none";
    description = "Equivalence ratio for fuel-air mixture";
}
real FAR {
    value = 0.0; IOstatus = "output"; units = "none";
    description = "Fuel-to-air ratio";
}
real FARDes {
    value = 0.0; IOstatus = "output"; units = "none";
    description = "Fuel-to-air ratio at design";
}
real fillFrac { //Added 17Jan2007 - IA
    value = 1.0; IOstatus = "input"; units = "none";
    description = "Fill fraction ";
}
real flowby { //added Dec09 - CT
    value = 1.0; IOstatus = "input"; units = "none";
    description = "Percentage of internal bypass into Mixer39";
}
real fuelFractV {
    value = 0.0; IOstatus = "input"; units = "none";
    description = "Fraction of the incoming flow velocity fuel
    enters the burner";
}
real iBPR { //added 17Jan2007 - IA
    value = 1.0; IOstatus = "output"; units = "none";
    description = "Bypass ratio internal to the PDC";
}

```

```

real iBPRdes {      //added 1Feb2007 - IA
    value = 1.0; IOstatus = "output"; units = "none";
    description = "Bypass ratio internal to the PDC at
design conditions";
}
real lTube { //added 17Jan2007 - IA
    value = 36; IOstatus = "input"; units = "none"; //inches??
    description = "length of the individual detonation tubes";
}
real n_tubes{ //added 17Jan2007 - IA
    value = 36; IOstatus = "input"; units = "none";
    description = "Total number of detonation tubes used
in the PDC";
}
real MCJ { //added 17Jan2007 - IA
    value = 3.0; IOstatus = "output"; units = "none";
    description = "Chapman-Jouguet Mach number of the
detonation wave.";
}
real Mvalve {      //added 15Feb2007 - IA
    value = 1.0; IOstatus = "input"; units = "none";
    description = "Mach number of flow passing through
the valve throat.";
}
real qadd{ //added 17Jan 2007- IA
    value = 0.0; IOstatus = "output"; units = "none";
    description = "Heat addition due to fuel combustion";
}
real Qhx {
    value = 0.0; IOstatus = "input"; units = "Btu/sec";
    description = "Heat loss to thermal mass storage";
}
real PqPRayleigh {
    value = 1.0; IOstatus = "output"; units = "none";
    description = "Adjusted Rayleigh pressure drop";
}
real PqPRayleighDelta {
    value = 0.0; IOstatus = "output"; units = "none";
    description = "Bounded Rayleigh pressure drop - for loop only";
}
real PqPRayleighError {
    value = 1.0; IOstatus = "output"; units = "none";
    description = "Adjusted Rayleigh pressure drop error";
}

```

```

}
real PqPRayleighMin {
  value = 0.05; IOstatus = "input"; units = "none";
  description = "Rayleigh pressure drop lower limit - for loop only";
}
real PqPRayleighStep {
  value = 0.05; IOstatus = "input"; units = "none";
  description = "Maximum step for Rayleigh pressure drop
- for loop only";
}
real PqPRayleighNew {
  value = 1.0; IOstatus = "output"; units = "none";
  description = "Previous adjusted Rayleigh pressure drop
- for loop only";
}
real purgeFrac {      //Added 17Jan2007 - IA
  value = 0.25; IOstatus = "input"; units = "none";
  description = "Purge fraction coefficient for flow";
}
real s_dPqP {
  value = 1.0; IOstatus = "input"; units = "none";
  description = "Duct friction pressure drop scalar";
}
real s_dPqPAud {
  value = 1.0; IOstatus = "unset"; units = "none";
  description = "Audit factor scalar applied to pressure ratio";
}
real s_eff {
  value = 1.0; IOstatus = "input"; units = "none";
  description = "Adiabatic efficiency scalar";
}
real s_effChem {
  value = 1.0; IOstatus = "input"; units = "none";
  description = "Chemical efficiency scalar";
}
real tauBlDn {      // Added 17Jan2007 - IA
  value = 5.; IOstatus = "input"; units="none";
  description = "Blowdown time constant";
}
real tauValveOpen {      // Added 18Jan2007 - IA
  value = 0.33333; IOstatus = "output"; units="none";
  description = "time valve open/ time cycle - from 0 to 1";
}

```

```

real tCycle{           // Added 17Jan2007 - IA
    value = 0.01; IOstatus = "output"; units = "none"; //seconds
    description = "Detonation engine cycle time (= 1/frequency)";
}
real tolRayleigh {
    value = 4e-05; IOstatus = "input"; units = "none";
    description = "Iteration tolerance on momentum pressure drop";
}
real tolWfuel {
    value = 1e-05; IOstatus = "input"; units = "none";
    description = "Iteration tolerance on temperature burn";
}
real TtCombOut {
    value = 0.0; IOstatus = "input"; units = "R";
    description = "Exit temperature";
}
real TtLast {
    value = 0.0; IOstatus = "input"; units = "R";
    description = "Previous exit temperature - for loop only";
}
real TTSSeff{           // Added 17Jan2007 - IA
    value = 1.0; IOstatus = "input"; units = "none";
    description = "Efficiency factor for the transition device.";
}
real TTSSdPqP{         // Added 17Jan2007 - IA
    value = 0.0; IOstatus = "input"; units = "none";
    description = "Change in Pressure divided by Pressure
    for transistion to steady state calculation.";
}
real tValve{           // Added 17Jan2007 - IA
    value = 0.0002; IOstatus = "input"; units = "none"; //seconds
    description = "Time for valves to open/close";
}
real Wfuel {
    value = 0.0; IOstatus = "input"; units = "lbm/sec";
    description = "Combustor fuel flow";
}
real WfuelError {
    value = 0.0; IOstatus = "input"; units = "lbm/sec";
    description = "Combustor fuel flow error";
}
real WfuelLast {
    value = 0.0; IOstatus = "input"; units = "lbm/sec";

```

```

    description = "Previous combustor fuel flow - for loop only";
}
real WfuelNew {
    value = 0.0; IOstatus = "input"; units = "lbm/sec";
    description = "Next combustor fuel flow - for loop only";
}
int countFuel {
    value = 0; IOstatus = "output";
    description = "Fuel loop counter";
}
int countFuelMax {
    value = 50; IOstatus = "input";
    description = "Fuel loop maximum counter";
}
int countRayleigh {
    value = 0; IOstatus = "output";
    description = "Rayleigh loop counter";
}
int countRayleighMax {
    value = 25; IOstatus = "input";
    description = "Rayleigh loop maximum counter";
}
int flagRayleighLossTooMuch {
    value = 0; IOstatus = "output";
    description = "If true, Rayleigh loop results in too much loss";
}
int flagRayleighChoked {
    value = 0; IOstatus = "output";
    description = "If true, Rayleigh loop results in supersonic flow";
}

// for backward compatibilty with old "aud"
FuncVariable a_dPqPAud {
    units = "none"; IOstatus = "input";
    getFunction = "get_aAud"; setFunction = "set_aAud";
}
real get_aAud() { return a_dPqPAud; }
void set_aAud(real userValue) { a_dPqPAud = userValue; }

FuncVariable s_dPqPAud {
    units = "none"; IOstatus = "input";
    getFunction = "get_sAud"; setFunction = "set_sAud";
}

```

```

real get_sAud() { return s_dPqPAud; }
void set_sAud(real userValue) { s_dPqPAud = userValue; }

//-----
// ***** OPTION VARIABLE SETUP *****
//-----

Option switchAud {
    allowedValues = { "BASE", "AUDIT" }
    description = "Determines if the audit factors are used";
    IOstatus = "input";
    trigger=TRUE;
}

Option switchBurn {
    allowedValues = { "FAR", "EQRATIO" }; //"FUEL", "WFUEL",
"TEMPERATURE", __ mod 18 Dec 2006 - IA - added "FILLFRACTION"
    description = "Switch determines if burner is running to fuel flow, FAR, or T4. Setting
option to FUEL will burn using the burner value as an input. Setting the option to
WFUEL will burn using the value coming in from the fuel station.";
    trigger=TRUE;
}

Option switchDes {
    allowedValues = { "DESIGN", "OFFDESIGN" };
    description = "Design switch";
    trigger=TRUE;
}
// input kept in for backward compatible (remove later)
Option switchHotLoss {
    allowedValues = { "INPUT", "CALCULATE", "input" };
    description = "Switch determines if the hot pressure loss is input or iterated on";
    trigger=TRUE;
}

//-----
// ***** SETUP PORTS, FLOW STATIONS, SOCKETS, TABLES *****
//-----

// FLUID PORTS
FluidInputPort Fl_I {
    description = "Incoming flow";

```

```

}

FluidOutputPort Fl_O1 {
    description = "Exiting combustion flow";
}

FluidOutputPort Fl_O2 {
    description = "Exiting bypass flow";
}

FluidOutputPort Fl_O3 {
    description = "Exiting bypass excess flow";
}
// FUEL PORTS

FuelInputPort Fu_I {
    description = "Incoming fuel flow";
}

// BLEED PORTS

// THERMAL PORTS

// MECHANICAL PORTS

// FLOW STATIONS

//_____flow stations modified 18 Dec 2006- IA
FlowStation Fl_Icomb {
    description = "Inlet station to detonation tube section
of burner (after the initial pressure loss is applied)";
}

FlowStation Fl_IcombAir {
    description = "Copy of the inlet station to detonation tube
section of burner(after the initial pressure loss is applied,
before flow is split and partitioned)";
}

FlowStation Fl_Iprg {
    description = "Station containing detonation tube purge fluid";
}

```



```

FlowStation Fl_Ocomb {
    description = "Exit station to combustion section of burner
(before thermal storage heat transfer is calculated)";
}

FlowStation Fl_Vit {
    description = "Vitiated Fluid flow station before detonation (cold)";
}
// _____----end flow station modifications

// SOCKETS

Socket S_dPqP {
    allowedValues = { "dPqPBase" };
    description = "Dry duct and valve pressure loss"; //__ mod -IA- 18 Dec 2006
    socketType = "dPqP";
}

Socket S_eff {
    allowedValues = { "effBase", "effChemBase" };
    description = "PulseDetonationCombustor adiabatic efficiency";
    socketType = "BURN_EFFICIENCY";
}

Socket S_Qhx {
    allowedValues = { "Qhx" };
    description = "Thermal storage socket";
    socketType = "HEATTRANSFER";
}

// TABLES

//-----
// ***** INTERNAL SOLVER SETUP *****
//-----

//-----
// ***** ADD SOLVER INDEPENDENTS & DEPENDENTS *****
//-----

//-----
// ***** VARIABLE CHANGED METHODOLOGY *****

```

```

//-----
void variableChanged( string name, any oldVal ) {
// Check to see what variables were changed....
// Change input/output status as necessary - IA- 18 Dec 06

if( name == "switchBurn" ) {
    if ( switchBurn == "FAR" ) {
        FAR.IOstatus = "input";
        Wfuel.IOstatus = "output";
        TtCombOut.IOstatus = "output";
        eqRatio.IOstatus = "output";
    }
//    else if ( switchBurn == "FUEL" ) {
//        FAR.IOstatus = "output";
//        Wfuel.IOstatus = "input";
//        TtCombOut.IOstatus = "output";
//    }
//    else if ( switchBurn == "WFUEL" ) {
//        FAR.IOstatus = "output";
//        Wfuel.IOstatus = "output";
//        TtCombOut.IOstatus = "output";
//    }
//_____ added 5 Feb 2007 -IA-
    else if ( switchBurn == "EQRATIO" ) {
        FAR.IOstatus = "output";
        Wfuel.IOstatus = "output";
        TtCombOut.IOstatus = "output";
        eqRatio.IOstatus = "input";
    }
//_____ end of additions -IA-
}

else if( name == "switchHotLoss" ) {
    if ( switchHotLoss == "INPUT" ) {
        dPqPRayleigh.IOstatus = "input";
    }
    else if ( switchHotLoss == "input" ){ switchHotLoss = "INPUT"; }
    else {
        dPqPRayleigh.IOstatus = "output";
    }
}

else if( name == "switchAud" ) {

```

```

    a_dPqPAud.IOstatus = "inactive";
    s_dPqPAud.IOstatus = "inactive";
    if( switchAud == "AUDIT" ) {
        a_dPqPAud.IOstatus = "input";
        s_dPqPAud.IOstatus = "input";
    }
}
}

//-----
// ***** PERFORM ENGINEERING CALCULATIONS *****
//-----

void calcPreLoss() {

    //-----
    // Check to see if the pressure sockets are empty, if not then execute
    //-----
    if ( !S_dPqP.isEmpty() ) {
        S_dPqP.execute();
    }
    dPqP = dPqPBase * s_dPqP + a_dPqP; // calculate pressure losses (dry duct and
    Valve)
    if( switchDes == "OFFDESIGN" ) {
        if( switchAud == "AUDIT" ) {
            dPqP = dPqP * s_dPqPAud + a_dPqPAud;
        }
    }
    //comment -IA- Collect total enthalpy at inlet
    real hin = Fl_I.ht;
    real Pin = ( 1 - dPqP ) * Fl_I.Pt; //comment -IA- apply pressure losses as calculated
    above
    //comment -IA- copy flow to combustor flow
    Fl_Icomb.copyFlowStatic( "Fl_I" );
    Fl_Icomb.setTotal_hP( hin, Pin );

}

void calcBurn() {

    real TtCombOutTemp;

```

```

real htStoich;
real WFuelLimit;
real WFuelHeat;

Fl_Ocomb.copyFlow( "Fl_Icomb" );

//-----
// Efficiency
//-----
if ( !S_eff.isEmpty() ) {
    S_eff.execute();
}
eff = effBase * s_eff + a_eff;
effChem = effChemBase * s_effChem + a_effChem;

//-----
// Burn
//-----
Fl_Ocomb.burn( "Fu_I", eff );

//-----
// if inputting a PW type of efficiency adjust the temperature
//-----
if ( effChem < 1.0 ) {
    TtCombOutTemp = effChem * ( Fl_Ocomb.Tt - Fl_Icomb.Tt ) +
        Fl_Icomb.Tt;
    Fl_Ocomb.setTotalTP( TtCombOutTemp, Fl_Icomb.Pt ); // use Pin
}
}

void calcRayleighLoss() {

    flagRayleighChoked = 0;
    flagRayleighLossTooMuch = 0;

    PqPRayleigh = 1.0;
    PqPRayleighError = 0.0;

    //-----
    // self-convergent iteration loop for internal momentum pressure drop calc
    //-----

```

```

for( countRayleigh=0; countRayleigh<=countRayleighMax;
    countRayleigh++) {

//-----
// input or output dPqPRayleigh
//-----
if( switchHotLoss == "INPUT" ) {
    PqPRayleigh = 1.0 - dPqPRayleigh;
}
else if( switchHotLoss == "CALCULATE" ) {
    dPqPRayleigh = 1.0 - PqPRayleigh;
}

//-----
// calculate momentum pressure drop
//-----
real PtCombOut = PqPRayleigh * Fl_Icomb.Pt;

Fl_Ocomb.setTotal_hP( Fl_Ocomb.ht, PtCombOut );

//-----
// Check momentum pressure drop
//-----
PqPRayleighNew = PqPRayleigh;

if ( switchHotLoss == "CALCULATE" ) {

//-----
// make this thing a constant area burner
//-----
Fl_Ocomb.A = Fl_Icomb.A;
flagRayleighChoked = 0;
if( Fl_Ocomb.MN > 1.0 ) {
    // when MN > 1.0 FlowStation static calc is
    // not consistent with Area
    // Fl_Ocomb.MN = 1.0;
    // do not do this - creates major iteration problems
    flagRayleighChoked = 1;
}
}
}

```

```

//-----
// Calculate the exit static pressure from the momentum equation
// assume the fuel has the same velocity as the entrance flow
//-----
real PsMomMeth1;
PsMomMeth1 = Fl_Icomb.W*Fl_Icomb.V - Fl_Ocomb.W*Fl_Ocomb.V;
PsMomMeth1 = PsMomMeth1/C_GRAVITY;
PsMomMeth1 = PsMomMeth1 + Fl_Icomb.Ps * Fl_Icomb.A;
PsMomMeth1 = PsMomMeth1/Fl_Ocomb.A;
real PsMomMeth2;
//PsMomMeth2 = Fl_Ocomb.W*Fl_Icomb.V;
PsMomMeth2 = Fl_Icomb.W*Fl_Icomb.V + Wfuel*Fl_Icomb.V*fuelFractV;
PsMomMeth2 = PsMomMeth2/C_GRAVITY;
PsMomMeth2 = PsMomMeth2 + Fl_Icomb.Ps * Fl_Icomb.A;
PsMomMeth2 = PsMomMeth2/Fl_Ocomb.A;
PsMomMeth2 =
    PsMomMeth2/(1.0+Fl_Ocomb.gams*Fl_Ocomb.MN*Fl_Ocomb.MN);
//PsMomMeth1 = PsMonMeth2;

//-----
// Note Meth1 = Meth2 when MN <= 1.0
// Use Meth2 - seems more stable the Meth1 when MN > 1.0
//-----
PqPRayleighNew = (PsMomMeth2/Fl_Ocomb.Ps) * PqPRayleigh;
}

// Check against tolerance
PqPRayleighError = PqPRayleighNew - PqPRayleigh;
if( abs(PqPRayleighError) < tolRayleigh ) { break; }

// Bounding of PqPRayleigh movement to PqPRayleighStep
real sign;
sign = PqPRayleighError/abs(PqPRayleighError);
PqPRayleighDelta = sign *
    min(abs(PqPRayleighError),PqPRayleighStep);
PqPRayleighNew = PqPRayleigh + PqPRayleighDelta;

// Lower limit of PqPRayleigh - limit too much loss to PqPRayleighMin
if( PqPRayleighNew < PqPRayleighMin ) {
    if( flagRayleighLossTooMuch == 1 ) {
        ESOREport( 1023901,"Rayleigh pressure loss limited, too much loss", FALSE );
        break;
    }
}

```

```

    }
    PqPRayleighNew = PqPRayleighMin;
    flagRayleighLossTooMuch = 1;
}
else {
    flagRayleighLossTooMuch = 0;
}

/*
// debug info
cout << Fl_Ocomb.A << " ";
cout << Fl_Ocomb.MN << " ";
cout << Fl_Ocomb.Ps << " ";
cout << PsMomMeth1 << " ";
cout << PsMomMeth2 << " ";
cout << PqPRayleigh << " ";
cout << PqPRayleighNew << " ";
cout << endl;
*/

//-----
// check for convergence
//-----
if( countRayleigh >= countRayleighMax ) {
    ESOreport( 1023901,"Rayleigh iteration failed to converge, counter exceed max",
FALSE );
    break;
}

PqPRayleigh = PqPRayleighNew;

}

if( flagRayleighChoked == 1 ) {
    ESOreport( 1023901,"Rayleigh Fl_Ocomb.MN exceed choked
condition", FALSE );
}
}

void calculate() {

```

```

//-----
// Preburning pressure loss
//-----
calcPreLoss(); // creates Fl_Icomb, applies pre-losses

real FARin = Fl_Icomb.FAR;
real WARin = Fl_Icomb.WAR;

//-----Added 6 Feb 2007 - IA-----
if (Fl_I.MN == 0. && Fl_I.Aphy == 0.){
    Fl_Icomb.MN = 0.4;
    Fl_Icomb.setTotal_hP(Fl_Icomb.ht, Fl_Icomb.Pt);
}
//-----End Additions 6 Feb 2007

//-----
// Pre-calculate Burning to obtain enthalpy, burned fuel attrib.
//-----
if ( switchBurn == "FAR" ) {
    //-----
    // determine the fuel weight flow from the input FAR
    //-----
    Wfuel = ( Fl_Icomb.W / ( 1. + FARin + WARin ))*( FAR - FARin );
    Fu_I.Wfuel = Wfuel;
    eqRatio = FAR/Fu_I.FARst; // Added 5 Feb 2007 - IA

    calcBurn();
    calcRayleighLoss();

    TtCombOut = Fl_Ocomb.Tt;

}
//#####
// Added 5 February 2007 - IA
// do an equivalence ratio calculation
else if (switchBurn == "EQRATIO") {
    FAR = eqRatio*Fu_I.FARst;
    Wfuel = ( Fl_Icomb.W / ( 1. + FARin + WARin ))*( FAR - FARin );
    Fu_I.Wfuel = Wfuel;

    calcBurn();
    calcRayleighLoss();
}

```



```

        TtCombOut = Fl_Ocomb.Tt;
    }

//-----
//make a flow station that has properties of cold vitiated air...
//-----
Fl_Vit.copyFlowStatic("Fl_Ocomb");
Fl_Vit.setTotalTP(Fl_Icomb.Tt, Fl_Icomb.Pt);

//-----
// copy inlet flow for pure air reference to be used later
//-----
//Take a snapshot of air after it has entered the detonation tubes
Fl_IcombAir.copyFlowStatic("Fl_Icomb");

// Copy input flow properties for internal bypass flow
// - W set later
Fl_O2.copyFlow("Fl_IcombAir");

//-----
// On-design loop
//-----
if (switchDes == "DESIGN"){

    //-----
    // Initialize iterated variables
    //-----
    real uCJ, a_1, rhoVit, freq, PcqPi, errors;
    real gamt, Cpt, beta, MCJ2, PcqPi2; // average (static gamma, Cp)
    real Atube, Vtube;//, mCycle, Wtube;
    real MFP, Wvalve, gma_I;
    real mFillAir, mPurgeAir, mPureAir; //tauVO, WvalveOpen,
    real tDetonation, tDetProp, tBlowdown, tPurge, tFill, iVel;
    real gam_s, gmm_fc;//, a_inlet;
    real WtotAir, Wbypass;

    int count;

    //---- initiated but not iterated -----
    //static density of cool vitiated fluid
    rhoVit = Fl_Vit.rhot; //(lbm/ft^3)

```

```

// speed of sound in pure air, stagnated in detonation tube
// that the detonation wave propagates in to
a_1 = sqrt(Fl_Icomb.gamt*Fl_Icomb.Rt*Fl_Icomb.Tt*25037.);

// =====
// Calculate Chapman-Jouguet Mach number for wave as described
// in Heiser and Pratt
// =====
//*** input variables: //
//*** output variables: //MCJ, deltaS, qadd //
//*** Flow Stations: //Fl_Ocomb, Fl_Icomb //
// local variables: //gamt, Cpt, qadd, beta, MCJ2 //

//----- Arithmetically average specific heats -----
gamt = (Fl_Ocomb.gamt + Fl_Icomb.gamt)/2.0; // arithmetic mean of
// gamma for stopped
// fluid
Cpt = (Fl_Ocomb.Cpt + Fl_Icomb.Cpt)/2.0; // arithmetic mean of Cp
// for a stopped fluid

//----- Calculate heat addition per Heiser-Pratt cycle -----
// calculate non-dimensional heat addition
qadd = (Fl_Ocomb.ht - Fl_Icomb.ht)/(Cpt*Fl_Icomb.Tt);

//----- Calculate Chapman-Jouget Mach number -----
beta = (gamt + 1.0)*qadd+1.0;
MCJ2 = beta + sqrt( beta**2 - 1.0 );
MCJ = sqrt(MCJ2);

//----- Calculate Entropy gain based on CJ detonation -----
deltaS = Cpt*(-log(MCJ2*((gamt+1.0)/
(1.0+gamt*MCJ2))**((gamt+1.0)/gamt)) );

//---- calculate the pressure rise using the H &P method -----
PcqPi = (1.0+ gamt*MCJ2)/(gamt+1.0);
uCJ = a_1*MCJ;

//----- Calculate tube volume and Area -----
Atube = (PI/4.)*dTube**2/144.; // ft^2
Vtube = Atube*(lTube/12); // ft^3

```

```

//----- calculate the valve inlet mass flow rate -----
gma_I=Fl_IcombAir.gamt;
MFP = Mvalve*sqrt( (gma_I*32.174)/(Fl_IcombAir.Rt*778.16) )
      *(1.+(gma_I-1.)/2.*Mvalve**2)**( (gma_I+1.)/(2.*(1.-gma_I)));
Wvalve = (Fl_IcombAir.Pt/sqrt(Fl_IcombAir.Tt))
          *(Atube*144.*ARvalve)*MFP;

//-----
// On-Design: Calculate bypass ratio
//-----
**** input Variables: //dTube, lTube, n_tubes, fillFrac
//                      // purgeFrac,
**** iterated Variables // freq
**** output Variables: // iBPR
**** local variables: //WfillAir, WpurgeAir, WpureAir, WtotAir
//                      Wbypass, WpurgeAir, Wvit, //
**** Flow Stations: // Fl_IcombAir, Fl_Icomb, Fl_Iprg, Fl_Vit, //

//----- Calculate the split and partition of flow -----
// amount of air that will be mixed with fuel - one tube
mFillAir = Vtube*(rhoVit*fillFrac)/(1.+FAR);

// amount of air that will purge during each cycle - one tube
mPurgeAir = Vtube*(Fl_IcombAir.rhos*purgeFrac);

// total air per cycle flowing though one tube
mPureAir = mFillAir + mPurgeAir;

//-----
// Timing - calculate frequency - Do I need to put this at the end?
//-----
**** input Variables: // DDT, tValve, Ltube, ff, pf, tCycle
**** iterated Variables: // uCJ, PcqPi
**** output Variables // tCycle, tauValveOpen, freq
**** local variables: // tDetonation, tDetProp, tBlowdown, tPurge,
//                      // tFill
//-----

//----- Detonation time -----
// DetProp time is relatively independant of fill fraction...
// tDetProp= lTube/(uCJ*12);

```

```

// DDT is input, tDetonationPropogatio calcd (may need to iterate)
// tDetonation = DDT + tDetProp;

//----- Blowdown time -----
// assume choked flow at tube exit and calculate blowdown based on
// draw-down time of a pressurized tank calculated on pressure
// differential
// gam_s = Fl_IcombAir.gams; // larger gamma is more conservative
// gmm_fc = ((gam_s + 1.)/2.)*(-(gam_s+1.)/( 2.*(gam_s-1.)) ); //

##### tBlowdown: Use ~1/2 calcd pressure (to match experimental data)
// we'll use CJ det wave velocity as the speed of sound in the gas
// since a cannot be directly calc'd
// note tBlowdown is proportional to tube length
// tauBlDn is proportional to tube length...
// tBlowdown = (log(0.4*PcqPi)/gmm_fc)*(lTube/uCJ);

//----- Fill and Purge time -----
// Use the choked flow at valve inlet and the mass flow rate as
// calculated outside the loop to calculate fill time (m/ mdot)
// tPurge = tValve + mPurgeAir/Wvalve; //(s)
// tFill = tValve + mFillAir/Wvalve; //(s)
//Improvement could be made by calculating vitiated air velocity...

//----- Cycle Time output calculation -----
// tCycle = tDetonation + tBlowdown + tPurge + tFill;
// tauValveOpen = (tPurge+tFill)/tCycle;
// freq = 1./tCycle; //tCycle is user input
//cout << "\n\n tDetonation, tBlowdown, tPurge, tFill PcqPi"<< " "<< tDetonation << "
"<< tBlowdown<< " "<< tPurge<< " "<< tFill<< " freq" << 1/tCycle << " " << PcqPi <<
endl;

//----- Set total mass flow through tubes -----
WtotAir = mPureAir*n_tubes*freq;
// steady-state flow rate into tubes

// conservation of mass check
if (WtotAir > Fl_I.W) {

    fillFrac = fillFrac*(Fl_I.W/WtotAir);
    purgeFrac = purgeFrac*(Fl_I.W/WtotAir);

    mFillAir = Vtube*(rhoVit*fillFrac)/(1.+FAR);

```

```

// amount of air that will be mixed with fuel - 1 tube

mPurgeAir = Vtube*(Fl_IcombAir.rhos*purgeFrac);
// amount of air that will purge during each cycle -1 tube

mPureAir = mFillAir + mPurgeAir;
// total air per cycle flowing though one tube

WtotAir = Fl_I.W;
//
cerr << "ATTENTION !pf & ff changed to: " << purgeFrac << " " <<
fillFrac << endl;

ESOreport( 2222100,"Purge and fill fractions changed in order to maintain
conservation of mass through the engine", FALSE );
//break;

}

//----- Set iBPR -----
Wbypass = (Fl_I.W - WtotAir)*flowby;
// steady-state flow rate sent to bypass

iBPR = Wbypass/WtotAir;
// steady-state internal PDC bypass ratio

iBPRdes = iBPR;

//----- Set bypass exit flow SPLIT -----
Fl_O2.W = Wbypass;
Fl_O3.W = (Fl_I.W - WtotAir)-((Fl_I.W-WtotAir)*flowby);

//----- Set purge and fill stations PARTITION -----
Fl_Iprg.copyFlowStatic("Fl_IcombAir");
// copy flow for purge function

// ----- PURGE AIR -----
Fl_Iprg.AphyDes = (Atube*144)*n_tubes; //Set physical area
Fl_Iprg.W = mPurgeAir*freq*n_tubes; // set mass flow rate

// ----- FILL AIR -----
Fl_Icomb.copyFlow("Fl_IcombAir");
Fl_Icomb.AphyDes = Atube*144.*n_tubes*tauValveOpen;
// Actual area is multiplied by tauVO to get equivalent

```

```

// area. - Fluid flows steadily through this area

Fl_Icomb.W = mFillAir*n_tubes*freq; //
Fl_Icomb.setTotal_hP(Fl_IcombAir.ht, Fl_IcombAir.Pt);
//sets time-averaged static conditions

//-----
// Burning
//-----
// FAR was calculated prior to enteringh this convergence loop -
// so we just need to modify Wfuel based on changed Fl_Icomb.W
Wfuel = ( Fl_Icomb.W /( 1. + FARin + WARin))*( FAR - FARin );
Fu_I.Wfuel = Wfuel;

calcBurn();
calcRayleighLoss();

TtCombOut = Fl_Ocomb.Tt;

//=====
// Apply Dyer-Kaemming correction to obtain tube flow at exit
// (ignores the kinetic energy of the shock wave.)
//=====
Fl_Ocomb.setTotal_hS(Fl_Ocomb.ht, Fl_Icomb.S+deltaS);

}

// OFF-DESIGN CODE //added Dec 09 - CT
if (switchDes == "OFFDESIGN"){

//-----
// Initialize iterated variables
//-----
//real uCJ, a_1, rhoVit, freq, PcqPi, errors;
//real gamt, Cpt, beta, MCJ2, PcqPi2; // average (static gamma, Cp)
//real Atube, Vtube;//, mCycle, Wtube;
//real MFP, Wvalve, gma_I;
//real mFillAir, mPurgeAir, mPureAir; //tauVO, WvalveOpen,
//real tDetonation, tDetProp, tBlowdown, tPurge, tFill, iVel;
//real gam_s, gmm_fc;//, a_inlet;
//real WtotAir, Wbypass;

//int count;

```

```

//---- initiated but not iterated -----
//static density of cool vitiated fluid
rhoVit = Fl_Vit.rhot; //(lbm/ft^3)

// speed of sound in pure air, stagnated in detonation tube
// that the detonation wave propagates in to
a_1 = sqrt(Fl_Icomb.gamt*Fl_Icomb.Rt*Fl_Icomb.Tt*25037.);

// =====
// Calculate Chapman-Jouguet Mach number for wave as described
// in Heiser and Pratt
// =====

=

**** input variables: //
**** output variables: //MCJ, deltaS, qadd //
**** Flow Stations: //Fl_Ocomb, Fl_Icomb //
// local variables: //gamt, Cpt, qadd, beta, MCJ2 //

//----- Arithmetically average specific heats -----
gamt = (Fl_Ocomb.gamt + Fl_Icomb.gamt)/2.0; // arithmetic mean of
// gamma for stopped
// fluid
Cpt = (Fl_Ocomb.Cpt + Fl_Icomb.Cpt)/2.0; // arithmetic mean of Cp
// for a stopped fluid

//----- Calculate heat addition per Heiser-Pratt cycle -----
// calculate non-dimensional heat addition
qadd = (Fl_Ocomb.ht - Fl_Icomb.ht)/(Cpt*Fl_Icomb.Tt);

//----- Calculate Chapman-Jouget Mach number -----
beta = (gamt + 1.0)*qadd+1.0;
MCJ2 = beta + sqrt( beta**2 - 1.0 );
MCJ = sqrt(MCJ2);

//----- Calculate Entropy gain based on CJ detonation -----
deltaS = Cpt*(-log(MCJ2*((gamt+1.0)/
(1.0+gamt*MCJ2))*((gamt+1.0)/gamt)) );

//---- calculate the pressure rise using the H &P method -----
PcqPi = (1.0+ gamt*MCJ2)/(gamt+1.0);
uCJ = a_1*MCJ;

```

```

//----- Calculate tube volume and Area -----
Atube = (PI/4.)*dTube**2/144.; // ft^2
Vtube = Atube*(lTube/12); // ft^3

//----- calculate the valve inlet mass flow rate -----
gma_I=Fl_IcombAir.gamt;
MFP = Mvalve*sqrt( (gma_I*32.174)/(Fl_IcombAir.Rt*778.16) )
      *(1.+(gma_I-1.)/2.*Mvalve**2)**( (gma_I+1.)/(2.*(1.-gma_I)));
Wvalve = (Fl_IcombAir.Pt/sqrt(Fl_IcombAir.Tt))
          *(Atube*144.*ARvalve)*MFP;

//-----
// OFF-Design: Calculate bypass ratio
//-----
//*** input Variables: //dTube, lTube, n_tubes, fillFrac
//                      // purgeFrac,
//*** iterated Variables // freq
//*** output Variables: // iBPR
//*** local variables: //WfillAir, WpurgeAir, WpureAir, WtotAir
//                      Wbypass, WpurgeAir, Wvit, //
//*** Flow Stations:   // Fl_IcombAir, Fl_Icomb, Fl_Iprg, Fl_Vit, //

//----- Calculate the split and partition of flow -----
// amount of air that will be mixed with fuel - one tube
mFillAir = Vtube*(rhoVit*fillFrac)/(1.+FAR);

// amount of air that will purge during each cycle - one tube
mPurgeAir = Vtube*(Fl_IcombAir.rhos*purgeFrac);

// total air per cycle flowing though one tube
mPureAir = mFillAir + mPurgeAir;

//-----
// Timing - calculate frequency – Not used for Thorn thesis, frequency is input
//-----
//*** input Variables: // DDT, tValve, Ltube, ff, pf, tCycle
//*** iterated Variables: // uCJ, PcqPi
//*** output Variables // tCycle, tauValveOpen, freq
//*** local variables: // tDetonation, tDetProp, tBlowdown, tPurge,
//                      // tFill
//-----

```



```

//----- Detonation time -----
// DetProp time is relatively independant of fill fraction...
// tDetProp= lTube/(uCJ*12);

//DDT is input, tDetonationPropogatio calcd (may need to iterate)
// tDetonation = DDT + tDetProp;

//----- Blowdown time -----
// assume choked flow at tube exit and calculate blowdown based on
// draw-down time of a pressurized tank calculated on pressure
// differential
// gam_s = Fl_IcombAir.gams; // larger gamma is more conservative
// gmm_fc = ((gam_s + 1.)/2.)*(-(gam_s+1.)/( 2.*(gam_s-1.)) ); //

##### tBlowdown: Use ~1/2 calcd pressure (to match experimental data)
// we'll use CJ det wave velocity as the speed of sound in the gas
// since a cannot be directly calc'd
// note tBlowdown is proportional to tube length
// tauBlDn is proportional to tube length...
// tBlowdown = (log(0.4*PcqPi)/gmm_fc)*(lTube/uCJ);

//----- Fill and Purge time -----
// Use the choked flow at valve inlet and the mass flow rate as
// calculated outside the loop to calculate fill time (m/ mdot)
// tPurge = tValve + mPurgeAir/Wvalve; //(s)
// tFill = tValve + mFillAir/Wvalve; //(s)
//Improvement could be made by calculating vitiated air velocity...

//----- Cycle Time output calculation -----
// tCycle = tDetonation + tBlowdown + tPurge + tFill;
// tauValveOpen = (tPurge+tFill)/tCycle;

freq = 1./tCycle; //frequency is input (Thorn thesis)

//cout << "\n \n tDetonation, tBlowdown, tPurge, tFill PcqPi"<< " "<< tDetonation << "
"<< tBlowdown<< " "<< tPurge<< " "<< tFill<< " freq" << 1/tCycle << " " << PcqPi <<
endl;

//----- Set total mass flow through tubes -----

```

```

WtotAir = mPureAir*n_tubes*freq;

// steady-state flow rate into tubes

// conservation of mass check

if (WtotAir > Fl_I.W) {

    fillFrac = fillFrac*(Fl_I.W/WtotAir);
    purgeFrac = purgeFrac*(Fl_I.W/WtotAir);

    mFillAir = Vtube*(rhoVit*fillFrac)/(1.+FAR);
    // amount of air that will be mixed with fuel - 1 tube

    mPurgeAir = Vtube*(Fl_IcombAir.rhos*purgeFrac);
    // amount of air that will purge during each cycle -1 tube

    mPureAir = mFillAir + mPurgeAir;
    // total air per cycle flowing though one tube

    WtotAir = Fl_I.W;
    // cerr << "ATTENTION !pf & ff changed to: " << purgeFrac << " " <<
    fillFrac << endl;

    ESOreport( 2222100,"Purge and fill fractions changed in order to maintain
conservation of mass through the engine", FALSE );
    //break;

}

//----- Set iBPR -----
Wbypass = (Fl_I.W - WtotAir)*flowby;
// steady-state flow rate sent to bypass

iBPR = Wbypass/WtotAir;
// steady-state internal PDC bypass ratio

//iBPRdes = iBPR;

//----- Set bypass exit flow SPLIT -----
Fl_O2.W = Wbypass;

```

```

    Fl_O3.W = (Fl_I.W - WtotAir)-((Fl_I.W-WtotAir)*flowby); //bleed flow needed
                                                                //for static pressure
                                                                //of iBPR entering
                                                                // Mixer39 to equal
                                                                // static pressure
                                                                //entering from tubes

//----- Set purge and fill stations PARTITION -----
Fl_Iprg.copyFlowStatic("Fl_IcombAir");
// copy flow for purge function

// ----- PURGE AIR -----
Fl_Iprg.AphyDes = (Atube*144)*n_tubes; //Set physical area
Fl_Iprg.W = mPurgeAir*freq*n_tubes; // set mass flow rate

// ----- FILL AIR -----
Fl_Icomb.copyFlow("Fl_IcombAir");
Fl_Icomb.AphyDes = Atube*144.*n_tubes*tauValveOpen;
// Actual area is multiplied by tauVO to get equivalent
// area. - Fluid flows steadily through this area

Fl_Icomb.W = mFillAir*n_tubes*freq; //
Fl_Icomb.setTotal_hP(Fl_IcombAir.ht, Fl_IcombAir.Pt);
//sets time-averaged static conditions

//-----
// Burning
//-----
// FAR was calculated prior to enteringh this convergence loop -
// so we just need to modify Wfuel based on changed Fl_Icomb.W
Wfuel = ( Fl_Icomb.W /( 1. + FARin + WARin))*( FAR - FARin );
Fu_I.Wfuel = Wfuel;

calcBurn();
calcRayleighLoss();

TtCombOut = Fl_Ocomb.Tt;

//=====
// Apply Dyer-Kaemming correction to obtain tube flow at exit
// (ignores the kinetic energy of the shock wave.)
//=====
Fl_Ocomb.setTotal_hS(Fl_Ocomb.ht, Fl_Icomb.S+deltaS);
}

```

```

//END OFF-DESIGN CODE
//-----
// Add split flows back to combusted flow
//-----
Fl_Ocomb.add("Fl_Iprg"); //add purge flow in (uncorrected)

//=====
// Apply corrections to the flow for transition to steady state...
// TTSS
//=====
//*** local Variables: // Snew, Pnew
//*** Input Variables: // deltaS, TTSSeff, TTSSdPqP
//*** Flwo stations: // Fl_Ocomb, Fl_Vit
real hnew, Pnew; //

//----- Calculate new Entropy and Pressure -----
//      eff = (dht)TTSF/(dht)comb + 1.
//      current h - ( h gained)*(1.-eff)
hnew = Fl_Ocomb.ht - (Fl_Ocomb.ht - Fl_Icomb.ht)*(1.0-TTSSeff);
Pnew = Fl_Ocomb.Pt*(1.0-TTSSdPqP);

//End of 12Jan2007 additinos - IA
//#####
Fl_O1.copyFlow( "Fl_Ocomb" );

//----- update fluid properties based on new Entropy and Pressure
Fl_O1.setTotal_hP(hnew, Pnew); //added 12Jan2007 - IA

//-----
// Thermal storage calculations
//-----
if ( !S_Qhx.isEmpty() ) {
    S_Qhx.execute();
}
real hout = Fl_O1.ht - Qhx / Fl_O1.W;
Fl_O1.setTotal_hP( hout, Fl_O1.Pt );

//-----
// store the design value of FAR for use in guessing
//-----

```

```

    if ( switchDes == "DESIGN" ) {
        FARDes = FAR;
    }

}

//-----
// register the appropriate errors at build time
//-----
void VCinit()
{
    ESoregCreate( 1023901, 8, "", TRUE, FALSE, TRUE ); // provisional
    ESoregCreate( 1093901, 8, "", TRUE, FALSE, TRUE ); // provisional
    ESoregCreate( 2222100, 2, "", TRUE, FALSE, TRUE ); // provisional
}

}

#endif

```

## Bibliography

- Andrus, Ionio Q. *Comparative Analysis of a High Bypass Turbofan Using a Pulsed Detonation Combustor*. MS thesis, AFIT/GAE/ENY/07-M02. Graduate School of Engineering and Management, Air Force Institute of Technology (AU), Wright-Patterson AFB OH, March 2007.
- Bussing, T. and Pappas, G. "An Introduction to Pulse Detonation Engines," 32<sup>nd</sup> Aerospace Sciences Meeting & Exhibit, AIAA-1994-0263. AIAA, Reno NV, 10-13 January 1994.
- Caldwell, Nicholas, and Gutmark, Ephraim. "Performance Analysis of a Hybrid Pulse Detonation Combustor/Gas Turbine Engine," 44<sup>th</sup> AIAA/ASME/SAE/ASEE Joint Propulsion Conference and Exhibit. AIAA-2008-4880, AIAA, Harford CT, 21-23 July 2008.
- Dyer, R.S. and Kaemming, T.A. "The Thermodynamic Basis of Pulsed Detonation Engine Thrust Production," 38<sup>th</sup> AIAA/ASME/SAE/ASEE Joint Propulsion Conference & Exhibit, AIAA-2002-4072. AIAA, Indianapolis IN, 7-10 July 2002.
- Glaser, Aaron, Allgood, Daniel, and Gutmark, Ephraim. "Experimental Investigation into the Off-Design Performance of a Pulse Detonation Engine," 42<sup>nd</sup> AIAA Aerospace Sciences Meeting and Exhibit, AIAA-2004-1208, AIAA, Reno NV, 5-8 January 2004.
- Glassman, Irvin. *Combustion*. New York: Academic Press, 1996.
- Heiser, William H. and Pratt, David T. "Thermodynamic Cycle Analysis of Pulse Detonation Engines," *AIAA Journal of Propulsion and Power*, 18(1):68-76, January-February 2002.
- Hoke, John, and Bradley, Royce. "Impact of DDT Mechanism, Combustion Wave Speed, Temperature, and Charge Quality on Pulsed-Detonation-Engine Performance," 43<sup>rd</sup> AIAA Aerospace Sciences Meeting, AIAA-2005-1342, AIAA, Reno NV, 10-13 January 2005.
- Hoke, John, Bradley, Royce, Stutrud, Jeff and Schauer, Fred. "Integration of a Pulsed Detonation Engine with an Ejector Pump and With a Turbo-Charger as Methods to Self-Aspirate," 20<sup>th</sup> AIAA Aerospace Sciences Meeting & Exhibit, AIAA-2002-0615, AIAA, Reno NV, 14-17 January 2002.

- Kuo, Kenneth Kuan-yun. *Principles of Combustion*. New York: John Wiley & Sons, 1986.
- Mattingly, Jack D., Heiser, William H., and Pratt, David T. *Aircraft Engine Design*. Reston VA: American Institute of Aeronautics and Astronautics (AIAA), 2002.
- NASA. *NPSS Reference Sheets*. National Aeronautics and Space Administration, NASA John H. Glenn Research Center at Lewis Field, 21000 Brookpark Rd., Cleveland, OH 44135-3191, Revision W Edition, March 12, 2008. Software Release NPSS\_1.6.5.
- NASA. *NPSS User Guide*. National Aeronautics and Space Administration, NASA John H. Glenn Research Center at Lewis Field, 21000 Brookpark Rd., Cleveland, OH 44135-3191, Revision W Edition, March 12, 2008. Software Release NPSS\_1.6.5.
- Oates, Gordon C. *Aerothermodynamics of Gas Turbine and Rocket Propulsion*. Reston VA: American Institute of Aeronautics and Astronautics (AIAA), 1997.
- Petters, Dean P. and Felding, James L. "Engine System Performance of Pulse Detonation Concepts Using the NPSS Program," 38<sup>th</sup> AIAA/ASME/SAE/ASEE Joint Propulsion Conference & Exhibit, AIAA-2002-3910. AIAA, Indianapolis IN, 7-10 July 2002.
- Rasheed, Adam, Furman, Anthony, and Dean, Anthony J. "Experimental Investigations of an Axial Turbine Drive by a Multi-tube Pulsed Detonation Combustor System," 41<sup>st</sup> AIAA/ASME/SAE/ASEE Joint Propulsion Conference & Exhibit, AIAA 2005-4209. AIAA, Tucson AZ, 10-13 July 2005.
- Rasheed, Adam, Furman, Anthony, and Dean, Anthony J. "Wave Interactions in a Multi-tube Pulsed Detonation Combustor-Turbine Hybrid System," 42<sup>nd</sup> AIAA/ASME/SAE/ASEE Joint Propulsion Conference & Exhibit, AIAA 2006-4447. AIAA, Sacramento CA, 9 - 12 July 2006.
- Schauer, Fred, Bradley, Royce, and Hoke, John. "Interaction of a Pulsed Detonation Engine With a Turbine," 41<sup>st</sup> Aerospace Sciences Meeting and Exhibit, AIAA-2003-0891. AIAA, Reno NV, 6-9 January 2003.
- Schauer, Fred, Bradley, Royce, and Stutrud, Jeff. "Detonation Initiation Studies and Performance Results for Pulsed Detonation Engine Applications," 39<sup>th</sup> AIAA Aerospace Sciences Meeting & Exhibit, AIAA-2001-1129. AIAA, Reno NV, 8-11 January 2001.

Shapiro, Ascher H. *The Dynamics and Thermodynamics of Compressible Flow, Vol. 1.*  
New York: John Wiley & Sons, 1953.

Strehlow, Roger A. *Combustion Fundamentals.* New York: McGraw Hill, 1984.

Williams, Forman A. *Combustion Theory.* USA: Perseus Books Publishing, L.L.C., 1985.

Wintenberger, E. and Shepherd, J. E. "Thermodynamic Analysis of Combustion  
Processes for Propulsion Systems," AIAA-2004-1033, Reno NV, 5-8 January 2004.



## **Vita**

Captain Caitlin Thorn graduated from Auburn University in 2004 summa cum laude with a degree in Mechanical Engineering before being commissioned as a 2<sup>nd</sup> Lieutenant in the United States Air Force. Her first assignment was at Patrick Air Force Base working as an Eastern Range engineer. There she oversaw the RSAII contract as a communications project engineer for the development and modernization of the Eastern Range. Her next assignment was at Cape Canaveral Air Force Station at the 5<sup>th</sup> Space Launch Squadron. There she worked as a Delta IV mechanical engineer and oversaw the first operational Delta IV heavy launch. In August of 2008 she entered the Air Force Institute of Technology in pursuit of a Master of Science degree in Aeronautical Engineering. Upon graduation, she will be assigned to the United States Air Force Academy as an undergraduate instructor in the Aeronautics Department.

REPORT DOCUMENTATION PAGE				Form Approved OMB No. 074-0188	
<p>The public reporting burden for this collection of information is estimated to average 1 hour per response, including the time for reviewing instructions, searching existing data sources, gathering and maintaining the data needed, and completing and reviewing the collection of information. Send comments regarding this burden estimate or any other aspect of the collection of information, including suggestions for reducing this burden to Department of Defense, Washington Headquarters Services, Directorate for Information Operations and Reports (0704-0188), 1215 Jefferson Davis Highway, Suite 1204, Arlington, VA 22202-4302. Respondents should be aware that notwithstanding any other provision of law, no person shall be subject to a penalty for failing to comply with a collection of information if it does not display a currently valid OMB control number.</p> <p><b>PLEASE DO NOT RETURN YOUR FORM TO THE ABOVE ADDRESS.</b></p>					
1. REPORT DATE (DD-MM-YYYY) 25-03-2010		2. REPORT TYPE Master's Thesis		3. DATES COVERED (From – To) September 2008 – March 2010	
4. TITLE AND SUBTITLE  Off-Design Analysis of a High Bypass Turbofan Using a Pulsed Detonation Combustor				5a. CONTRACT NUMBER	
				5b. GRANT NUMBER	
				5c. PROGRAM ELEMENT NUMBER	
6. AUTHOR(S)  Thorn, Caitlin R., Captain, USAF				5d. PROJECT NUMBER	
				5e. TASK NUMBER	
				5f. WORK UNIT NUMBER	
7. PERFORMING ORGANIZATION NAMES(S) AND ADDRESS(S) Air Force Institute of Technology Graduate School of Engineering and Management (AFIT/ENY) 2950 Hobson Way, Building 640 WPAFB OH 45433-8865				8. PERFORMING ORGANIZATION REPORT NUMBER  AFIT/GAE/ENY/10-M26	
9. SPONSORING/MONITORING AGENCY NAME(S) AND ADDRESS(ES)  Intentionally left blank				10. SPONSOR/MONITOR'S ACRONYM(S)	
				11. SPONSOR/MONITOR'S REPORT NUMBER(S)	
12. DISTRIBUTION/AVAILABILITY STATEMENT  APPROVED FOR PUBLIC RELEASE; DISTRIBUTION UNLIMITED.					
13. SUPPLEMENTARY NOTES  This material is declared a work of the U.S. Government and is not subject to copyright protection in the United States.					
14. ABSTRACT Past research has indicated that implementation of a pulsed detonation combustor (PDC) into a high-bypass turbofan engine yields a more efficient engine at design conditions. It is proposed that performance gains can be made utilizing this hybrid engine off-design. A hybrid high-bypass turbofan engine with a PDC model was evaluated for a range of Mach numbers, altitudes, and fill fractions in the Numerical Propulsion System Simulation (NPSS). Results were compared to a conventional baseline high-bypass turbofan engine that shares the same architecture with the hybrid. The NPSS baseline engine was validated using the Aircraft Engine Design System (AEDsys) program and the net thrust and specific fuel consumption agreed to within one percent. The effect of detonation on the core air flow is calculated using a closed form solution for the Chapman-Jouguet Mach number with a total energy correction applied. Results indicate that fill fraction can be adjusted to reduce the TSFC to that of the baseline engine and lower at some thrust levels. With careful selection of design parameters, results suggest a pulsed detonation combustor may be an appropriate candidate for inclusion in a hybrid turbofan engine.					
15. SUBJECT TERMS High Bypass Turbofans, Turbofan Engines, Detonation Waves, Combustion, Hybrid Propulsion, Hybrid Simulation, Aircraft Engines, Air Breathing Engines, Air Breathing Engines (Unconventional), Thermodynamic Cycles					
16. SECURITY CLASSIFICATION OF:			17. LIMITATION OF ABSTRACT	18. NUMBER OF PAGES	19a. NAME OF RESPONSIBLE PERSON
a. REPORT	b. ABSTRACT	c. THIS PAGE			Dr. Paul I. King ADVISOR
U	U	U	UU	154	19b. TELEPHONE NUMBER (Include area code) (937) 255-3636, ext 4628 (paul.king@afit.edu)